Varactor Based Tunable Planar Filters and Post-Fabrication Tuning of Microwave Filters

by

Alborz Rezazadeh Sereshkeh

A thesis
presented to the University of Waterloo
in fulfillment of the
thesis requirement for the degree of
Master of Applied Science
in
Electrical and Computer Engineering

Waterloo, Ontario, Canada, 2012

AUTHOR'S DECLARATION

I hereby declare that I am the sole author of this thesis. This is a true copy of the thesis, including any required final revisions, as accepted by my examiners.

I understand that my thesis may be made electronically available to the public.

Abstract

Post-fabrication tuning of filters is usually realized by adding number of elements for tuning the frequency and/or controlling the couplings between the resonators. The task of these tuning elements is to control resonators center frequency, inter-resonators coupling and input/output couplings. While the most common tool for the post-fabrication tuning is to use tuning screws and rods, it is not usually practical to tune a planar filter with these tools.

This thesis introduces a novel method for global post-fabrication tuning of microwave filters by designing and adding a passive distributed-element circuit in parallel to the detuned filter. The idea, which is demonstrated by experimental results, has several advantages over traditional techniques for filter tuning that use screws. The quality factor of resonator reduces significantly after adding the tuning screws while the proposed method does not affect the Q of resonators.

The most important advantage of the proposed compensator circuit is that it can be employed without knowing details of the detuned filters. Since the compensator circuit will be added in parallel to the detuned filter, it will not affect the elements of filter individually. So whether the filter is planar or cavity, the proposed circuit can be used for the tuning. The experimental results obtained demonstrate the validity of this method.

The dissertation also presents a novel concept for designing a center frequency and bandwidth tunable microstrip filter by using GaAs varactors. The proposed isolated coupling structure which is used in this filter makes the bandwidth tuning possible by reducing the loading effect of coupling elements on the resonators. The center frequency of this filter can be also tuned by using a different set of varactors connected to resonators. A 3-pole filter based on this concept has been designed and simulated. The concept can be expanded to higher order filters.

Acknowledgements

I would like to express my sincere thanks and appreciation to my supervisor, Professor R. R. Mansour, for his mentorship, guidance, ideas, encouragement and full support. His great personality made this research a pleasant and wonderful journey. I will be forever thankful to him for introducing me to the world of RF/Microwave engineering. I would not have been able to accomplish all that I have over the past two years without his supervision.

I would also like to thank the many members of the Centre for Integrated RF Engineering at the University of Waterloo who were my friends and confidants for the last two years. Thanks to Sara Attar for always being available to listen and provide guidance; to Mostafa Azizi for his valuable insight and hands-on RF experiments; to Sormeh Setoodeh for sharing her expertise in RF design; to Bill Jolley for providing his bountiful experience and expertise with RF measurement and assembly; to Siamak Fouladi for his great personality, his depth of RF knowledge, and his enduring support; and to Geoffrey Lee for always encouraging me and for being a great office-mate and friend.

My warm wishes and thanks go as well to my dear friends, Farhad Haghighizadeh, Koosha Khalvati, Mahdi Mirhoseini, Bahram Ehsandoust, Omid Zobeiri, Houshmand Shiranimehr, Arash Khatibi, Amir Safaripour, Sasan Taghizadeh and Mohammadreza Fakhari who have enriched my life beyond my studies. I have been lucky to have such good friends by my side.

And most importantly my deepest appreciation goes to my family, whom I love and cherish dearly.I would like to express my deepest gratitude to my parents, Fatemeh Nakhaee and Yadollah Rezazadeh, for their infinite love and continuous support and dedication. I would also like to thank my sister, Azadeh Rezazadeh, for her unconditional love and inspiration. Last but not least, I owe a world of thanks to my best friend and my beloved wife, Rozhin Yousefi, for enduring this journey with me, providing her unwavering support and continuous encouragement during these years. I would like to dedicate this work to her, my parents, and my sister to show my appreciation for their unconditional love and sacrifice.

Table of Contents

List of Figures

List of Tables

Chapter 1
Introduction

1.1 Motivations

Two main purposes of bandpass filters are band selection and image-rejection. However, the implementation of transceivers is challenging due to the occurrence of multi-frequency bands in different regions and diverse applications. Because of this, a single bandpass filter cannot carry out the filtering needs of all bands. The most common solution is to use a filter-bank and switching network, which necessitates a larger circuit size and greater complexity. Figure 1-1 shows a block diagram of a traditional multi-band transceiver.

A viable solution for eliminating the bulky filter-bank and switching network is replacing them with a tunable bandpass filter. Over the past two decades, radio frequency (RF) tunable filters have received increasing attention due to their potential to reduce the complexity and size of modern multi-band transceivers. The focus of recent work on tunable filters has shifted from maximizing the tuning range to controlling filter behavior as it is tuned. However, achieving clear-cut tuning has proven difficult due to manufacturing process inaccuracies, operational temperature, and long-term drift.

The most important demand for tunable filters is in multi-band wireless communication systems. The filter-banks followed by switch networks in multi-band cell phones usually take up 60-80% of the area on an RF board. Another important application of RF tunable filters is cognitive radios, which can decide on a usable communication channel by sensing the available spectrum. These do not have a fixed frequency band.

One of the most important steps in manufacturing commercial microwave filters is post-production tuning. As this step usually entails the input of expensive vector network analyzers (VNA) and skilful experts, it significantly impacts the filter's overall cost. Full control of a tunable filter requires the use of tunable elements to tune the center frequency of resonators as well as the coupling between two adjacent resonators and the input/output coupling. There are number of tuning techniques for reducing the complexity of filter tuning, such as time domain, group delay and fuzzy logic methods [1, 2, 3]. However, all of these techniques require the use of several tuning elements.

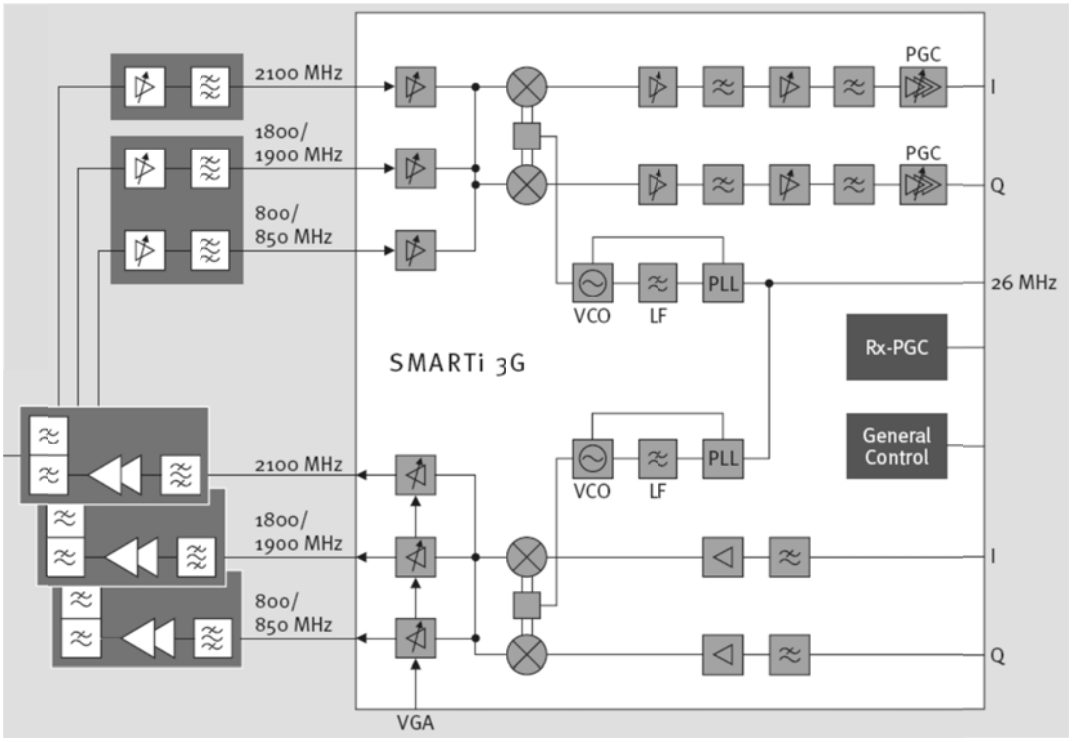

Figure 1-1: Block diagram of a traditional transceiver, PMB 5701 [4]

1.2 Objective

The objective of this research is to:

1) Develop a novel solution for the post-fabrication tuning of a microwave filter by employing passive elements parallel to the detuned filter.

2) Develop a novel structure for center frequency and bandwidth tunable microstrip filters.

1.3 Thesis Organization

The organization of this thesis is as follows. Chapter 2 presents a literature review of the work completed thus far in the areas of microwave tunable planar and cavity filters. The design steps of a microstrip filter as well as different methods of compensating a lossy fabricated filter are also provided in Chapter 2.

Chapter 3 introduces a novel method for the post-fabrication tuning of a microwave filter. A detailed theoretical analysis is provided for the proposed concept. EM simulation and experimental results are presented to demonstrate the validity of the concept.

Chapter 4 presents a new varactor-based structure for a center frequency and bandwidth tunable microstrip filter. At the end of Chapter 4, EM-simulation results of this structure are provided.

Chapter 5 presents the work's conclusions and possible future improvements.

Chapter 2
Background

2.1 Introduction

In this chapter, we cover some of the most important work that has been done in the area of microwave bandpass tunable filters. In section 2.2, a literature review of various tunable filters is presented. Section 2.3 outlines the fundamentals and design steps of a bandpass microstrip microwave filter. Finally, a literature survey of different methods of compensating a detuned fabricated filter is provided in Section 2.4, which is primarily concerned with the post-production tunability of filters.

2.2 Tunable Filters

This section overviews the major improvements in tunable cavity and planar filter design and is divided into three subsections. Subsection 2.2.1 outlines the planar tunable filters, while a literature review on bandwidth tunable filters is provided in 2.2.2.

Most tunable filters presented in this section fall into three main types: mechanically tunable, magnetically tunable, and electronically tunable [5].

Due to their large size and low tuning speed, mechanically tunable filters are not practical for modern communication systems. Their main advantage is low insertion loss [6].

The most widely held examples of magnetically tunable filters are filters with Yttrium-Iron-Garnet (YIG)-based resonators. The ferromagnetic resonators of these filters enable them to be tuned by applying an external DC magnetic field and variation of the ferromagnetic resonant frequency of YIG spheres. Although YIG filters have low insertion loss and high quality factor (Q) resonators, they suffer from large power consumption (0.1-1 W) [7]. Another disadvantage of YIG filters is their non-planar structure, which prevents their wide application in modern communication systems.

Electronically tunable filters come in three different types: varactor diodes; Barium Stronium Titanate (BST); and Radio-Frequency Micro-Electro-Mechanical Systems (RF MEMS).

The concept used in varactor diode-based tunable filters centers on changes in the depletion region width and resultant changes in capacitance. A reverse-bias DC voltage is utilized to effect this

change. Although these filters have zero power consumption and relatively fast tuning speed, they suffer from moderate Q of the resonators [8].

A ferroelectric thin-film BST tunable capacitor is the fundamental element of BST tunable filters. An electric field can change the relative dielectric constant of ferroelectric materials. The major advantages of BST filters are that they are planar, easy to integrate, and have zero power consumption [9]. However, they suffer from poor linearity and moderate Q.

The tuning element of RF MEMS tunable filter is usually a capacitance network based on RF MEMS. In these devices, an applied DC voltage can result in variations in the capacitance by employing micrometer level movements. Low insertion loss, high linearity, and low power consumption are some advantages of these filters. On the other hand, as they need a high voltage drive to operate (25-90 V), relatively more complex circuitry for high-voltage drive circuits is required.

2.2.1 Tunable Planar Filters

Planar filter are difficult to tune mechanically or magnetically since the electric field is trapped inside the dielectric. While varactors are the most common tuning element in the planar tunable filter technology, BST tunable capacitors and RF MEMS are other common methods for tuning planar filters. In this section, several publications in each category are reviewed. The selection criteria include having wide and nearly continuous frequency coverage, high Q, low insertion-loss, and good frequency response.

2.2.1.1 Varactor-based Planar Tunable Filters

Brown et al. presented an electronically tunable filter by applying a suspended substrate design and varactors as the tuning element [10]. The filter has a 60% center frequency tuning range from 700 MHz to 1.33 GHz, and the insertion loss is less than 3 dB for half of the tuning range. However, the filter suffers from bandwidth uncontrollability, and the fractional bandwidth reduces from 14% to 0.5% as the center frequency is tuned from 1 GHz to 700 MHz.

Sanchez-Renedo et al. demonstrated a tunable combline filter with additional transmission zeros by applying multiple couplings between the source/load and resonators [11]. The center frequency of

this filter is tunable from 400 MHz to 800 MHz. Along with a non-controllable bandwidth, the filter suffers from high insertion loss in the tuning range, especially at lower center frequencies.

One of the pioneer publications in controlling bandwidth in varactor-based planar filter tuning technology is presented by Park et al. [12]. This 2-pole filter has three different fractional bandwidth variations and a center frequency tuning range of 850 to 1400 MHz. The insertion loss performance of this filter is less than 3 dB for most frequencies in the tuning range, which represented state-of-the art insertion-loss performance at the time. However, the proposed 2-pole filter structure is not expandable to more resonators.

2.2.1.2 MEMS-based Planar Tunable Filters

Entesari et al. developed a 4-bit, 2-pole tunable filter by employing switched capacitors, metal-contact switches, and fixed-value capacitors [13]. The lumped inductors are air-coil type and the Q is 114 at 50 MHz. The Radant-MEMS switches are bonded on the FR-4 filter substrate; the measured insertion loss is 3–5 dB at 25–75 MHz; the relative bandwidth is $4.2\pm0.5\%$, and the measured IIP3 of the tunable filter is greater than +65 dBm. A resonator Q of 52–75 was measured over all tuning states.

Reines et al. presented a high-Q filter by employing suspended strip-line configurations. They developed the first suspended three-pole high-Q tunable combline RF MEMS tunable filter with a frequency coverage of 1.6–2.4 GHz, built on a quartz substrate [14]. The essential element for a 3-pole low-loss filter is a high-Q resonator and the suspended topology is chosen to fulfill the Q requirement. Both the resonators and the input/output matching networks are tunable. The insertion loss of the filter is 1.34–3.03 dB over the tuning range and a 3-dB bandwidth of 201–279 MHz. The quality factor is tunable and its value is 50–150 over the frequency range.

By investigating the loss mechanism of the multi-bit capacitance network, Park et al. used a high-Q 3-bits orthogonally-biased RF MEMS capacitance network and developed a low-loss 3-bit tunable filter [15]. The orthogonal biasing networks ensure high-Q operation because of a very low RF leakage through the bias lines. The measured filter has an insertion loss of 1.5–2.8 dB with a 1-dB bandwidth of $4.35\pm0.35\%$ over the 4–6 GHz tuning range. The tunable Q is 85–170 and can be improved to 125–210 with the use of a thicker bottom electrode for the RF MEMS capacitive switch.

At 5.91 GHz, the measured IIP3 is greater than 40 dBm while 1-dB power compression point is greater than +27.5 dBm.

The tunable filters for wireless applications need to have constant absolute bandwidth. El-Tanani et al. developed high performance tunable filters with this feature [16]. The filter is fabricated on ceramic substrates ($\varepsilon_r = 9.9$) for miniaturization and the design is based on corrugated coupled-lines. As the 3-bit tuning network is fabricated using a digital/analog RF MEMS device, it can provide a large capacitance ratio and continuous frequency coverage. The insertion loss of 1.9-2.2 dB at 1.5-2.5 GHz is measured in narrowband (bandwidth of 72 ± 3 MHz) and wideband (bandwidth of 115 ± 10 MHz) 2-pole filters. The power handling is 25 dBm and IIP3 is greater than 35 dBm. A quality factor of 85–165 was reported for this filter, which was the highest reported at this frequency range at the time of publication of this paper.

2.2.1.3 BST-based Planar Tunable Filters

Sanderson et al. presented a tunable IF filter by employing thin-film BST varactors [17]. The filter center frequency is tunable from 30 MHz to 88 MHz in three separate switch-selectable bands. The fractional bandwidth is relatively constant in the tuning range, and the insertion loss is less than 5 dB for the entire frequency range.

Chun et al. demonstrated a bandpass tunable bandwidth filter by employing an interdigital BST varactor [18]. The center frequency of this filter is 1.8 GHz while the 3-db bandwidth is tunable from 276 MHz to 318 MHz.

Nguyen et al. applied high-Q, tunable ICs to demonstrate a tunable bandpass filter [19]. The ICs are fabricated by applying Paratek's proprietary doped BST material. The presented 3-pole filter has a center frequency tuning range of 74% from 230 MHz to 400 MHz, and the insertion filter is less than 2.5 dB for the entire tuning range.

2.2.2 Bandwidth Tunable Filters

Unlike the tunability of the center frequency, little effort has been made with regards to the bandwidth tunability of filters. One probable reason for this lack of research interest is that, in the design steps of a microwave filter, bandwidth is taken into consideration in the designing of coupling elements. However, methods for varying the inter-resonator couplings are currently inadequate. Thus,

proposed solutions in the past have focused primarily on providing discrete bandwidth tuning while keeping the center frequency fixed [20, 21].

One of the main applications of tunable-bandwidth microwave filters is the design of high-frequency multifunction receivers that can simultaneously support multiple data signals at different power levels and frequency bands. As mentioned earlier, tuning the bandwidth is usually achieved by adjusting the filter's internal inter-resonator coupling. This can be implemented by discrete diode-varactors, switches [22, 23, 24, 12], or MEMS-cantilevers [25, 26, 27]. In this section, a few examples of each of these methods are provided and explained.

Sanchez-Renedo et al. presented a new combline filter structure with continuous tunabilty for both bandwidth and center frequency. They achieved the tunability of the bandwidth (passband width) by placing a variable coupling reducer between the resonators to control filter coupling. Variable coupling reducers are designed as detuned resonators, which are comprised of a line segment ending in a variable capacitor. Figure 2-1 shows the layout of the tunable filter prototype [22].

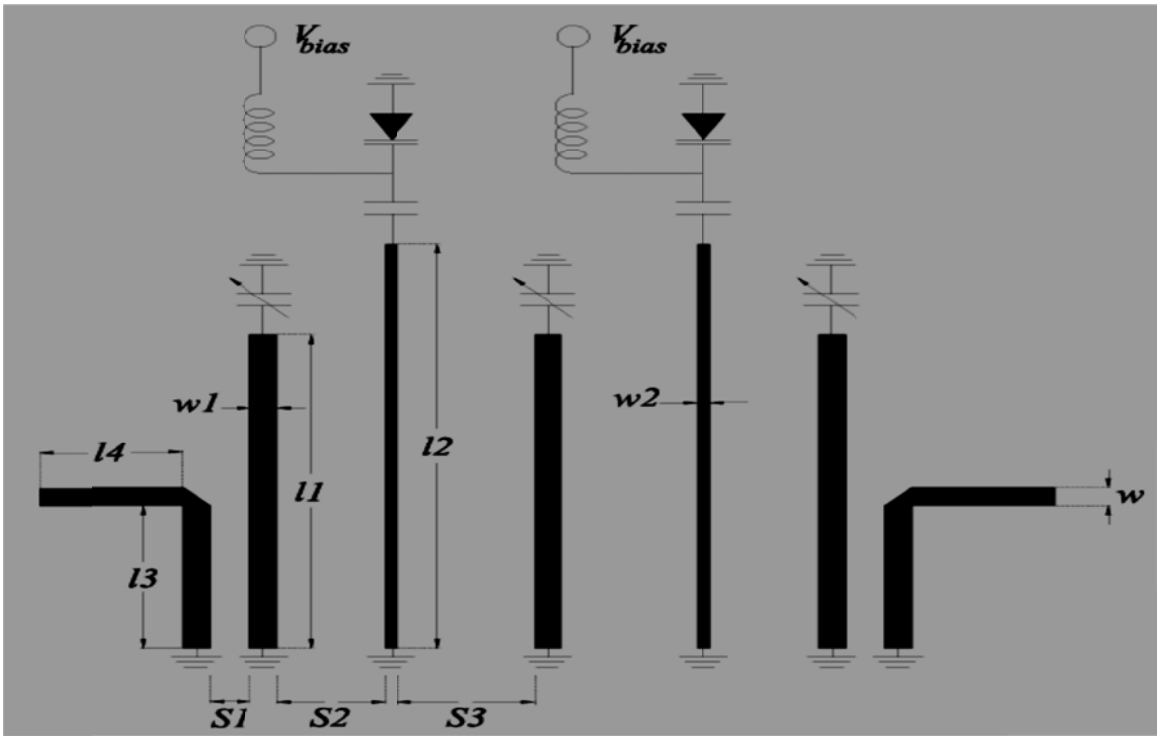

Figure 2-1: Layout of the tunable filter prototype [22]

The proposed structure in [22] is experimentally validated with the design and construction in suspended stripline technology. The characterization of the constructed filter is a cost-effective filter prototype for terrestrial digital video broadcasting receiver, simultaneously handling analog and digital TV channels in the UHF band (470-862 MHz). Figure 2-2 shows the constructed tunable filter prototype.

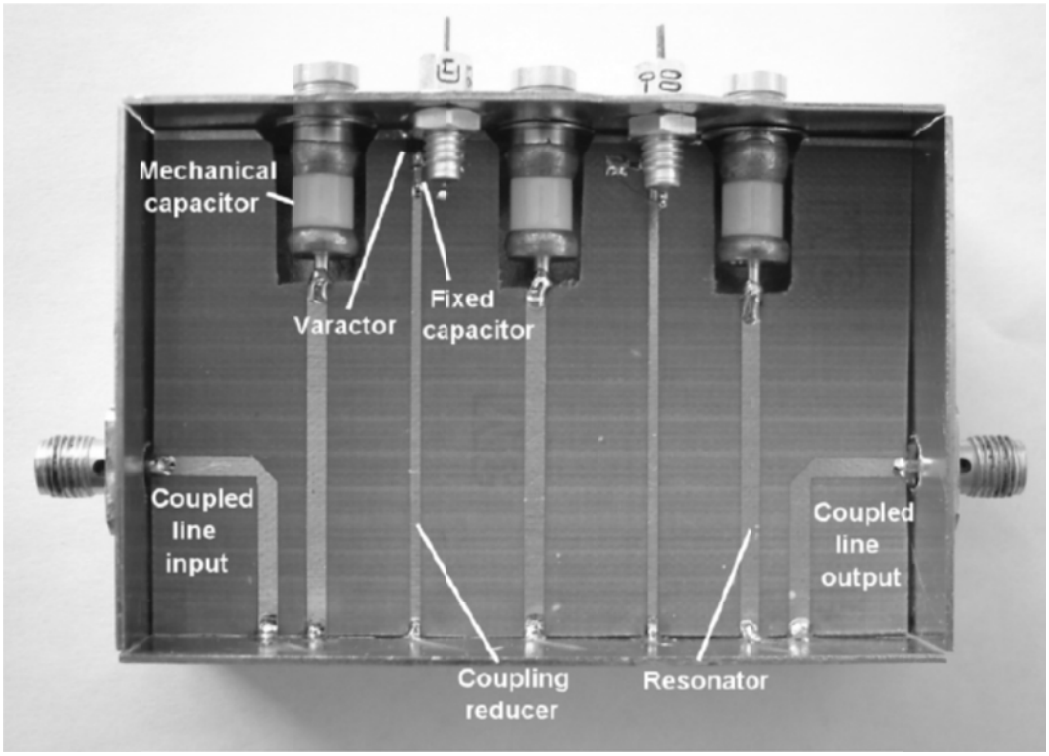

Figure 2-2: Constructed tunable filter prototype [22]

Kawai et al. demonstrated a digital tunable pass-band filter that controls bandwidth and center frequency individually [23]. Tunability is achieved by using tunable J-inverters and tunable $\lambda/4$ -length resonators. The tunable J-inverter consists of a microstrip gap with multiple switches, metal bars and metal islands in the gap. The applied tunable resonator comprises a transmission line with a comb-shaped pattern on both sides of the transmission line. There are multiple switches on the surface of the teeth of the comb-shaped pattern. The tuning ratios of the measured bandwidth and center frequency of the fabricated prototype filter are 2.67 and 1.14, respectively [23]. Figure 2-3 shows a schematic and fabricated prototype filter.

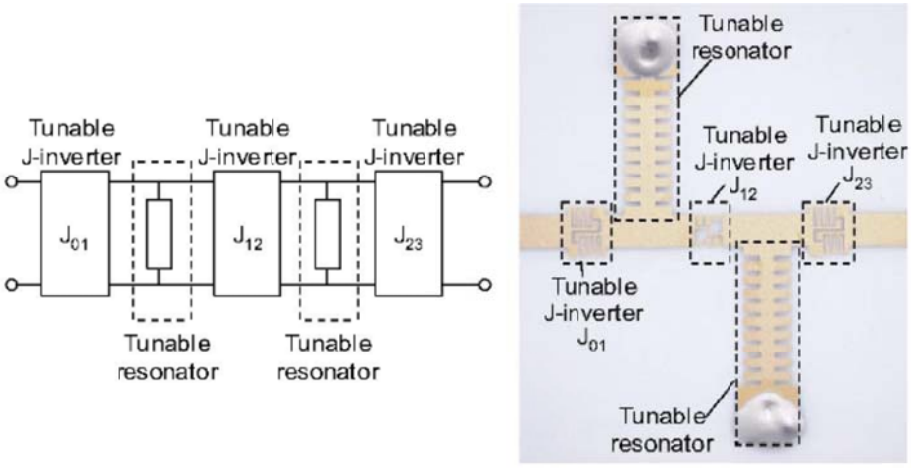

Figure 2-3: Schematic and fabricated prototype filter in [23]

The fabricated tunable resonator and tunable J-inverter of the proposed structure in [23] is provided in Figures 2-4 (a) and (b), respectively. The resonant frequency of the resonator can be changed discretely by controlling the status of the switches. Here, the function of the J-inverter will be the same as a varactor in which the capacitor discretely changes.

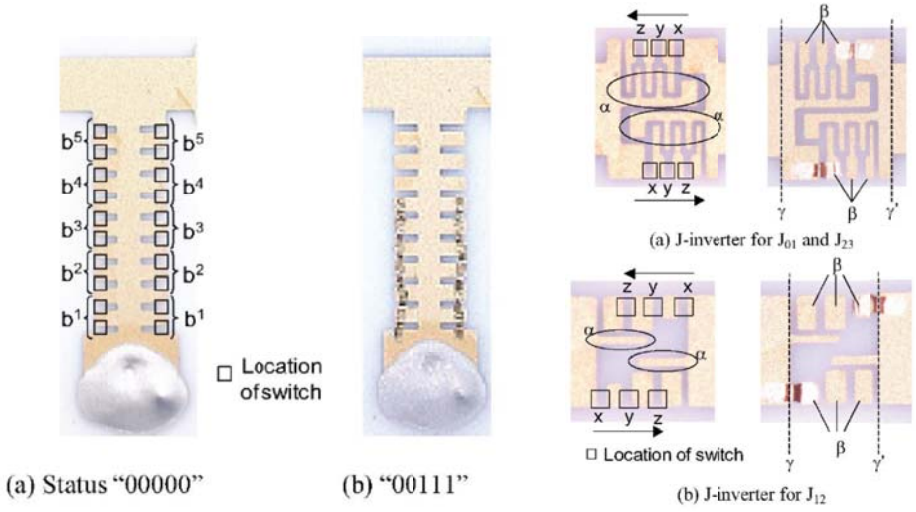

Figure 2-4: (a) Fabricated tunable resonator in [23]; (b) **F**abricated tunable J-inverters in [23]

Park et al. demonstrated varactor-diode 2-pole tunable filters with three different fractional-bandwidth characteristics [12]. The tunable resonator model they used is shown in Figure 2-5 (a). By employing this model, both the coupling and the resonance frequency of each resonator can be tuned. The full-wave simulation model for the tunable filter is shown in Figure 2-5 (b).

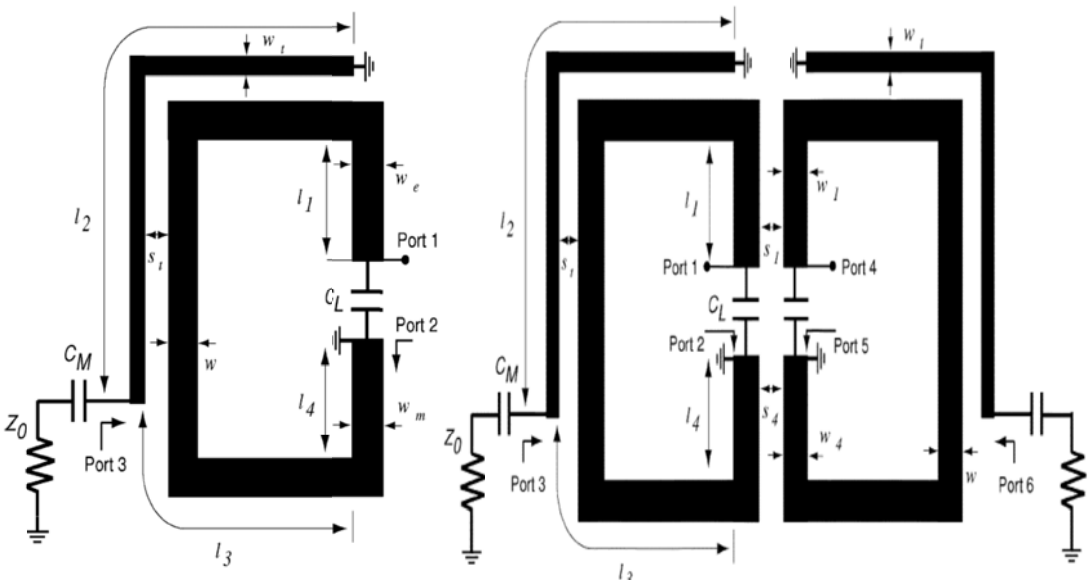

Figure 2-5: (a) Full-wave simulation model for a tunable resonator; (b) full-wave simulation model for a tunable filter [12]

Three different filters were constructed by employing Schottky varactor diodes with a tuning range from 850 MHz to 1400 MHz. The first filter, a constant fractional-bandwidth filter, shows a 1-dB bandwidth of 5.4% $\pm$ 0.3% with an insertion loss of 2.88 - 1.04 dB. The second filter, a constant absolute-bandwidth filter, has a 1-dB bandwidth decrease from 5.2% to 2.9% and an insertion loss of 2.89 – 1.93 dB. The last filter, an increasing fractional bandwidth filter, has a 1-dB bandwidth increase from 4.3% to 6.5% and an insertion loss of 3.47-1.18 dB. The fabricated filter for the third proposed structure (the increasing fractional-bandwidth one) is provided in Figure 2-6 [12]. The problem with this structure is that it cannot be extended to a higher order tunable filter in planar technology.

Palego et al. demonstrated a 2-pole lumped-element programmable filter with bandwidth and center frequency tuning [28]. This filter is built on alumina substrate and employs five 3-bit capacitor banks controlled with MEMS ohmic switches. The filter has 12 states with a 37.5% tuning range between 1.51 GHz to 2.26 GHz and an insertion loss of 2.9-5.9 dB. Because of the lumped-element components used in the inter-resonator coupling structure, the filter suffers from poor selectivity and high insertion loss. Figure 2-7 shows a microphotograph of the fabricated filter.

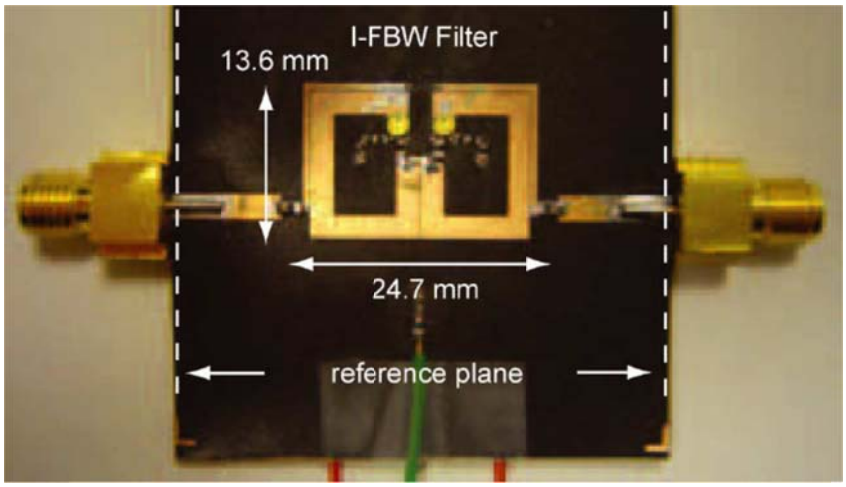

Figure 2-6: Fabricated increasing fractional-bandwidth filter [12]

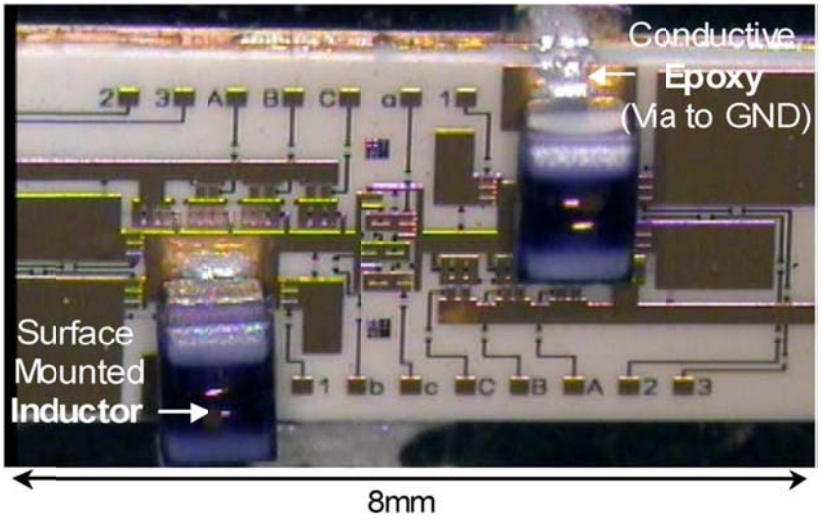

Figure 2-7: Microphotograph of the fabricated filter in [28]

Joshi et al. demonstrated a fully reconfigurable high-quality factor (Q) tunable band-pass filter [29]. They proposed a design technique that enables controlling the external coupling and inter-resonator by employing low Q varactors. The bandwidth is controlled to be constant, while the tuning range of the filter is from 0.8 GHz to 1.43 GHz, with an insertion loss of 1.6 dB to 3.1 dB. However, as with most microstrip combline filters, this filter has an asymmetric transmission response and poor selectivity in the lower band due to having the transmission zeros in the higher stop-band [24]. Figure 2-8 shows the layout of the proposed filter in [29].

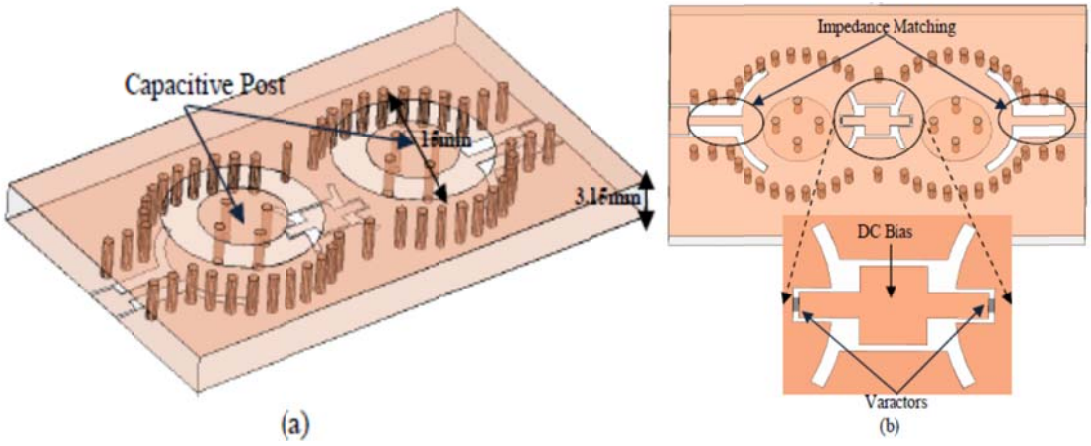

Figure 2-8: Filter layout (a) top side having the capacitive posts and (b) bottom side having the feed-lines with the tunable bandwidth section [29]

Hsu et al. recently demonstrated an RF-MEMS structure for bandwidth tuning by employing a movable nickel electrode to implement tunable broad-side coupling [30]. To avoid performance degradation, high resistivity-SiCr is used in the fabrication of the bottom electrode. The tunable coupling structure is realized in a planar MEMS tunable filter that comprises $\lambda/2$ coplanar waveguide (CPW) resonators and nickel RF-MEMS varactors. The tunability of the center frequency is from 28.55 GHz to 27.22 GHz, and the bandwidth is tunable and can be increased by 5%. The measured insertion loss of this filter is about 9.4 dB. This value is higher than typical values for the insertion loss of planar tunable filters due to the moderate Q of tunable resonators [30]. The schematic of the RF-MEMS tunable coupling structure of this filter is shown in Figure 2-9.

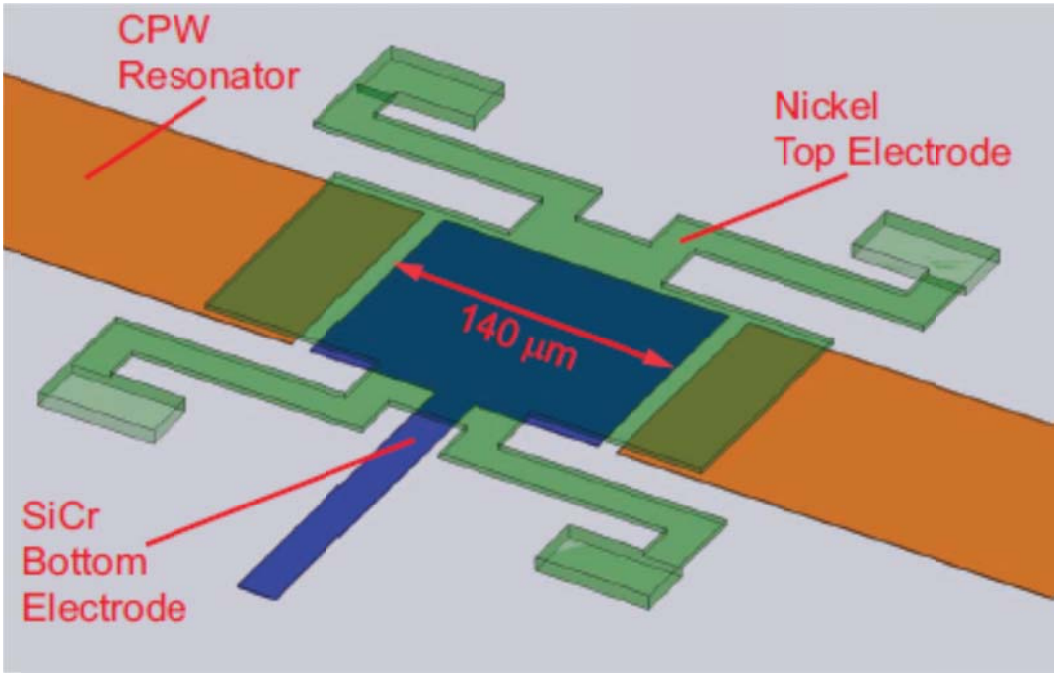

Figure 2-9: Schematic of an RF-MEMS tunable coupling structure whose bottom electrode is made of high resistivity SiCr [30]

Chiou et al. demonstrated a center frequency and bandwidth tunable 3-pole combline bandpass filter with transmission zero control [31]. To achieve center frequency tunability, the filter comprises three straight short-ended resonators with varactor diodes (D_1). For bandwidth control, two pairs of diodes (D_2) are located between two adjacent resonators. To resolve the common problems arising from microstrip combline filters, and having no transmission zero in the lower band, two diodes (D_3) are placed at the input and output matching networks. The task of these diodes is to generate additional tunable zero in the lower band. The schematic of the 3-pole combline filter is shown in Figure 2-10 [31].

The center frequency range of the fabricated filter is from 1.5 GHz to 2.2 GHz, while the 1-dB bandwidth is tunable from 50 MHz to 170 MHz (2.2% to 11.2 % fractional bandwidth). A photograph of the fabricated bandpass tunable filter is shown in Figure 2-11 [31].

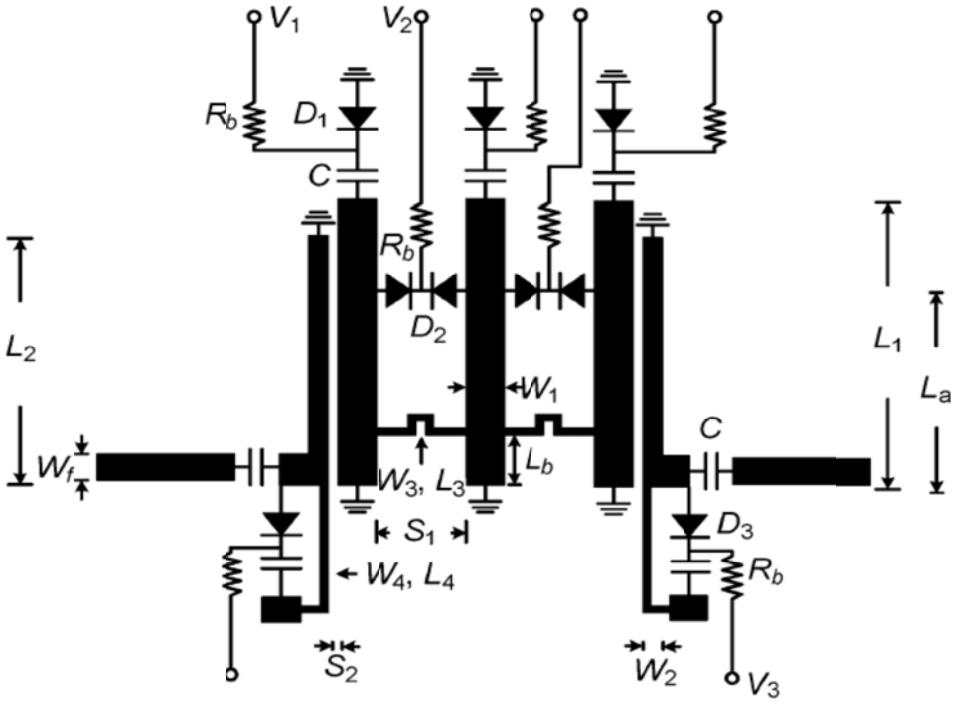

Figure 2-10: Schematic of the proposed combline center frequency and BW tunable filter in [31]

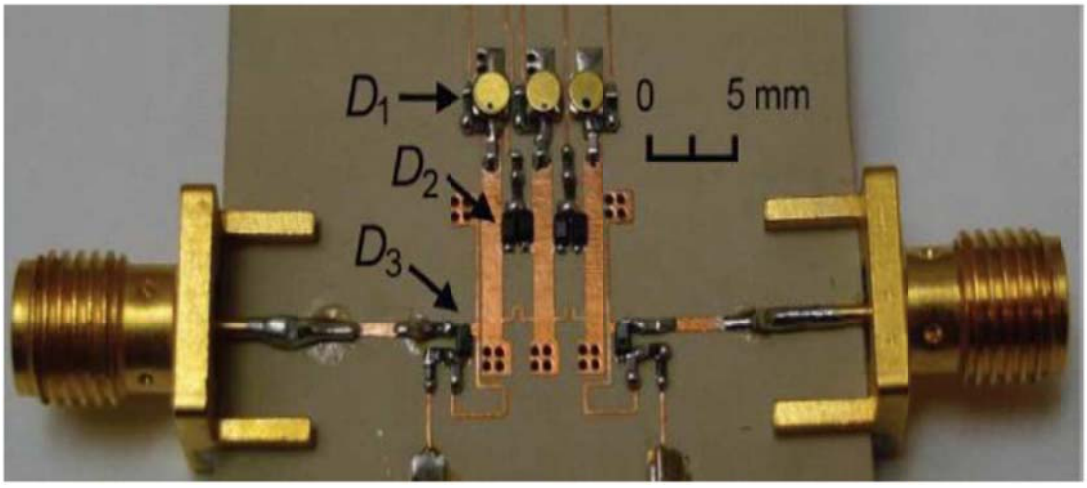

Figure 2-11: Photograph of the center frequency and bandwidth tunable bandpass filter in [31]

2.3 Fundamentals and Design Steps of a Microstrip Filter

2.3.1 Microstrip Transmission Line

A microstrip transmission line is a type of electrical transmission line that consists of a conducting strip suspended above a ground plane by a dielectric layer called a substrate. The dielectric constant of the substrate (ε_r), width of the strip (w), thickness of the substrate (d) and thickness of the strip (t) can change the characteristic impedance of a microstrip line. Figure 2-12 shows a microstrip transmission line.

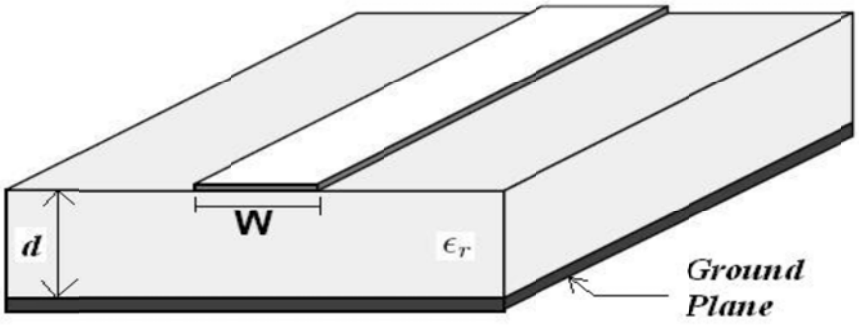

Figure 2-12: Microstrip transmission line [32]

2.3.2 Design Steps of a Chebyshev Bandpass Microstrip Filter

The design steps of a Chebyshev band-pass microstrip filter, when the equal ripple value and number of poles are given, are provided in [33].

Step 1: Finding the element values (g-values) for equal-ripple low-pass filter prototypes based on number of poles and the value of the equal ripple is outlined as follows.

Suppose that we show the ripple level in a passband with LR and a filter order with n. The g-values of this filter can be calculated as following [33]:

$$g_0 = 1 \tag{2-1}$$

$$\beta = \ln\left(\coth\left(\frac{LR}{17.37}\right)\right) \tag{2-2}$$

$$\gamma = \sinh(\frac{\beta}{2n}) \tag{2-3}$$

$$a_k = \sin\left(\frac{(2k-1)\pi}{2n}\right), \qquad k = 1,2,\dots,n \tag{2-4}$$

$$b_k = \gamma^{\,2} + \sin^2\left(\frac{k\pi}{n}\right), \qquad k = 1,2,\dots,n \tag{2-5}$$

$$g_1 = \frac{2a_1}{\gamma} \tag{2-6}$$

$$g_k = \frac{4a_{k-1}a_k}{b_{k-1}g_{k-1}}, \qquad k = 2,3,\dots,n \tag{2-7}$$

$$g_{n+1} = \begin{cases} 1 & n\ odd \\ coth^2\left(\frac{\beta}{4}\right) & n\ even \end{cases} \tag{2-8}$$

Step 2: Finding J values for J-admittance inverters based on g values from Step 1 and percentage bandwidth (Δ)

J values can be calculated with the following formulas [33]. Figure 2-13 shows a bandpass filter with J-admittance inverters.

$$\frac{J_{01}}{Y_0} = \sqrt{\frac{\pi\Delta}{2g_0g_1}} \tag{2-9}$$

$$\frac{J_{k,k+1}}{Y_0} = \frac{\pi\Delta}{2\sqrt{g_kg_{k+1}}} \qquad k = 1,2,\dots,n-1 \tag{2-10}$$

$$\frac{J_{N,N+1}}{Y_0} = \sqrt{\frac{\pi\Delta}{2g_Ng_{N+1}}} \tag{2-11}$$

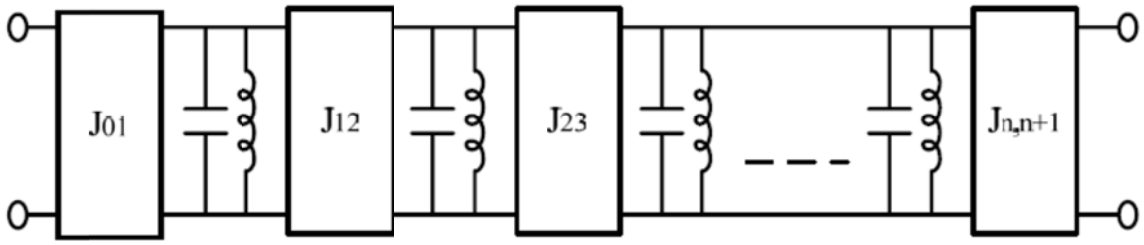

Figure 2-13: A bandpass filter with J-admittance inverters

Step 3: Designing inverters with desired values of J, calculated in Step 2 by using microstrip gaps

An admittance inverter is shown in Figure 2-14. The value of J varies in different admittance inverters.

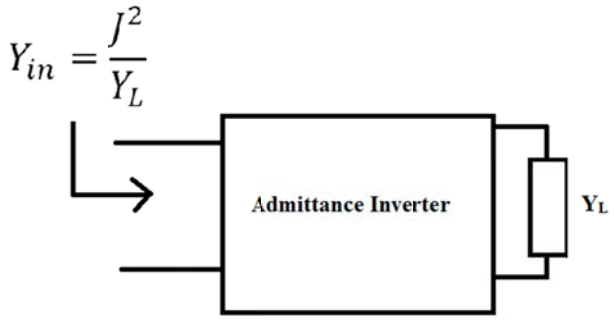

Figure 2-14: Admittance inverter

There are numerous ways to implement an admittance inverter. Two equivalent circuits, one with capacitors and the other with inductors, are shown in Figures 2.15(a) and 2.15(b), respectively.

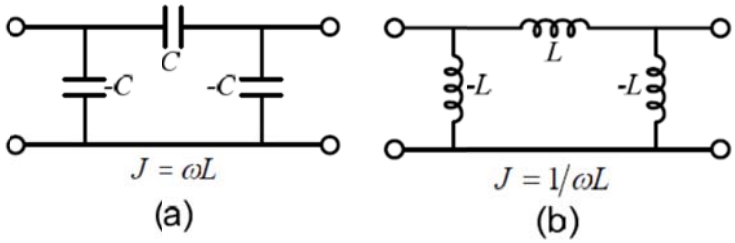

Figure 2-15: Equivalent circuits and J values for an admittance inverter with (a) capacitors and (b) inductors

As shown in Figure 2-16, it is possible to model a microstrip gap in a circuit with three capacitors [33].

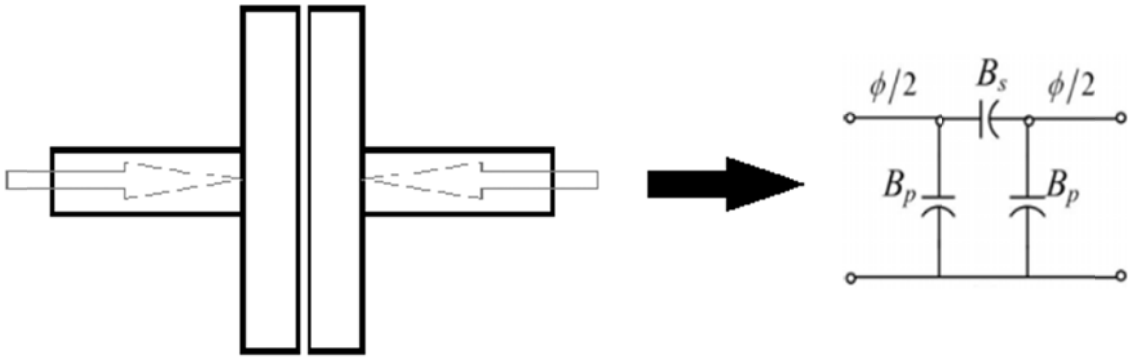

Figure 2-16: Modeling a microstrip gap with three capacitors

The equivalent circuit for a microstrip gap is shown in Figure 2-17. The only differences between this model and the circuit of Figure 2-15(a) are the two transmission lines on both sides of the admittance inverter. Hence, in modeling a complete inverter, and other than the gap, we need two specified length of transmission lines on both sides of the gap.

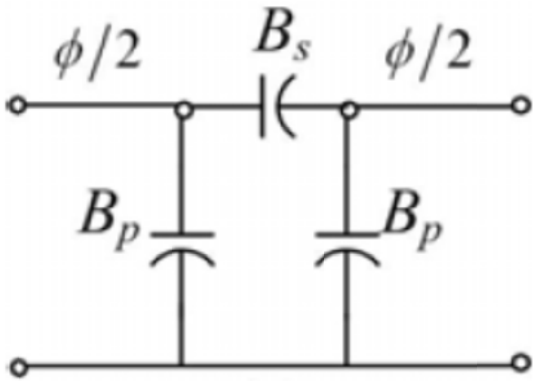

Figure 2-17: Equivalent circuit for admittance inverter

The desire values for J of the inverters are calculated in Step 2. Now we need find a method for calculating the J values of the microstrip gaps, after which we can change the parameters of the gap (for example, D, L and W in Figure 2-18) until we generate the same J values as Step 2.

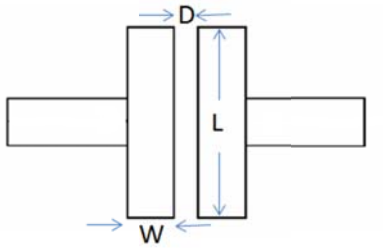

Figure 2-18: Different parameters of a microstrip gap

The J value of the circuit in Figure 2-41 can be calculated from the following formulas:

$$\frac{J}{Y_0} = \left|\tan\left(\frac{\phi}{2} + arctan\frac{B_p}{Y_0}\right)\right| \tag{2-12}$$

$$\phi = -\arctan\left(2\frac{B_s}{Y_0} + \frac{B_p}{Y_0}\right) - arctan\frac{B_p}{Y_0} \tag{2-13}$$

where the values of B_s and B_p are derived from the S parameters, as in the following:

$$\frac{B_p}{Y_0} = \frac{1 - S_{12} - S_{11}}{1 + S_{11} + S_{12}} \tag{2-14}$$

$$\frac{B_s}{Y_0} = \frac{2S_{12}}{(1 + S_{11})^2 - {S_{12}}^2} \tag{2-15}$$

Step 4: Finding the length of resonators based on the center frequency, the microstrip line specifications, and the ϕ of inverters

Figure 2-19 shows a microstrip filter with gaps as inverters and microstrip transmission lines as resonators. For a transmission line to resonate, its length should be:

$$L_{resonate} = k\frac{\lambda_g}{2} \qquad k = 1,2,\ldots \tag{2-16}$$

where λ_g is the effective wavelength of the transmission line. In the case of microstrip lines, λ_g can be calculated as follows:

$$\lambda_g = \frac{\lambda_0}{\sqrt{\varepsilon_{eff}}} \tag{2-17}$$

Figure 2-19: A microstrip filter

However, we cannot use the length of $\frac{\lambda_g}{2}$ for all resonators, as we need to add a specific length to each transmission line in order to complete the admittance inverters. After completing Step 3, we have n+1 (from $J_{0,1}$ to $J_{n,n+1}$) admittance inverters, generated by microstrip gaps, and also n+1 phases (ϕ) for each inverter (referring to the relevant formula). As shown in Figure 2-17, we need to add the phase of $\phi/2$ on each side of each gap to the transmission lines. For a transmission line to have a phase of $\phi/2$, its length should be:

$$L_{phase=\phi/2} = \frac{\lambda_{g0}}{2\pi} \times \frac{\phi}{2} \tag{2-18}$$

This means that the length of the transmission line (between the gaps) number k should be sum of the length needed for the resonance (refer to formula) and two lengths for the phases of two inverters on each side of the resonator (refer to formula). The formula for the length of each transmission line is as follows:

$$L_k = \frac{\lambda_{g0}}{2\pi}\left(\pi + \frac{1}{2}(\phi_{k-1} + \phi_k)\right) \qquad k = 1,2,\dots,n \tag{2-19}$$

After finishing this step, all of the elements of the microstrip filter are determined and the filter is complete.

2.4 Post-Production Tuning

Nowadays, a filter designer can accurately model and simulate a microwave filter with commercially available software such as HFSS, ADS [34] and Sonnet [35]. Nevertheless, after the fabrication, the experimental response can differ from the simulation results for any number of reasons, including inaccuracies in the material properties or fabrication process. As a result, post-production tuning is usually necessary.

One of the most popular ways of tuning an as-made filter is employing mechanical tuning screws. These screws enable adjustment of the center frequency of resonators and/or coupling between them. Despite their popularity, tuning screws have many disadvantages. For instance, in compact circuit design, due to the relatively small maximum size of tuning screws, the possible tuning range is limited [36]. Also, for detuned filters with a deviated center frequency of 5% or more, tuning screws alone usually cannot compensate for the difference and hence a new fabrication is required [37].

Harscher et al. proposed and demonstrated an automated filter tuning method for microwave filters [38]. Their method comprises two steps. The first step is determining the sensitivity of different parameters relating to the tuning elements by performing a number of S-parameters measurements. In the second step, the filter's measured parameters are compared to the corresponding parameters of an ideal filter, from which optimal screw positions can be determined. The measured response of the filter before and after tuning is provided in Figures 2-20 (a) and (b).

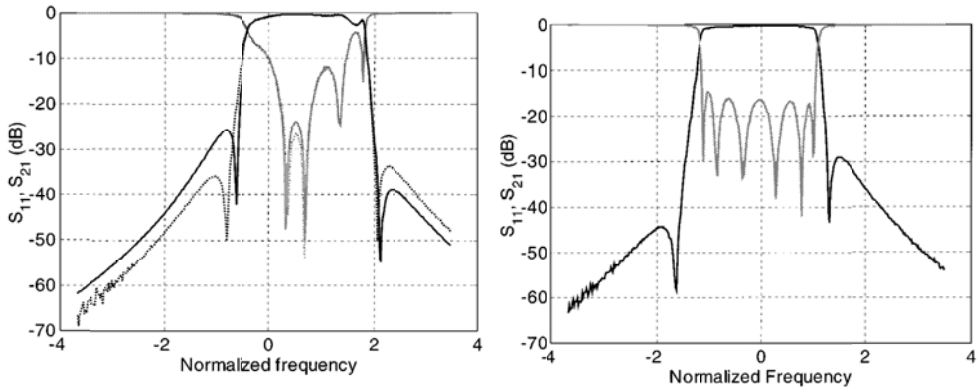

Figure 2-20: Measured response of a filter used in [38] before, left, and after, right, tuning [38]

In [39], Hsu et al. presented a model for calculating the inter-resonator couplings and resonant frequencies of each individual resonator and then developed a deterministic finite step-tuning algorithm based on the model. They have also employed this model in the automated tuning of a 5-pole combline Chebyshev filter.

Miraftab et al. employed fuzzy logic to introduce an algorithm for tuning microwave filters [2]. They extracted fuzzy rules from the sampled data and successfully applied their algorithm to tune an 8-pole elliptic filter and a 4-pole Chebyshev filter. Further efforts to apply curve-fitting software to extract the coupling matrix of a fabricated filter were made by Pepe et al. in [40].

A different and interesting approach for tuning a microwave filter is presented in [41]. The main concept of this research is overlaying thin dielectric materials over the surface of the circuit to decrease center frequency. However, along with the disability of increasing center frequency, this method suffers from additional losses caused by the overlaid material.

Parker et al. suggested the use of laser trimming for tuning superconducting microwave filters as a novel method in [42]. This method requires expensive equipment and is irreversible. Zuo et al., in [43], proposed tuning HTS filters by developing a computer-aided method of tuning through optimization and neural networks. This technique identifies the detuning of individual resonators quantitatively during the tuning step and determines the required tuning of the correspondence tuning screw by employing neural network models. Figures 2-21 and 2-22 show the S parameters of the filter before and after the tuning process, respectively.

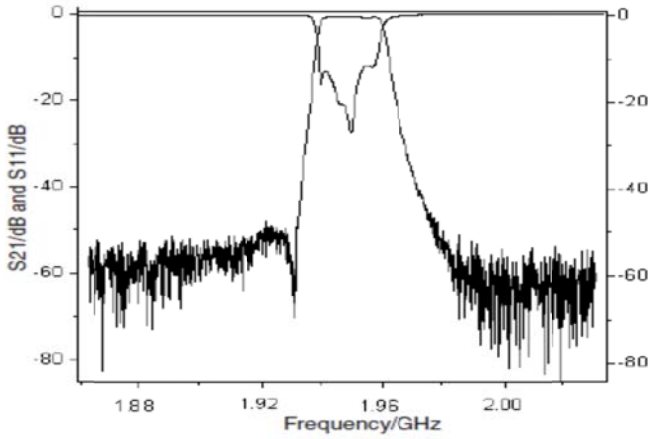

Figure 2-21: Response of an HST filter used in [43] before tuning

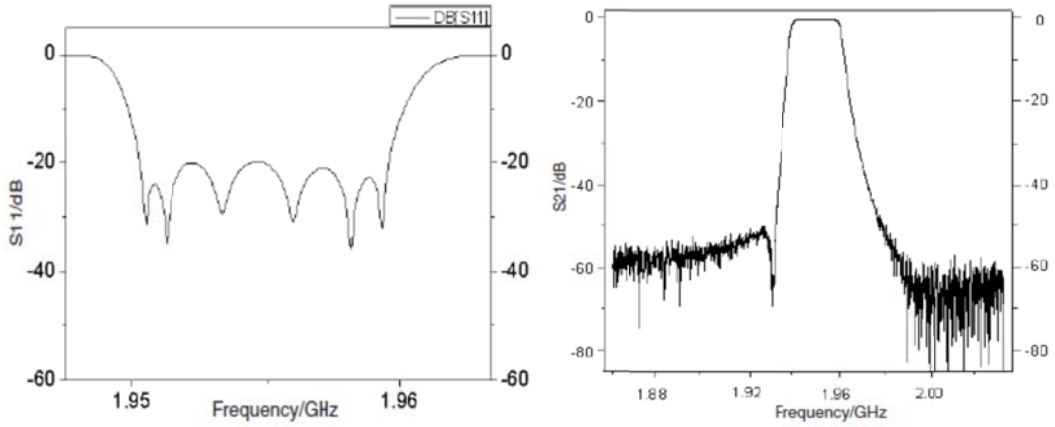

Figure 2-22: Response of an HST filter used in [43] after tuning

Chapter 3
Post-Fabrication Tuning of Microwave Filters

3.1 Introduction

Controlling a tunable Chebyshev filter is usually realized by adding a number of elements to tune the frequency and/or control the couplings between resonators. Some of the most common tuning elements are tuning screws, MEMS switches, and semiconductor varactors. The task of each tuning element can be one the following: tuning the center frequency of one or more resonator; controlling the coupling between two adjacent resonators; or adjusting the input and output couplings. The complexity of tuning microwave filter stems from the interaction between the resonance frequencies of resonators and the coupling between them. In other words, tuning one parameter without affecting the value of other parameters is virtually impossible.

One of the most important steps in manufacturing commercial microwave filters is post-production tuning. This step requires the skill of experts and consequently significantly affects the final cost of the filter. There are number of different tuning techniques for reducing the complexity of filter tuning such as time domain, group delay, and fuzzy logic methods [1, 2, 3]. The base parameters in implementing these methods are the phase and magnitude of the filter's reflection coefficient.

Meng et al. proposed an analytical approach to extract the coupling matrix of a bandpass Chebyshev filter and utilized it for computer-aided tuning of bandpass microwave filters [44]. This parameter extraction relies on pole and zero identification of the transfer function and, as a result, requires a VNA for the measurement. Prior to [44], two similar approaches for computer-aided tuning of a microwave filter based on coupling matrix extraction and use of VNA were published in [39, 45].

In this chapter, a novel idea for the post production tuning of microwave filters is presented. This method relies on adding a passive microwave circuit parallel to the original filter by creating a path between the input and the output. The structure of an added circuit can be determined by calculating the difference between the Y parameters of a detuned and an ideal filter (ΔY). Since creating the exact shape of ΔY may be complicated, an approximation model is used as the added circuit. The idea is demonstrated by tuning a detuned cavity filter and a detuned microstrip filter, with the experimental results being provided at the end of this chapter.

Chapter 3 is organized as follows. In section 3.2, the idea is explained and circuit implementation for tuning a Chebyshev filter with high insertion loss in the passband is presented. In section 3.3, we use the stated method to tune several detuned filters. Finally, the EM simulation and experimental results are provided in sections 3.4 and 3.5, respectively.

3.2 Theory

A Chebyshev bandpass filter can be specified by the number of poles, ripple level (or, alternatively, the return loss), center frequency, and bandwidth. The limited quality factor (Q) of the resonators, i.e., having a non-ideal Chebyshev filter, has a considerable influence on the final shape of the S parameters [46]. On average, achieving a return loss less than -20 dB is considered a success in filter manufacturing.

In this section, the theory behind the tuning method will be explained. The goal of this section is decreasing the ripple level of a Chebyshev filter in the bandpass by adding a simple passive circuit parallel to the filter. Henceforth in this dissertation, this parallel circuit will be called the auxiliary circuit. The bandwidth of the filter will show only a slight decrease during this process. The design steps of the auxiliary circuit are also provided in this section.

3.2.1 Pole Matching of Admittance Parameters

An in-line ideal Chebyshev filter can be determined by number of poles, ripple level, center frequency, and bandwidth. As will be explained in this section, if all of these parameters (except the ripple level) are similar for two Chebyshev filters, the location of their admittance parameters poles will be different. When designing a proper auxiliary circuit, these poles need to be exactly matched.

The g-values of a filter, regardless of its center frequency and bandwidth, can be calculated by the given formulas in Chapter 2 (2-1 to 2-8). Having calculated the g-values, the coupling matrix can then be calculated as shown in expression (3-1) [33]. Two other necessary parameters for determining the filter response are input and output resistance (R_S and R_L, respectively). If n is the degree of the filter, the value of the input and output resonators can be calculated as follows:

$$M = \begin{bmatrix} 0 & \frac{1}{\sqrt{g_1 g_2}} & 0 & 0 & \cdots & 0 \\ \frac{1}{\sqrt{g_1 g_2}} & 0 & \frac{1}{\sqrt{g_2 g_3}} & 0 & \cdots & 0 \\ 0 & \frac{1}{\sqrt{g_2 g_3}} & 0 & \ddots & \cdots & 0 \\ 0 & 0 & \ddots & \ddots & \frac{1}{\sqrt{g_{n-2} g_{n-1}}} & 0 \\ \vdots & \vdots & \vdots & \frac{1}{\sqrt{g_{n-2} g_{n-1}}} & 0 & \frac{1}{\sqrt{g_{n-1} g_n}} \\ 0 & 0 & 0 & 0 & \frac{1}{\sqrt{g_{n-1} g_n}} & 0 \end{bmatrix} \quad (3\text{-}1)$$

$$R_s = \frac{1}{g_1} \quad (3\text{-}2)$$

$$R_L = \frac{1}{g_n g_{n+1}} \quad (3\text{-}3)$$

Another matrix needs to be defined for the calculation of S parameters. This matrix is called R and can be calculated as follows:

$$R\ Matrix = \begin{bmatrix} R_s & 0 & 0 & \cdots & 0 \\ 0 & 0 & 0 & \cdots & 0 \\ 0 & 0 & \ddots & \cdots & 0 \\ \vdots & \vdots & \vdots & \ddots & 0 \\ 0 & 0 & 0 & 0 & R_L \end{bmatrix} \quad (3\text{-}4)$$

The S parameters of a microwave band-pass filter can be easily calculated using the following equations [33]:

$$\lambda = \frac{f_0}{BW}\left(\frac{f}{f_0} - \frac{f_0}{f}\right) \quad (3\text{-}5)$$

$$\delta = \frac{f_0}{BW.Q_u} \quad (3\text{-}6)$$

$$(Effect\ of\ adding\ losses) \qquad \lambda \to \lambda - j\delta$$

$$A = \lambda I - jR + M \quad (3\text{-}7)$$

$$S_{11} = 1 + 2jR_s[A^{-1}]_{11} \tag{3-8}$$

$$S_{21} = -2j\sqrt{R_s R_L}[A^{-1}]_{n1} \tag{3-9}$$

where f_0 is the center frequency, BW is the bandwidth, and Q_u is the unloaded quality factor. The effect of losses in resonators is taken into consideration as the value of δ. In the case of an ideal filter with an infinite quality factor, δ is equal to zero.

The admittance parameters of a Chebyshev filter have different poles from the scattering matrix parameters. The Y parameter matrix can be expressed as follows [47]:

$$Y = (M - \lambda I - jR)^{-1} \tag{3-10}$$

The input admittance, y_{11}, can be calculated as follows:

$$y_{11}(\lambda) = (-\lambda I + M)^{-1}{}_{11} = \frac{|-\lambda I + M_{n-1}|}{|-\lambda I + M|} \tag{3-11}$$

where M_{n-1} is the coupling matrix after the elimination of the first row and first column. In the case of an in-line 3-pole Chebyshev filter, the poles of admittance parameters can be determined by calculating the denominator of y_{11} in the above equation.

$$\det(-\lambda I + M) = \det\left(\begin{bmatrix} -\lambda & \frac{1}{\sqrt{g_1 g_2}} & 0 \\ \frac{1}{\sqrt{g_1 g_2}} & -\lambda & \frac{1}{\sqrt{g_2 g_3}} \\ 0 & \frac{1}{\sqrt{g_2 g_3}} & -\lambda \end{bmatrix}\right)$$

$$= -\lambda\left(\lambda^2 - \frac{1}{g_2 g_3}\right) - \frac{1}{\sqrt{g_1 g_2}}\left(\frac{-\lambda}{\sqrt{g_1 g_2}}\right) \xrightarrow{\frac{1}{\sqrt{g_1 g_2}} = \frac{1}{\sqrt{g_2 g_3}}}$$

$$\det(-\lambda I + M) = -\lambda\left(\lambda^2 - \frac{2}{g_1 g_2}\right) \tag{3-12}$$

Thus, the location of the three poles can be calculated by equating the above equation to zero.

$$-\lambda\left(\lambda^2-\frac{2}{g_1g_2}\right)=0\Rightarrow Poles:\begin{cases}\lambda=0\\ \lambda=\sqrt{\dfrac{2}{g_1g_2}}\\ \lambda=-\sqrt{\dfrac{2}{g_1g_2}}\end{cases} \tag{3-13}$$

Since λ is equal to $\frac{f_0}{BW}\left(\frac{f}{f_0}-\frac{f_0}{f}\right)$, the location of the poles on the frequency axis, f_1, f_2 and f_3, can be calculated as follows:

$$\lambda=0\Rightarrow\frac{f_0}{BW}\left(\frac{f}{f_0}-\frac{f_0}{f}\right)=0\Rightarrow f_1=f_0 \tag{3-14}$$

$$\lambda=\sqrt{\frac{2}{g_1g_2}}\Rightarrow\frac{f_0}{BW}\left(\frac{f}{f_0}-\frac{f_0}{f}\right)=\sqrt{\frac{2}{g_1g_2}}\Rightarrow f^2-\left(BW\sqrt{\frac{2}{g_1g_2}}\right)f-{f_0}^2=0\Rightarrow$$

$$f_2=\frac{BW\sqrt{\dfrac{2}{g_1g_2}}+\sqrt{4{f_0}^2+\dfrac{2BW^2}{g_1g_2}}}{2}\xrightarrow{for\ narrow-band\ filters\ \frac{2BW^2}{g_1g_2}\ll 4{f_0}^2}$$

$$f_2=f_0+\frac{BW}{2}\sqrt{\frac{2}{g_1g_2}} \tag{3-15}$$

$$\lambda=-\sqrt{\frac{2}{g_1g_2}}\Rightarrow\frac{f_0}{BW}\left(\frac{f}{f_0}-\frac{f_0}{f}\right)=-\sqrt{\frac{2}{g_1g_2}}\Rightarrow f^2+\left(BW\sqrt{\frac{2}{g_1g_2}}\right)f-{f_0}^2=0\Rightarrow$$

$$f_3=\frac{-BW\sqrt{\dfrac{2}{g_1g_2}}+\sqrt{4{f_0}^2+\dfrac{2BW^2}{g_1g_2}}}{2}\xrightarrow{for\ narrow-band\ filters\ \frac{2BW^2}{g_1g_2}\ll 4{f_0}^2}$$

$$f_3=f_0-\frac{BW}{2}\sqrt{\frac{2}{g_1g_2}} \tag{3-16}$$

The above expressions show that the two in-line 3-pole Chebyshev filters, with the same center frequency, have similar poles in the admittance parameters if the value of $(BW/2)\times\sqrt{2/g_1g_2}$ is

equal for both of them. The reduction in the ripple level causes an increase in the elements of the coupling matrix [33]. So, for $(BW/2) \times \sqrt{2/g_1 g_2}$ to remain constant, the bandwidth needs to be reduced.

$$Ripple\ Level\ \downarrow \Rightarrow Coupling\ Matrix\ Elements\ \uparrow \xrightarrow{For\ \frac{BW}{2}\sqrt{\frac{2}{g_1 g_2}}\ to\ remain\ constant} B\downarrow$$

The ratios of this change in the ripple level and the bandwidth are not the same. For example, to decrease the ripple level from 0.1396 dB, which represents a return loss of -15 dB, to 0.0436 dB (i.e., a return loss of -20 dB), the admittance matrix poles will remain constant if the bandwidth decreases to 85.4% of the original bandwidth. This indicates an approximately 70% decrease in ripple level, in the dB scale, results in an approximately 15% decrease in bandwidth.

$$Same\ poles\ of\ admittance\ matrix \begin{cases} ripple\ level = 0.1396\ dB, & Bandwidth = BW \\ ripple\ level = 0.0436\ dB, & Bandwidth = 0.854 * BW \end{cases}$$

3.2.2 Phase Loading Effect Addition

The Y parameters of a two-port circuit can be calculated from S parameters by using the following equations [48].

$$Y_{11} = Y_0 \frac{(1 - S_{11})(1 + S_{22}) + S_{12}S_{21}}{(1 + S_{11})(1 + S_{22}) - S_{12}S_{21}} \tag{3-17}$$

$$Y_{12} = Y_0 \frac{-2S_{12}}{(1 + S_{11})(1 + S_{22}) - S_{12}S_{21}} \tag{3-18}$$

$$Y_{21} = Y_0 \frac{-2S_{21}}{(1 + S_{11})(1 + S_{22}) - S_{12}S_{21}} \tag{3-19}$$

$$Y_{22} = Y_0 \frac{(1 + S_{11})(1 - S_{22}) + S_{12}S_{21}}{(1 + S_{11})(1 + S_{22}) - S_{12}S_{21}} \tag{3-20}$$

Analyzing a filter based on its Y parameters is complicated due to the phase-loading effect, which represents the difference between the reference phase at the input of an ideal coupled resonator filter and the reference phase calculated from the reference plane at the filter input in measurement. In order to accurately compare the Y parameters of two filters, the effect of phase-loading must first be removed. After its removal, the system's poles will emerge at the correct positions on the real

frequency axis [49]. Figure 3-1 shows the Y parameter of the 3-pole Chebyshev filter with and without the phase-loading effect.

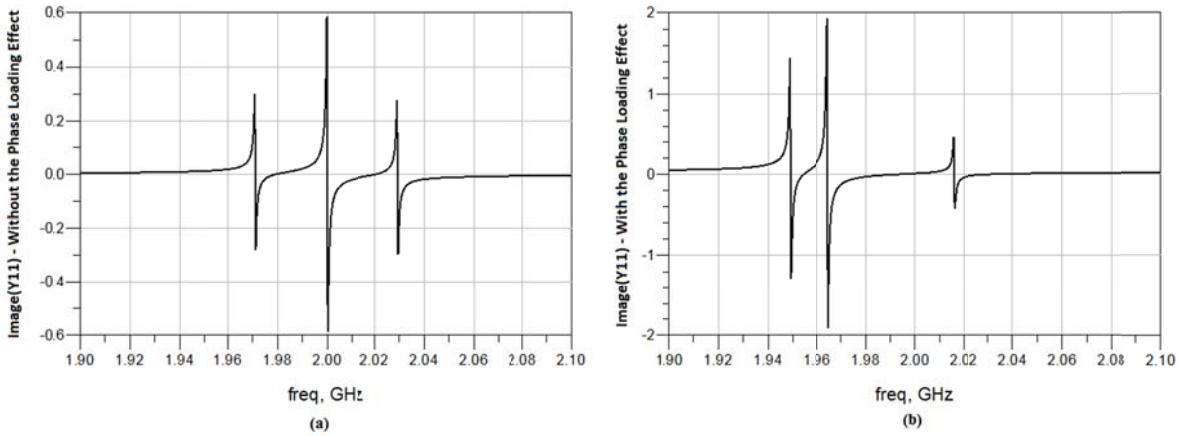

Figure 3-1: Y parameters of a Chebyshev filter (a) without and (b) with the phase loading effect

As depicted in Figure 3-1, the Y11 diagram has three poles equal to the degree of filter. The Y matrix of a filter without the phase-loading effect can be expressed as follows [49]:

$$Y(s) = \begin{bmatrix} y_{11} & y_{12} \\ y_{21} & y_{22} \end{bmatrix} = \sum_{k=1}^{n} \frac{1}{s - j\lambda_k} \begin{bmatrix} r_{11k} & r_{12k} \\ r_{21k} & r_{22k} \end{bmatrix} \tag{3-21}$$

where $\lambda_k (k = 1,2, \dots, n)$ are the poles, placed on the real frequency axis and at their correct positions to the phase-loading effect removal, s is the complex frequency variable, and $r11k, r12k, r21k$ and $r22k$ are the residues of partial expansion fractions.

In the previous section, we presented a method for matching the admittance parameter poles of two Chebyshev filters with different ripple levels. Figure 3-2 shows the difference between the Y_{11} of two 3-pole Chebyshev filters ($Y_{Desired\ Filter} - Y_{Primary\ Filter}$) with the same center frequency of 2 GHz. Here, the phase-loading effect is removed from both filters. The ripple level of the original filter is 0.1396 dB with a fraction bandwidth of 2%. The ripple level of the desired filter is 0.0436 dB. As calculated in the previous section, in order to match the admittance parameters poles of these two filters, the bandwidth of the desired filter is chosen to be 85.4% of the original filter bandwidth.

Figure 3-2 shows that the Y parameter between the two filters has three poles. Although the peak values of this diagram are considerably smaller than the peaks in the Y parameters of the filter (from 0.6 dB to 0.06 dB), the circuit extraction for this behaviour will still be complicated. If the poles could be moved outside the bandwidth or close to the passband edges, the Y parameter difference would be simpler and more easily modeled by a passive circuit. As shown in Figure 3-1(b), the phase loading effect has the ability to move the poles.

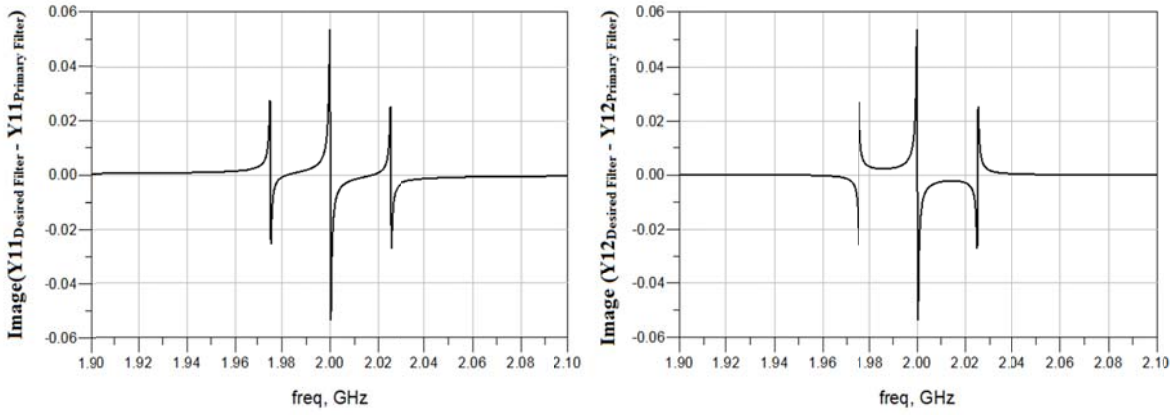

Figure 3-2: Differences between the Y parameters of desired and primary filters

The ABCD matrix of a transmission line with a length of $\lambda/4$ is calculated in [33].

$$ABCD_{\ T.L.with\ the\ length\ of\ \lambda/4} = \begin{bmatrix} 0 & jZ_0 \\ j/Z_0 & 0 \end{bmatrix} \tag{3-22}$$

The ABCD matrix of a primary filter can be calculated from the Y parameters by the following expression:

$$ABCD_{\ Primary\ Filter} = \begin{bmatrix} A_{PF} & B_{PF} \\ C_{PF} & D_{PF} \end{bmatrix} = \begin{bmatrix} -\frac{Y_{22}}{Y_{21}} & -\frac{1}{Y_{21}} \\ -\frac{Y_{11}Y_{22} - Y_{12}Y_{21}}{Y_{21}} & -\frac{Y_{11}}{Y_{21}} \end{bmatrix} \tag{3-23}$$

If the transmission line is located before the input port of a primary filter, as shown in Figure 3-3, the ABCD matrix of the net two pole network can be calculated as follows:

$$ABCD_{Phase-Loaded\ Filter} = ABCD_{T.L.} \times ABCD_{Primary\ Filter} =$$

$$\begin{bmatrix} A_{net} & B_{net} \\ C_{net} & D_{net} \end{bmatrix} = \begin{bmatrix} jZ_0C_{PF} & jZ_0D_{PF} \\ jA_{PF}/Z_0 & jB_{PF}/Z_0 \end{bmatrix} \quad (3\text{-}24)$$

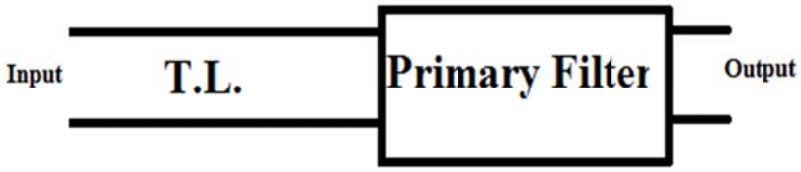

Figure 3-3: Adding the phase-loading to the primary filter

The Y parameters of the net network can be calculated by converting the ABCD matrix to a Y matrix. The calculation of $Y11$ is provided in the following expression:

$$Y_{11\,net} = \frac{D_{net}}{B_{net}} = \frac{B_{PF}}{{Z_0}^2 D_{PF}} = \frac{1}{{Z_0}^2} \times \frac{\frac{1}{Y_{21}}}{\frac{Y_{11}}{Y_{21}}} = \frac{1}{{Z_0}^2} \times \frac{1}{Y_{11}} \quad (3\text{-}25)$$

This means that the zeros in the primary filter's Y11 will be the new poles of the net circuit. As mentioned in expression (3-11), the numerator of Y11 is $|-\lambda I + M_{n-1}|$. Therefore, the poles of the net circuit can be calculated by finding the roots of this expression.

$$|-\lambda I + M_{n-1}| = 0 \Rightarrow \lambda^2 - \frac{1}{g_1 g_2} = 0 \Rightarrow Poles: \begin{cases} \lambda = \sqrt{\frac{1}{g_1 g_2}} \\ \lambda = -\sqrt{\frac{1}{g_1 g_2}} \end{cases} \quad (3\text{-}26)$$

$$\lambda = \sqrt{\frac{1}{g_1 g_2}} \Rightarrow \frac{f_0}{BW}\left(\frac{f}{f_0} - \frac{f_0}{f}\right) = \sqrt{\frac{1}{g_1 g_2}} \Rightarrow f^2 - \left(BW\sqrt{\frac{1}{g_1 g_2}}\right) f - {f_0}^2 = 0 \Rightarrow$$

$$f_1 = \frac{BW\sqrt{\frac{1}{g_1 g_2}} + \sqrt{4{f_0}^2 + \frac{BW^2}{g_1 g_2}}}{2} \xrightarrow{for\ narrow-band\ filters\ \frac{BW^2}{g_1 g_2} \ll 4{f_0}^2}$$

$$f_1 = f_0 + \frac{BW}{2}\sqrt{\frac{1}{g_1 g_2}} \quad (3\text{-}27)$$

$$\lambda = -\sqrt{\frac{1}{g_1 g_2}} \Rightarrow \frac{f_0}{BW}\left(\frac{f}{f_0} - \frac{f_0}{f}\right) = -\sqrt{\frac{1}{g_1 g_2}} \Rightarrow f^2 + \left(BW\sqrt{\frac{1}{g_1 g_2}}\right) f - {f_0}^2 = 0 \Rightarrow$$

$$f_2 = \frac{BW\sqrt{\frac{1}{g_1 g_2}} - \sqrt{4{f_0}^2 + \frac{BW^2}{g_1 g_2}}}{2} \xrightarrow{for\ narrow-band\ filters\ \frac{BW^2}{g_1 g_2} \ll 4{f_0}^2} \Longrightarrow$$

$$f_2 = f_0 - \frac{BW}{2}\sqrt{\frac{1}{g_1 g_2}} \tag{3-28}$$

In other words, the number of admittance matrix poles, on the real frequency axis, is reduced to two poles placed symmetrically around the center frequency. Note that the actual number of poles is still three, but their locations have been changed. Figure 3-4 shows the Y parameter of the net network, a $\lambda/4$ transmission line connected to the primary filter. By reducing one of the poles outside of the passband and pushing the two remaining poles close to the edges of passband, the Y parameter difference is made simpler and thus easier to implement. The fractional bandwidth of the primary filter is 2%, i.e., 40 MHz.

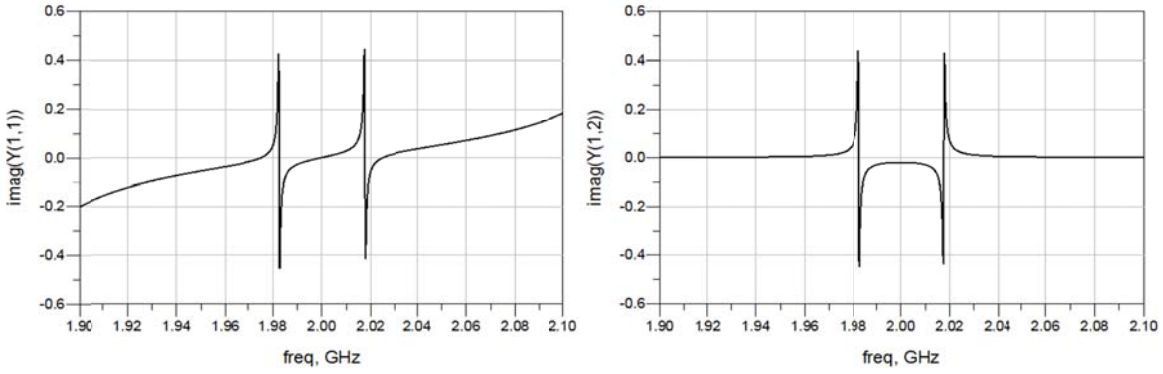

Figure 3-4: Y parameters of the net network, with a $\lambda/4$ transmission line connected to the primary filter

If we calculate the Y parameters of both the desired and primary filters after adding the $\lambda/4$ transmission line to their input ports, the location of the poles will remain matched due to the fact that $BW/2\sqrt{g_1 g_2}$ is equal in these two filters. Hence, the matched poles make the Y parameter differences diagrams simple and easy to implement. Figure 3-5 shows the differences between the Y

parameters of two networks, i.e., desired and primary Chebyshev filters, each connected to $\lambda/4$ transmission lines.

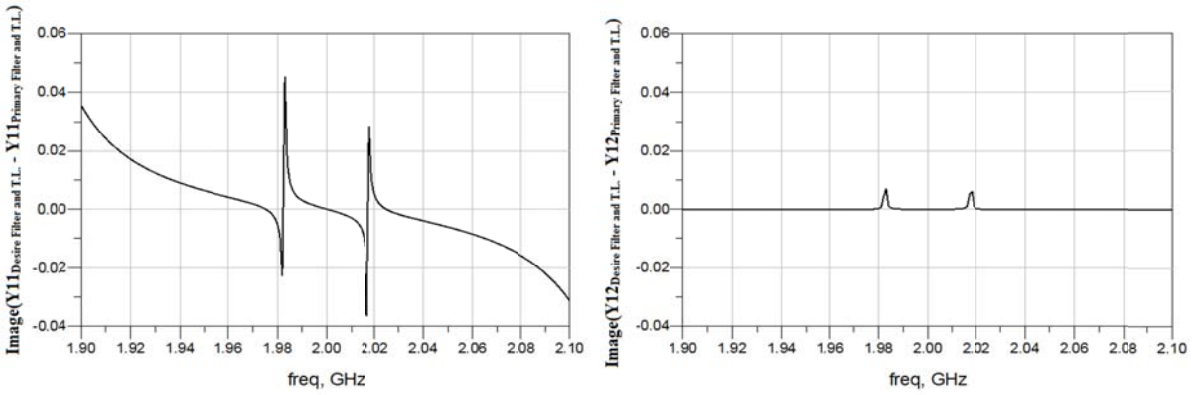

Figure 3-5: Differences between Y parameters of desired and primary filters (with a $\lambda/4$ T.L.)

Before proceeding to the next section and explaining the circuit extraction of the calculated admittance parameters, it is necessary to analyze the symmetric phase-loading effect. Adding two similar transmission lines to both sides of the filter will move the poles of admittance parameters. Calculating the exact locations of the new poles is more complicated than for one-sided transmission line cases. Figure 3-6 shows the Y parameters of a primary filter, in its passband, with two $\lambda/8$ transmission lines on each side. As depicted in this figure, two poles are located inside the bandwidth, close to the edges of the passband.

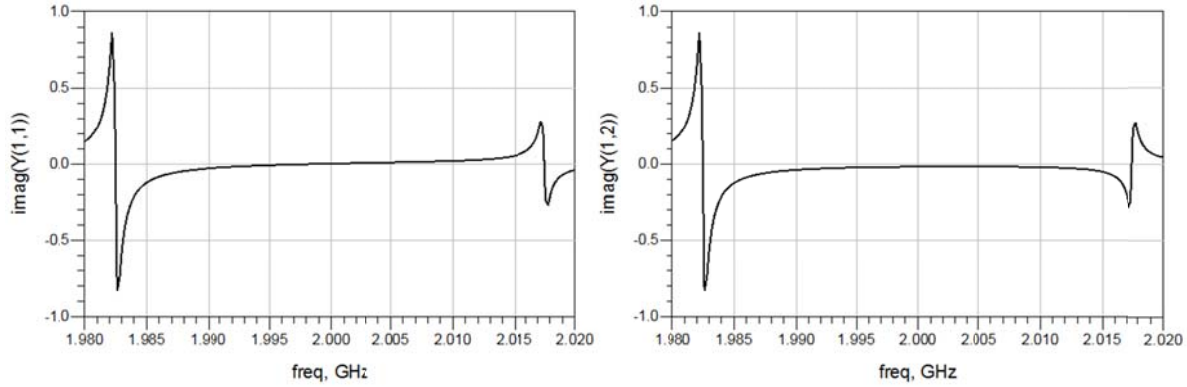

Figure 3-6: Y parameters of the net network, with two $\lambda/8$ transmission lines connected to each side of the primary filter

If we add two $\lambda/8$ transmission lines to each side of both Chebyshev filters, primary and desired, their admittance parameters poles will not remain exactly matched. The length of the transmission lines around the desired filter needs to be slightly tuned (around $\lambda/8$) to minimize the difference between the poles of the two admittance parameter sets. Figure 3-7 shows the difference between the admittance parameters of these two phase-loaded filters in the passband of the primary filter. While the transmission lines around the primary filter have a length of $\lambda/8$, the transmission lines around the desired filter are chosen to be $\lambda/8.62$ in length to minimize the difference between the poles. Note that since the important specification of the desired filter is the magnitude of its S parameters (which needs to remain unchanged), changing the phase-loading effect will not affect this specification.

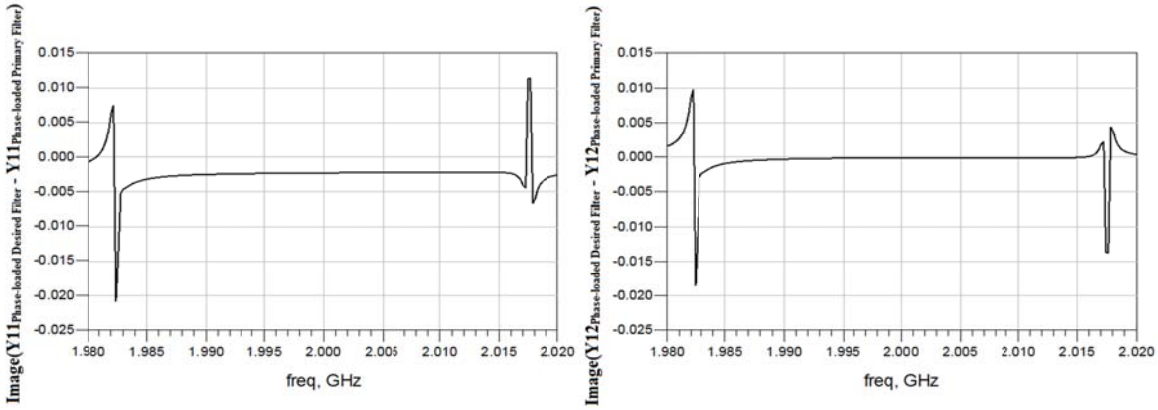

Figure 3-7: The difference between the Y parameters of the desired filter, after applying the phase-loading effect, and the primary filter with two $\lambda/8$ transmission lines added to both sides

3.2.3 Extracting the Circuit of Calculated Admittance Parameters

Adding a circuit parallel to a filter will affect the S-parameters of the filter, but calculating this influence in terms of S parameters is complicated. However, if we analyze the Y parameters of the filter and parallel circuit, quantifying the effect of the circuit will be simple. Namely, the Y-parameters of the net circuit will be the Y parameters of the filter plus the Y parameters of the added circuit. As a result, the Y parameters of the proper parallel circuit can be calculated by finding the difference between the Y parameter of the desired and primary filters. After that, we need to come up with a circuit to model the extracted Y parameters, or an approximation of it.

Figure 3-8 shows the calculated admittance parameter differences in the passband of a desired filter. In the previous sections, the difference between the admittance parameters had been simplified by the addition of the phase-loading effect. However, here there is no pole in the desired filter passband, which makes the circuit extraction that much easier. In this section, a passive circuit will be proposed to model the calculated admittance parameters.

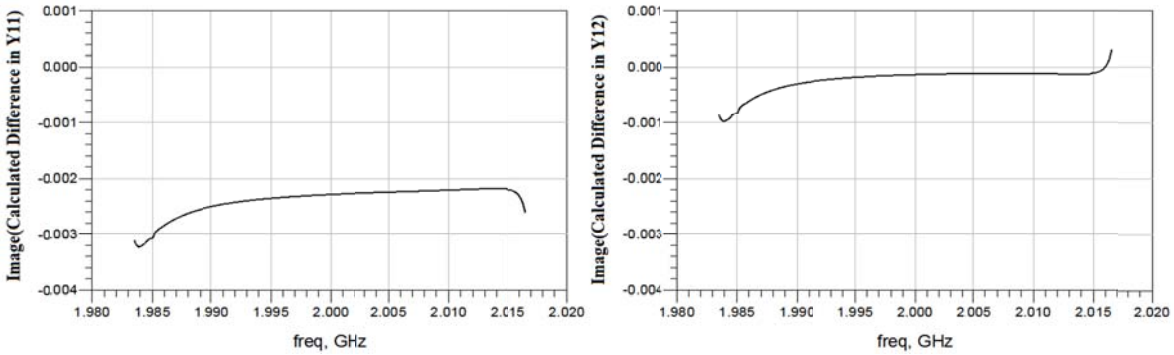

Figure 3-8: The calculated difference between the Y parameters in the desired filter's passband

The first and simplest model for approximating the calculated admittance parameter difference is a linear model. The Curve Fitting toolbox of MATLAB [50] is used to find the linear approximation. Figure 3-9 shows the calculated admittance parameter difference in the passband of a desired filter and the calculated linear model for approximating it in dotted lines.

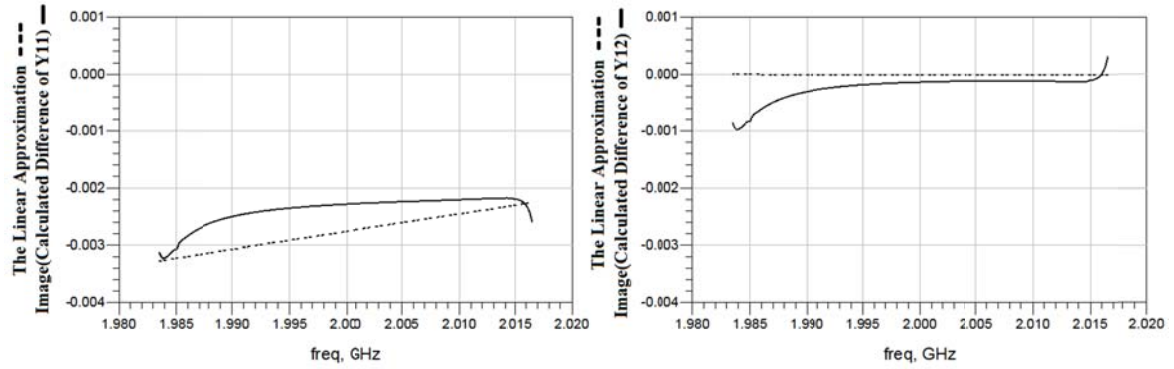

Figure 3-9: Linear approximation of the calculated difference between Y parameters in the desired filter's passband

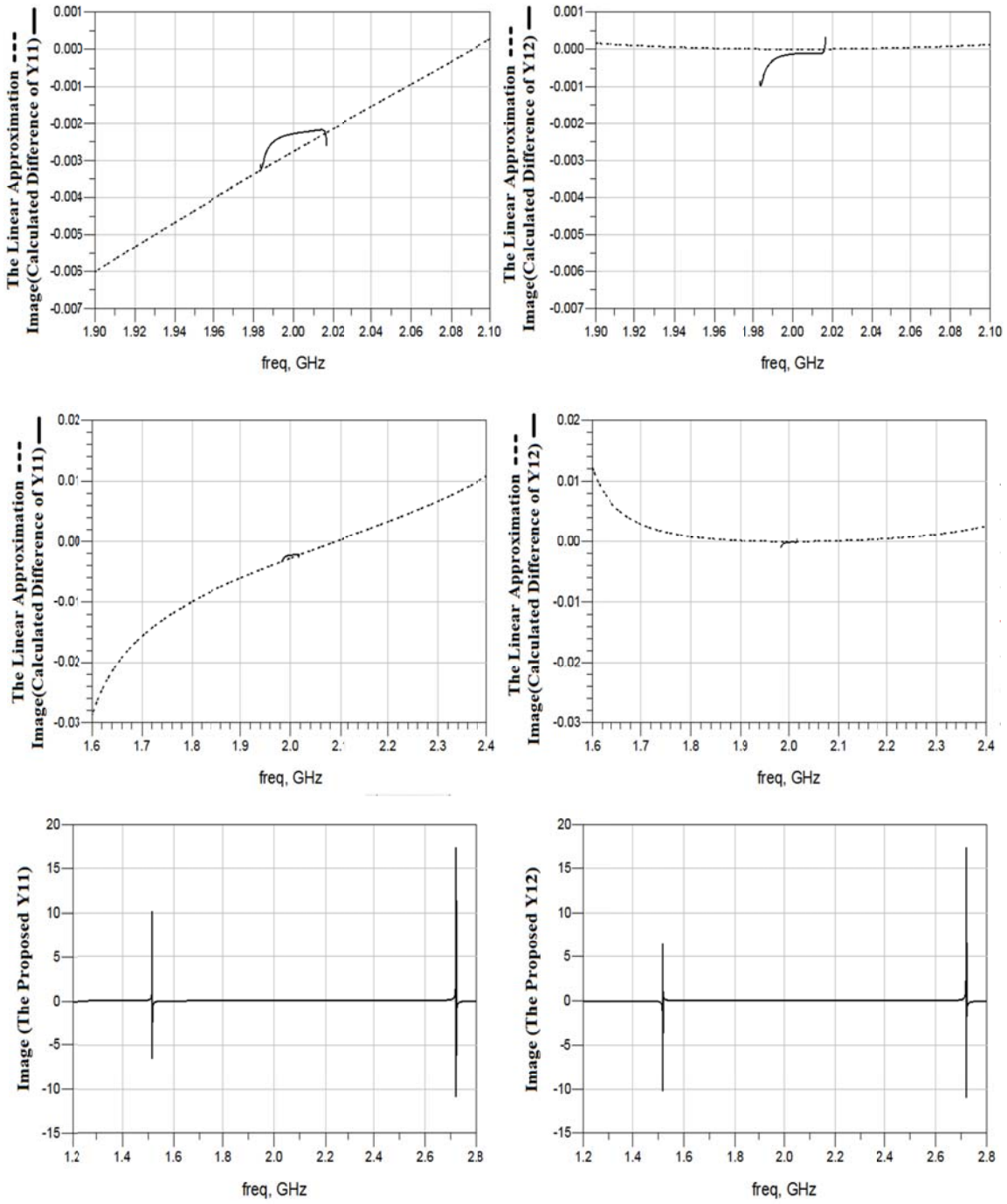

Figure 3-10: The proposed Y parameter behaviour for the parallel auxiliary circuit in the frequency ranges of $f_0 \pm 2.5\Delta f$, $f_0 \pm 10\Delta f$, and $f_0 \pm 20\Delta f$

Extracting a circuit in modeling a linear approximation does not have one preferred method. Rather, there is an unlimited number of circuits with the same admittance parameters in the mentioned frequency range. The key is to choose a circuit with the least harmful effects outside the passband, especially in the required frequency range of a filter based on its application. In this dissertation, our criteria is having a similar Chebyshev behaviour in the frequency range of $f_0 \pm 10\Delta f$, where f_0 is the center frequency and Δf is the bandwidth of the desired filter.

Figure 3-10 shows the proposed Y parameter behaviour for the parallel auxiliary circuit in the frequency ranges of $f_0 \pm 2.5\Delta f$, $f_0 \pm 10\Delta f$ and $f_0 \pm 20\Delta f$. As illustrated, the poles in the Y parameters of the proposed behaviour are placed further than $f_0 \pm 10\Delta f$ from the passband to minimize the undesired effects on the primary filter's behaviour.

The proposed admittance parameters can easily be realized as a lumped-element circuit by applying two parallel LC networks. Figure 3-11 shows the realized circuit for the proposed Y parameters. Note that, depending on the ripple level of the primary and desired filters, different values of lumped elements may be required.

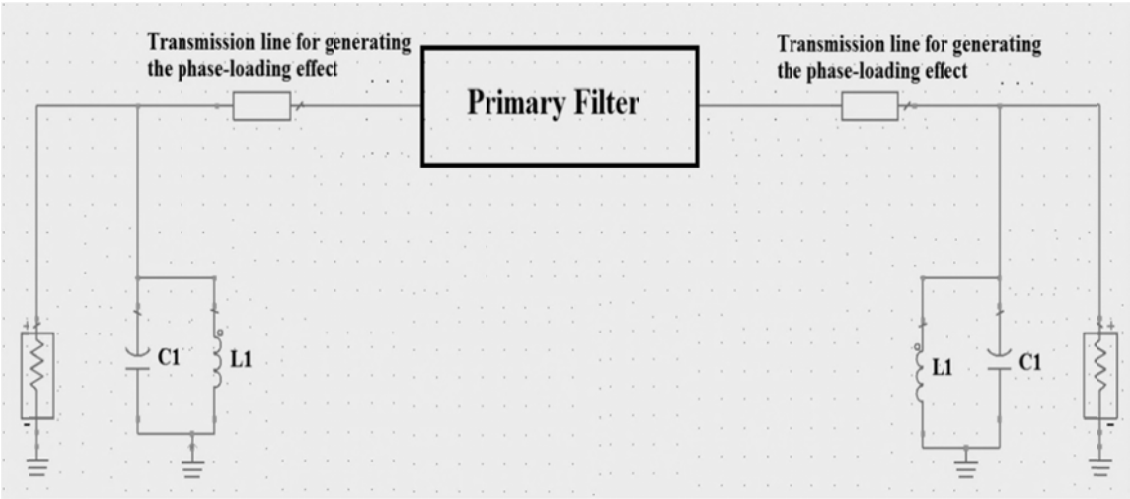

Figure 3-11: A general prototype of the proposed auxiliary circuit

Figure 3-12 shows the effect of adding the proposed auxiliary circuit parallel to the primary filter on the scattering matrix parameters. The applied values of lumped elements are provided in Table 3-1. As shown in this figure, the ripple level has decreased from 0.1396 dB to 0.0436 dB while the

bandwidth is reduced 14.6%, as expected. Also noteworthy is that, based on Figure 3-13, the S parameter of the net circuit, including the primary and auxiliary circuits, has not changed considerably in the frequency range of $f_0 \pm 10\Delta f$.

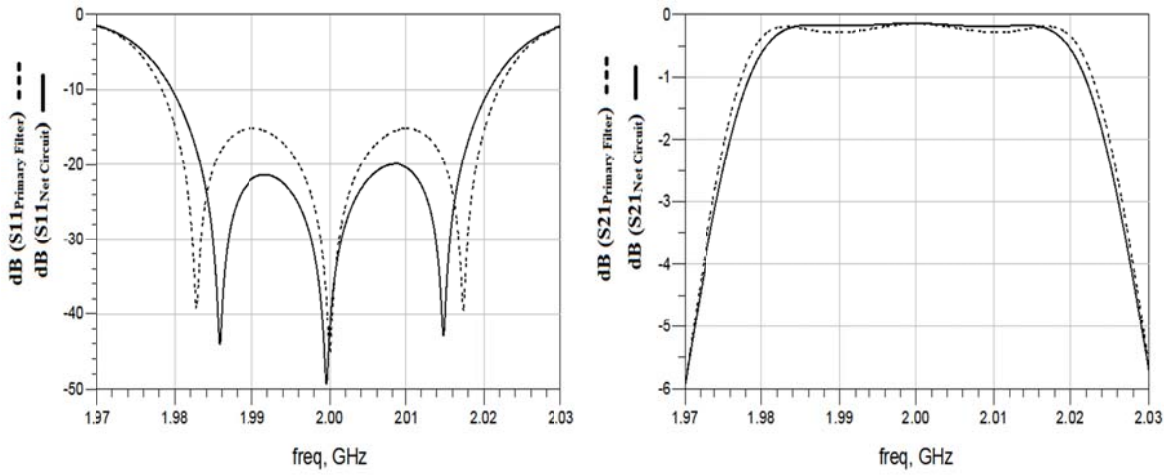

Figure 3-12: The effect of adding the proposed auxiliary circuit parallel to the primary filter on the scattering matrix parameters

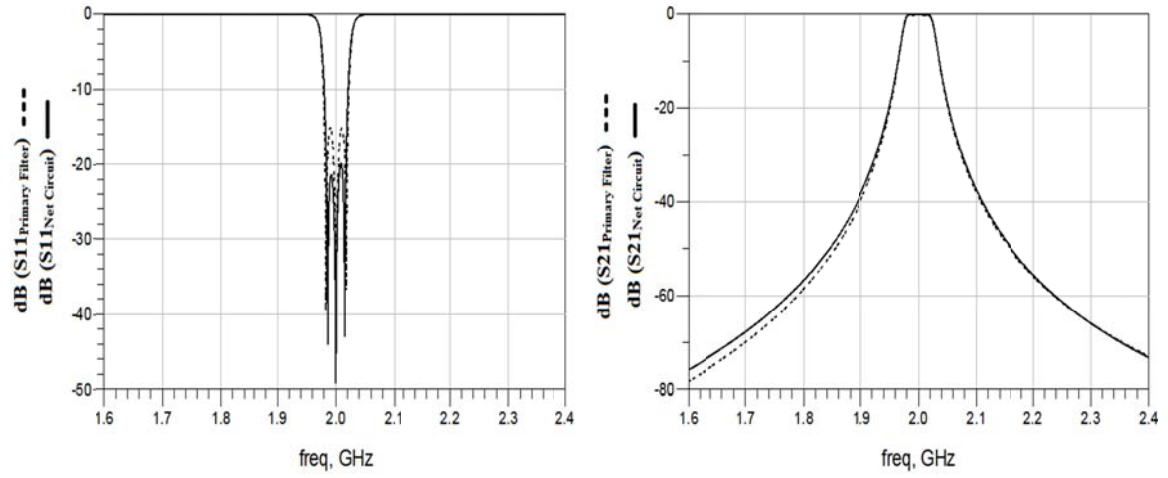

Figure 3-13 : The effect of adding the proposed auxiliary circuit parallel to the primary filter on the scattering matrix parameters in the frequency range of $f_0 \pm (10 \times Bandwidth)$

Table 3-1 : The element values of the auxiliary circuit to improve the ripple level from 0.14 dB to 0.044 dB

Element	C1	L1
Value	0.6 pF	8 nH

3.2.4 Varactor-Based Tuning of Different Low Return-Loss Chebyshev Filters

In the previous sections, the passband return loss of a Chebyshev filter was shown to be enhanced by adding a lumped-element auxiliary circuit parallel to the filter. Thus, for each fabricated detuned filter, a new auxiliary circuit needed to be designed and placed parallel to the filter. In this section, the same concept is employed for improving a number of different Chebyshev filters with different return losses by using a single fabricated auxiliary circuit.

The proposed auxiliary circuit consists of two capacitors and two inductors. Although the capacitance of capacitors can easily be tuned by using varactors, tuning inductors is more difficult to implement. Therefore, if the tuning of different detuned filters is possible only by tuning the capacitors of an auxiliary circuit, then all of these detuned filters should be able to be tuned by a single auxiliary circuit with tunable capacitors. Figure 3-14 shows the proposed auxiliary circuit with varactors.

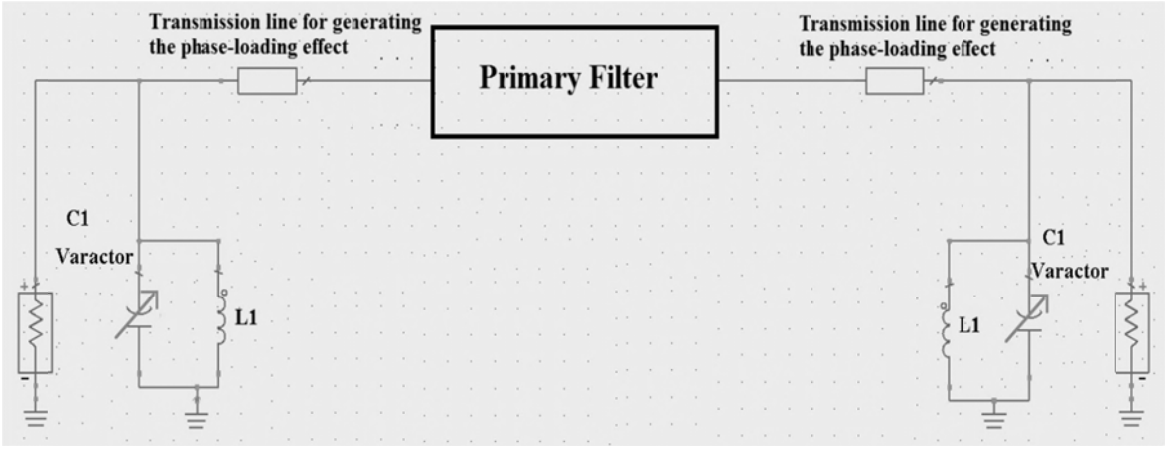

Figure 3-14: Proposed auxiliary circuit with varactors

As primary filters, four 3-pole Chebyshev filters with the same center frequency (2 GHz) and bandwidth (2%) but with different return losses (18 dB, 16 dB, 14 dB and 12 dB) are used. The goal is to improve the return losses of these filters to 20 dB by using the proposed auxiliary circuit. The inductance of the inductors is fixed at a value of 8 nH, which was calculated in the previous section for improving the return loss of 15 dB to 20 dB.

The simulation results show that the proposed auxiliary circuit has the ability to improve the return loss of all four filters to 20 dB by tuning the varactor from 390 fF to 720 fF. As was expected (based on the previous sections), the bandwidth of the net circuit is smaller than the bandwidth of the primary filter. Table 3-2 shows the required capacitance of varactors in each case and the bandwidth of the net circuit with a return loss of 20 dB. Figure 3-15 shows an S parameters diagram of four primary filters before and after adding the auxiliary circuit. These results clearly show that a single auxiliary circuit with varactors has the ability to tune different detuned filters.

Table 3-2: shows the required capacitance of varactors in each case and the bandwidth of the tuned filter

	18 dB	16 dB	14 dB	12 dB
C1	720 fF	640 fF	540 fF	390 fF
L1	8 nH	8 nH	8 nH	8 nH
Bandwidth of the Tuned Filter	1.9%	1.75%	1.62%	1.5%

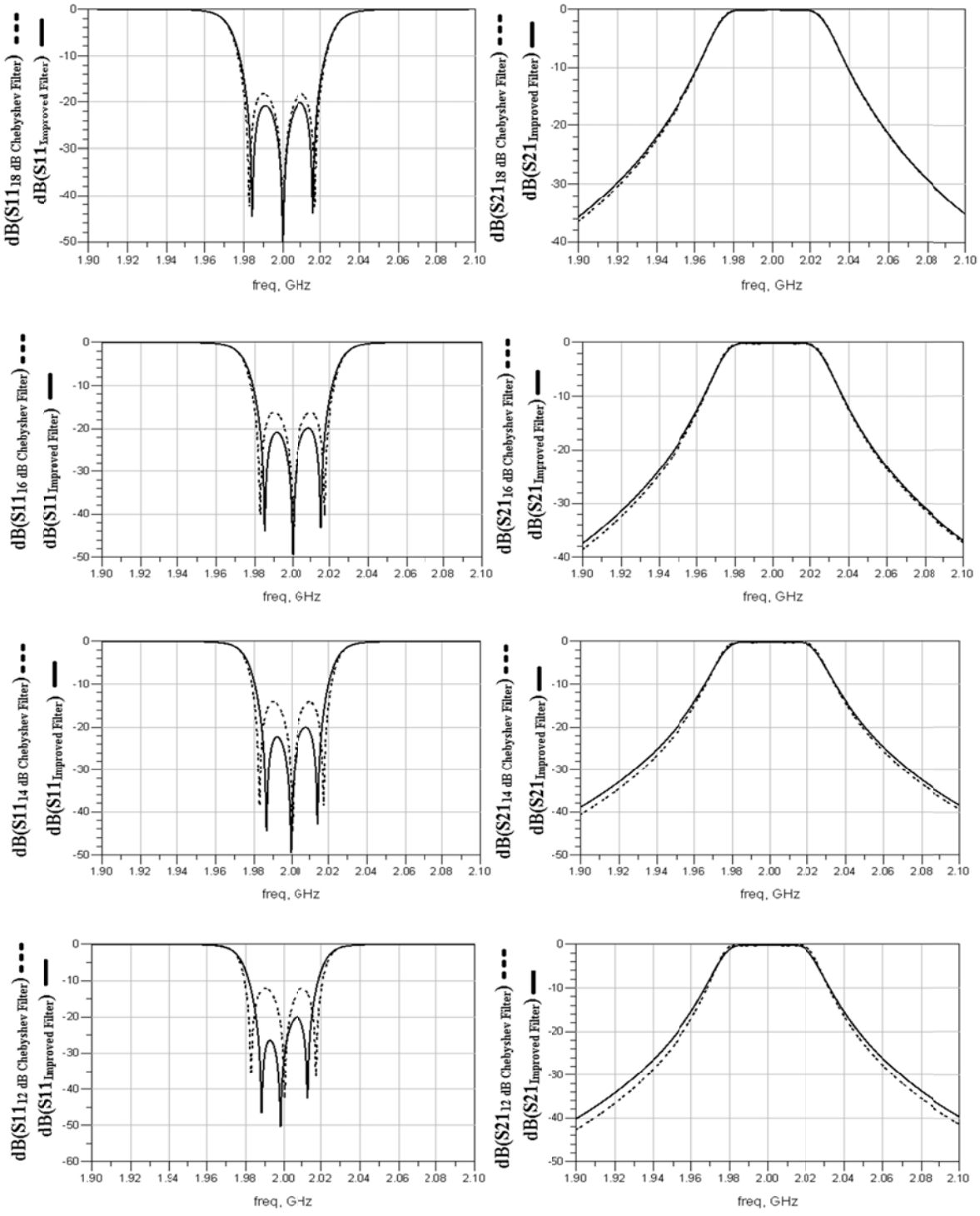

Figure 3-15: The effect of adding the proposed auxiliary circuit parallel to the Chebyshev filters

3.2.5 Extracting the Distributed-Element Circuit of Calculated Impedance Parameters

The proposed auxiliary circuit is passive and low-cost. Regardless of the type (microstrip, dielectric, combline, etc.) of manufactured microwave filter, it only depends on its transmission response. The problem here, however, is providing the applied lumped elements with their different sizes and values. This issue can be resolved by replacing the lumped-element circuit with a distributed-element one.

Figure 3-16 shows the proposed distributed-element circuit for an auxiliary network. It consists of five transmission lines of four different lengths. These four lengths are variable parameters, corresponding to the lumped element values, which will be determined based on the ripple level and passband of the primary and desired filters. Two of the transmission lines (T2 and T4) are open-circuit ended and their values will be the same if the primary filter has a symmetric behaviour (e.g., an in-line Chebyshev filter). The characteristic impedance of transmission lines in an auxiliary circuit needs to match that of the primary network.

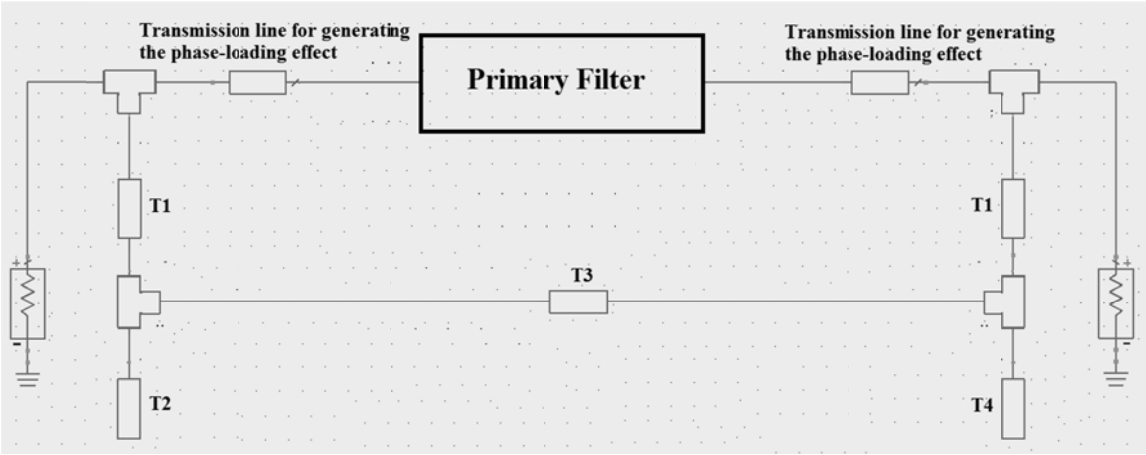

Figure 3-16: Prototype of the proposed auxiliary circuit implemented with distributed elements

Figure 3-17 shows the effect of adding the proposed auxiliary distributed-element circuit parallel to the primary filter on the scattering matrix parameters. The applied values for the transmission line lengths are provided in Table 3-3. Like the lumped-element circuit, the ripple level has decreased from 0.1396 dB to 0.0436 dB while the bandwidth has been reduced by 14.6%.

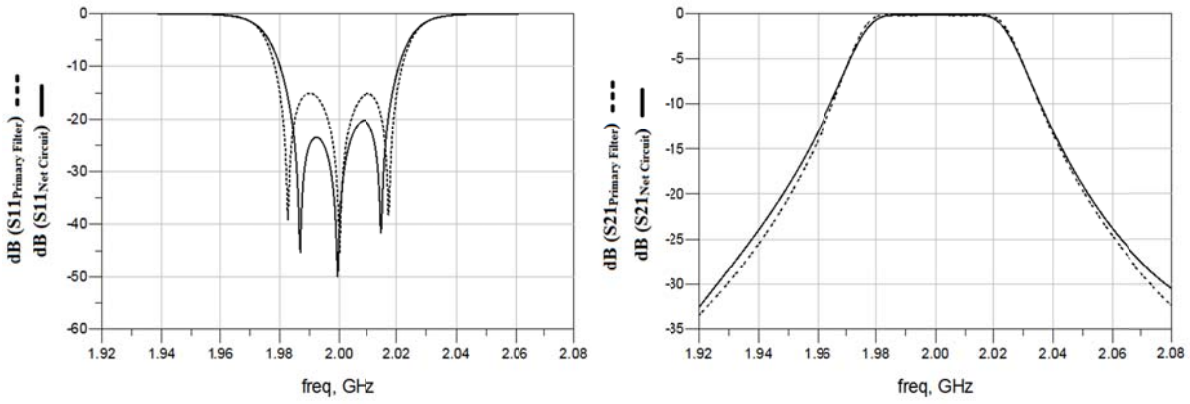

Figure 3-17: S parameters of a primary filter and net circuit, including the primary filter in parallel with the proposed distributed-element auxiliary circuit

Table 3-3: The lengths of transmission lines in the auxiliary circuit to improve the ripple level

T.L.	T1	T2	T3	T4
Length	$\lambda/4.52$	$\lambda/4.12$	$\lambda/4.6$	$\lambda/4.12$

3.3 Tuning a Detuned Chebyshev Bandpass Filter

After the fabrication of a microwave filter, the measured S-parameters of the filter are usually not as good as the EM simulation results. Some common mismatches are shift in center frequency, change in bandwidth, and increase in the insertion loss in the pass band. A common method for tuning a fabricated filter is using tuning screws. This method is not useful for all different types of microwave filters (for example, it is usually not applicable to planar filters). In this section, we use the technique proposed in section 3.2 to improve the return loss of a microwave detuned filter.

The goal in this section is to design a passive circuit that can be connected parallel to the detuned filter to change its transmission response to the desired performance. Here, we will use the term “detuned filter” instead of primary filter (used in Section 3.2), due to the fact that a primary filter is

designed to have specific insertion and return losses and is not detuned. Conversely, the performance of a detuned filter is different from the design due to fabrication inaccuracy.

3.3.1 Tuning a Detuned Chebyshev Bandpass Filter Using Distributed Elements

The fabrication inaccuracy of a microstrip filter will cause detuning in a filter's transmission response. Figure 3-18 shows the scattering matrix parameters of the detuned filter resulting from changing the dimensions of microstrip filter in a same diagram with the ideal Chebyshev filter. The maximum error in the dimensions of the microstrip filter is, in this case, 5%.

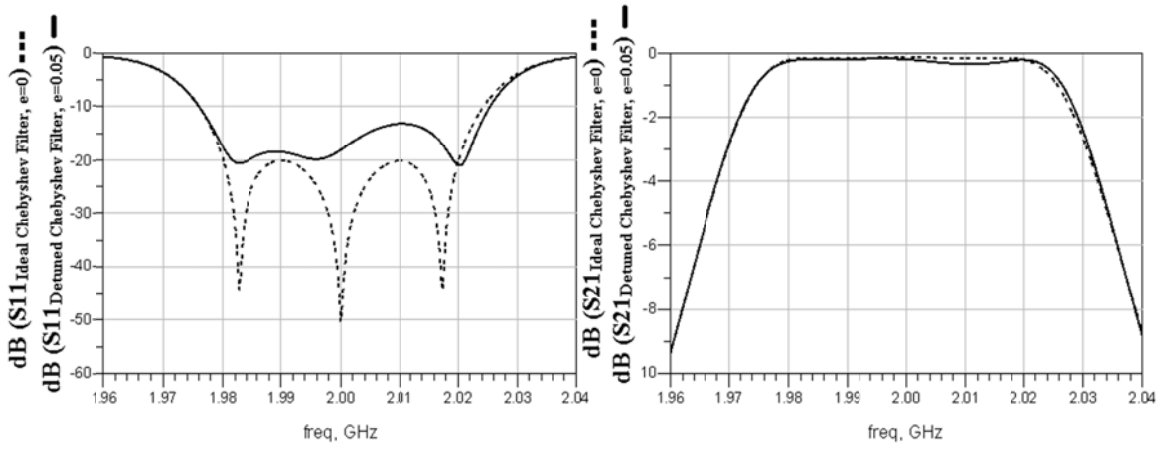

Figure 3-18: A detuned Chebyshev filter compared to an ideal correspondence

The first step is to locate a proper auxiliary circuit to improve the detuned filter by finding a proper desired filter that matches the admittance parameter poles with the detuned filter. In the second step, the phase-loading effect will be applied to the detuned filter to move the admittance matrix poles to the edges of the passband, thereby making the Y parameters difference simple to extract. This effect can be implemented by adding proper length transmission lines next to the detuned filter. Finally, in the last step, the auxiliary circuit will be extracted from the approximation of the differences between the admittance parameters. Figure 3-19 shows the effect of adding the proposed auxiliary distributed-element circuit, based on Figure 3-16, parallel to the detuned filter on the scattering matrix parameters. Applied values for the transmission line lengths are provided in Table 3-4.

Table 3-4: Lengths of transmission lines in the auxiliary circuit for tuning a detuned filter

T.L.	T1	T2	T3	T4	Phase-loading Effect
Length	$\lambda/4.81$	$\lambda/4.079$	$\lambda/11.504$	$\lambda/3.94$	$\lambda/5.57$

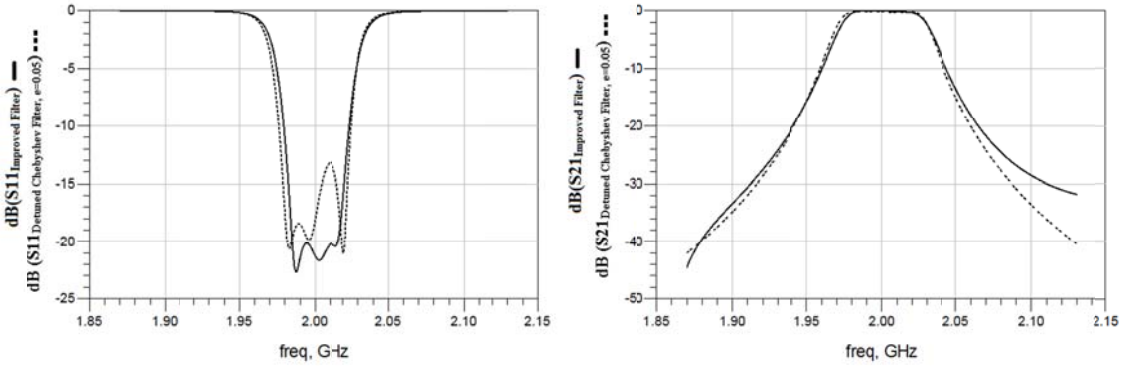

Figure 3-19: S parameters of a detuned filter and net circuit, including the detuned filter parallel with the proposed distributed-element auxiliary circuit

While this method is also practical for filters with more poles, the auxiliary circuit design does become more complicated as more poles are added. Figures 3-20 shows the effect of the auxiliary circuit in tuning a 4-pole detuned Chebyshev filter in the frequency ranges of $f_0 \pm \Delta f$ and $f_0 \pm 4\Delta f$. The filter is tuned to have a maximum ripple of 0.0436 dB in its passband, with a fractional bandwidth of 2% at 2 GHz. The applied values for transmission line lengths are provided in Table 3-5.

Table 3-5: Lengths of transmission lines in the auxiliary circuit for tuning a detuned 4-pole filter

T.L.	T1	T2	T3	T4	Phase-loading Effect
Length	$\lambda/3.814$	$\lambda/4.142$	$\lambda/5.854$	$\lambda/3.923$	$\lambda/5.404$

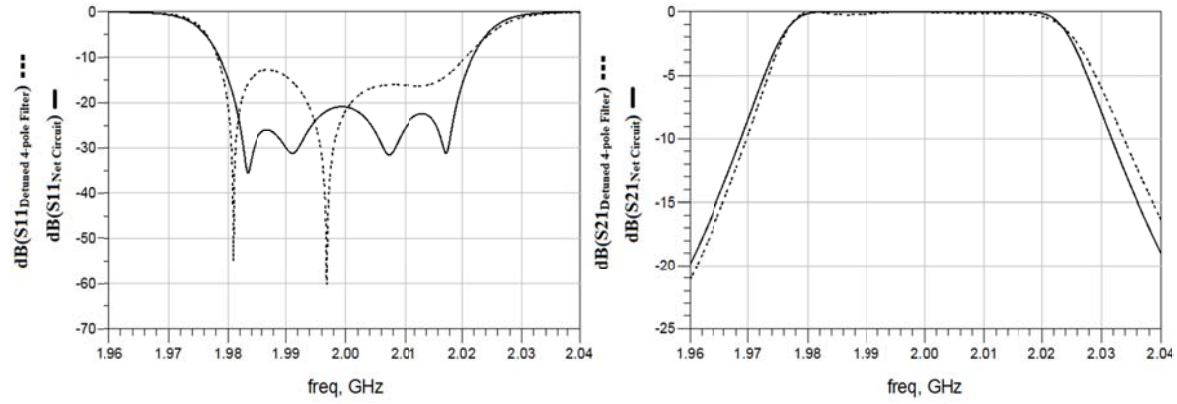

(a)

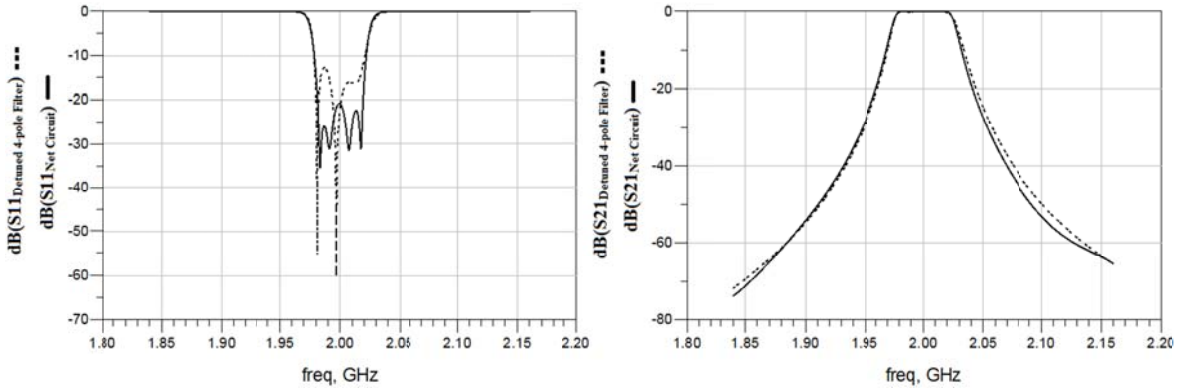

(b)

Figure 3-20: S parameters of a detuned 4-pole filter and net circuit, including the filter parallel with the proposed distributed-element auxiliary circuit, in the frequency ranges of (a) $f_0 \pm \Delta f$ and (b) $f_0 \pm 4\Delta f$

3.3.2 Tuning a Detuned Chebyshev Bandpass Filter Using Varactors

In the previous section, the passband return loss of a detuned Chebyshev filter was shown to be enhanced by adding a distributed-element auxiliary circuit parallel to the filter. Thus, for each fabricated detuned filter, a new auxiliary circuit needed to be designed and placed parallel to the filter. In this section, the same concept is employed for improving a number of different detuned Chebyshev filters with different return losses by using a single fabricated auxiliary circuit.

Same as the Section 3.2.4, the proposed auxiliary circuit consists of two capacitors and two inductors. Although the capacitances can easily be tuned by using varactors, tuning inductors is more difficult to implement. Therefore, if the tuning of different detuned filters is possible only by tuning the capacitors of an auxiliary circuit, then all of these detuned filters should be able to be tuned by a single auxiliary circuit with tunable capacitors. Figure 3-21 shows the proposed auxiliary circuit with varactors. Despite of the proposed circuit in Figure 3-16, this circuit has two different values for varactors in each side to tune asymmetric detuned filters.

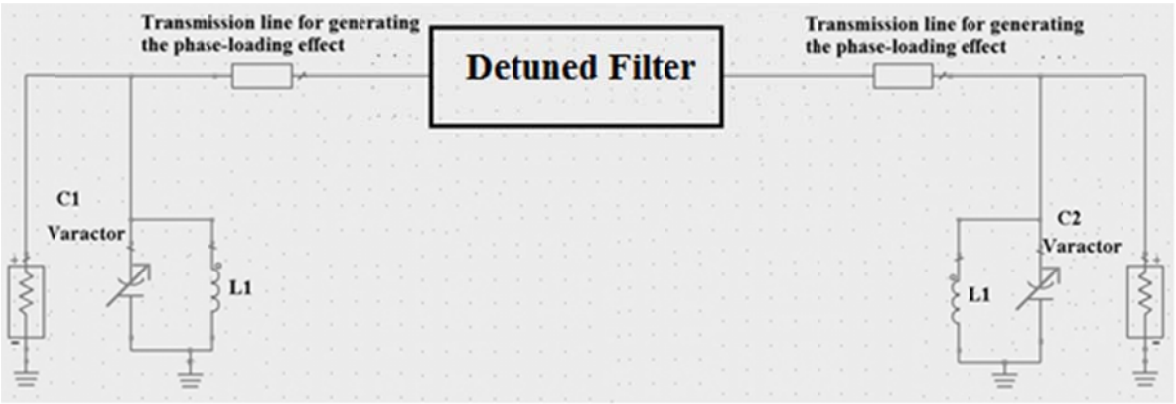

Figure 3-21: Proposed auxiliary circuit with varactors C1 and C2

As detuned filters, three 3-pole detuned Chebyshev filters with the same center frequency (2 GHz) and bandwidth (2%) are used. The return loss of detuned filters is not equal ripple and ranging from 10 dB to 15 dB. The goal is to improve the return losses of these filters to 20 dB by using the proposed auxiliary circuit. The inductance of the inductors is fixed at a value of 8 nH, which was calculated in the previous section for improving the return loss of 15 dB to 20 dB.

The simulation results show that the proposed auxiliary circuit has the ability to improve the return loss of all three filters to 20 dB by tuning the varactor from 390 fF to 720 fF. Figures 3-22, 3-23 and 3-24 show the S parameters diagram of three primary filters before and after adding the auxiliary circuit and the required capacitance of varactors in each case. These results clearly show that a single auxiliary circuit with varactors has the ability to tune different detuned filters.

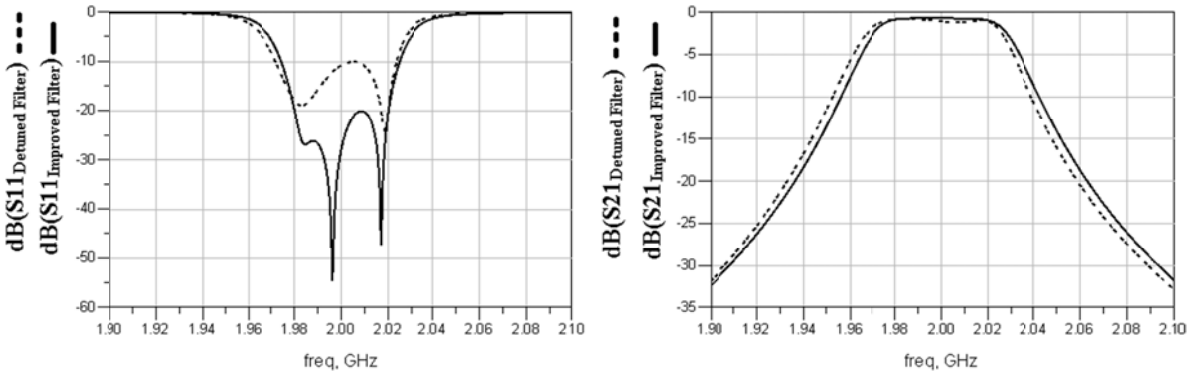

Figure 3-22: A varactor based tuned Chebyshev filter compared to the detuned correspondence (L1=8 nH, C1=302 fF, C2=398 fF)

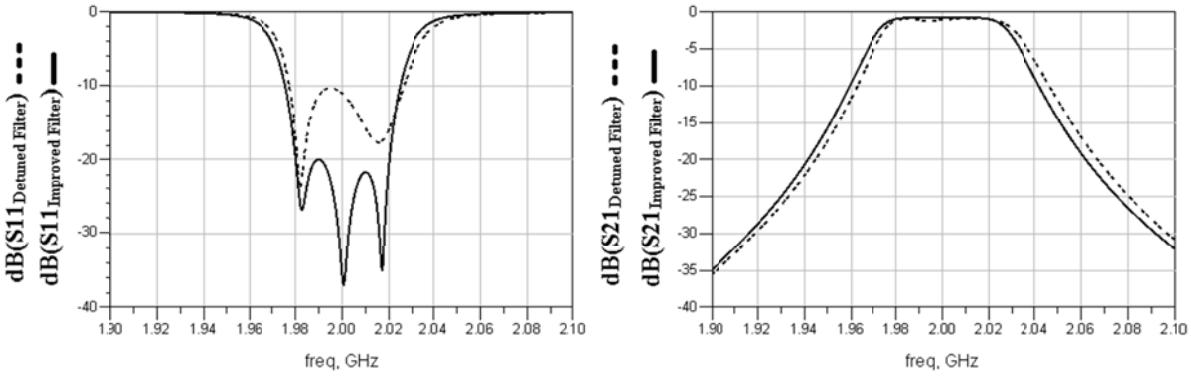

Figure 3-23: A varactor based tuned Chebyshev filter compared to the detuned correspondence (L1=8 nH, C1=1259 fF, C2=1301 fF)

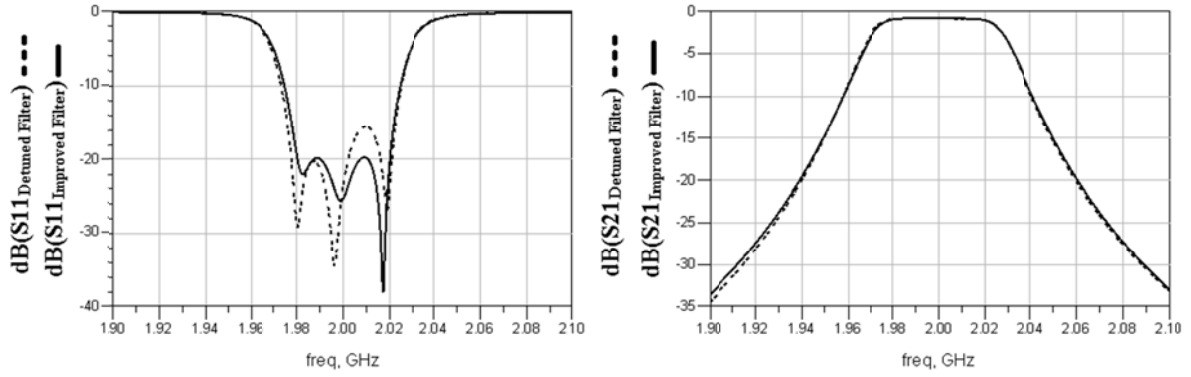

Figure 3-24: A varactor based tuned Chebyshev filter compared to the detuned correspondence (L1=8 nH, C1=544 fF, C2=803 fF)

3.4 Simulation Results

In this section, the EM simulation results after applying the proposed tuning method on a detuned microstrip Chebyshev filter are presented. The EM simulation is run in Momentum 2011. Figure 3-25 shows the layout of the 3-pole filter used in this experiment. The filter is designed to have a return loss of -20 dB and a fractional bandwidth of 2% at 2 GHz. Rogers Duroid 6010.2 is employed as the substrate. Figure 3-26 shows the EM simulation S parameters of the microstrip filter in a frequency range of $f_0 \pm 2.5\Delta f$.

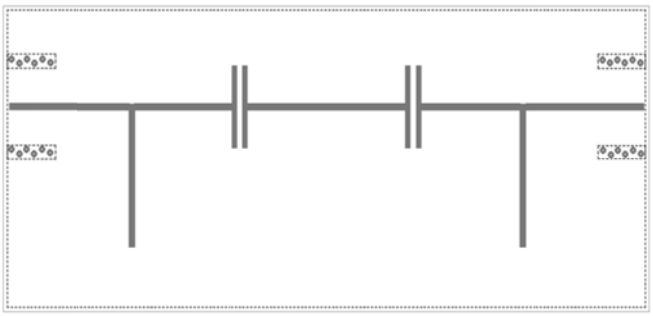

Figure 3-25: Layout of the applied 3-pole microstrip filter

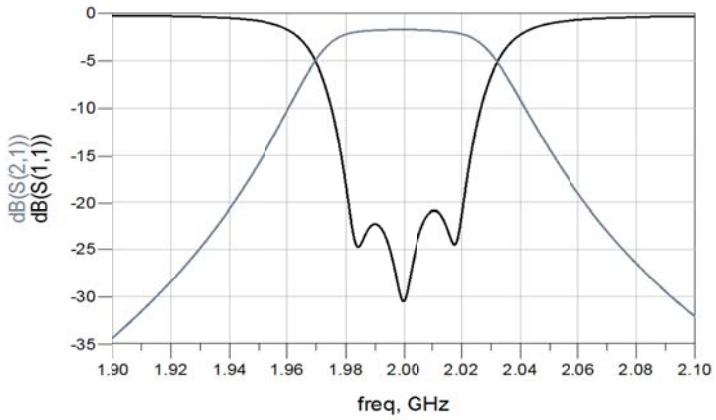

Figure 3-26: S-parameters of a microstrip filter before detuning

An error in the dimensions of the microstrip filter will cause detuning in the filter's transmission response. Figure 3-27 shows the scattering matrix parameters of a detuned filter resulting from a change in the microstrip filter's dimensions. Here, the maximum error is 5%. As shown in the following figure, the magnitude of return loss is less than -15dB for about half of the passband.

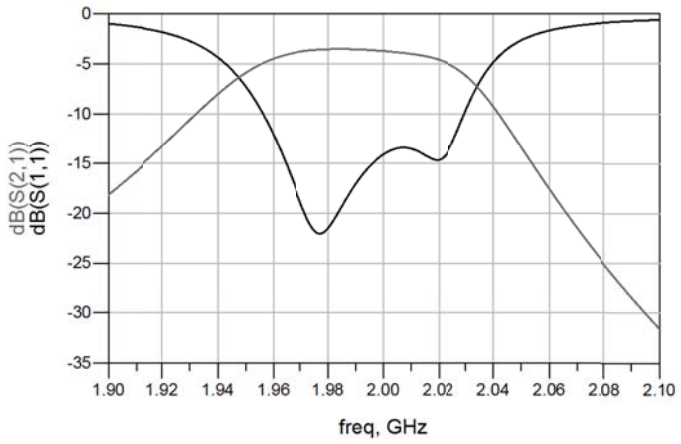

Figure 3-27: S-parameters of a microstrip filter after detuning

After performing the tuning steps mentioned in sections 3.2 and 3.3, the proper auxiliary circuit can be calculated. Figure 3-28 shows the layout of the net circuit, including the detuned filter parallel to the calculated auxiliary circuit.

Figure 3-29 shows the scattering matrix parameters of a net circuit, including the detuned filter and auxiliary circuit. As shown, the magnitude of the return loss has increased from 14 dB to more than 25 dB in the passband. Figure 3-30 illustrates the S parameter of the net circuit in a wider frequency range of $f_0 \pm 4\Delta f$.

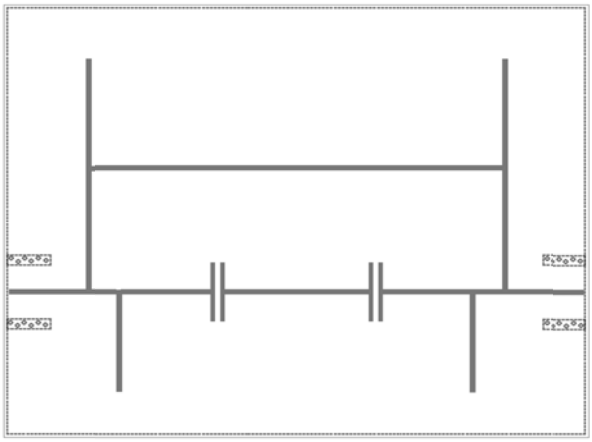

Figure 3-28: Layout of a net circuit, including a detuned filter, parallel to the calculated auxiliary circuit

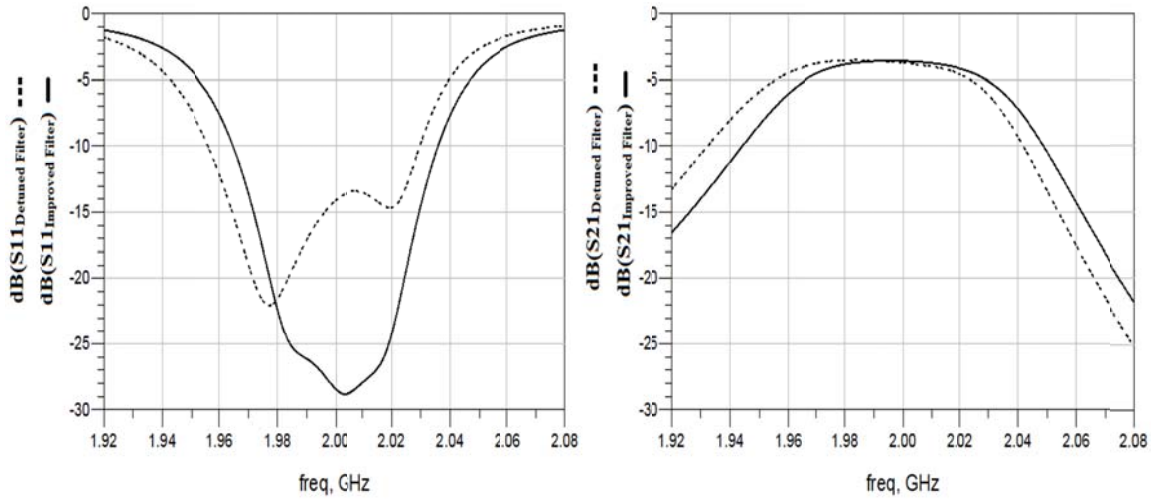

Figure 3-29: S parameters of a net circuit compared to S parameters of a detuned filter

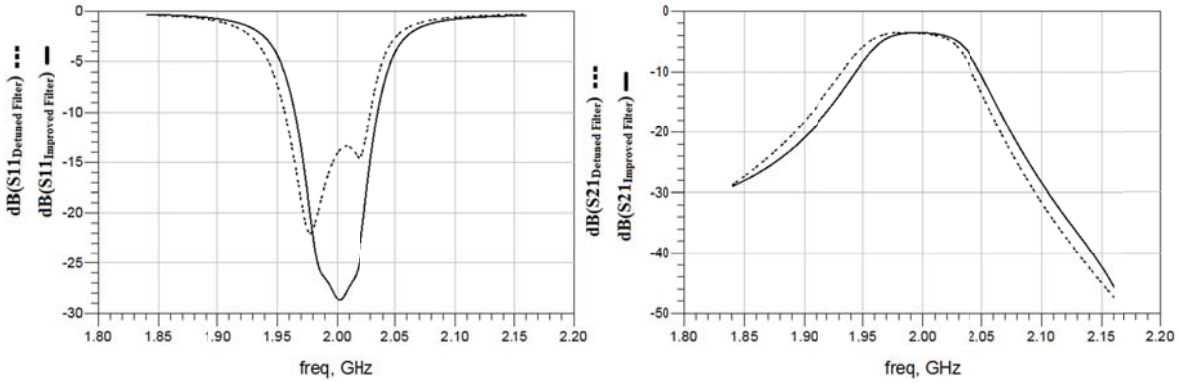

Figure 3-30: S parameters of a net circuit compared to S parameters of a detuned filter in the frequency range of $f_0 \pm 4\Delta f$

3.5 Experimental Results

In this section, the proposed method has been applied to two different microwave filters: a microstrip filter at 2 GHz, and a cavity filter at 20 GHz. The microstrip filter is fabricated on a 0.635 mm Duroid substrate ($\varepsilon_r = 10.2$, Rogers RT/Duroid 6010.2). The scattering matrix parameters of both filters were measured with an Agilent PNA, and the calibration is executed using an Agilent E-cal kit. The reference planes are located at the SMA connectors. The design of the fabricated microstrip filter is based on the simulation results in the previous section.

3.5.1 Microstrip Filter

A fabricated and intentionally detuned microstrip filter is shown in Figure 3-31. The measured S-parameters of this filter are illustrated in Figure 3-32, whereas Figure 3-33 shows the S parameters of the desired filter, based on the EM simulation and the measured S parameters of the detuned filter. The measured return loss is less than 10 dB in some frequencies in the passband, and the 1-dB bandwidth is 3.68% (72 MHz), with a center frequency of 1.957 GHz.

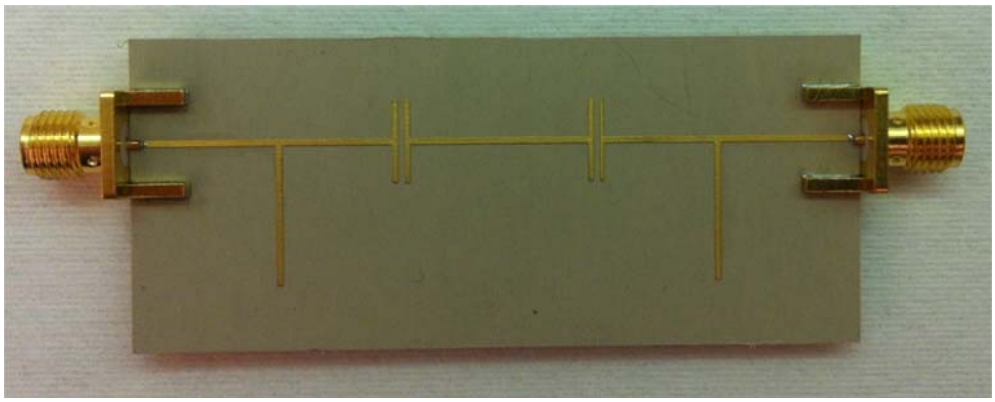

Figure 3-31: Fabricated microstrip filter

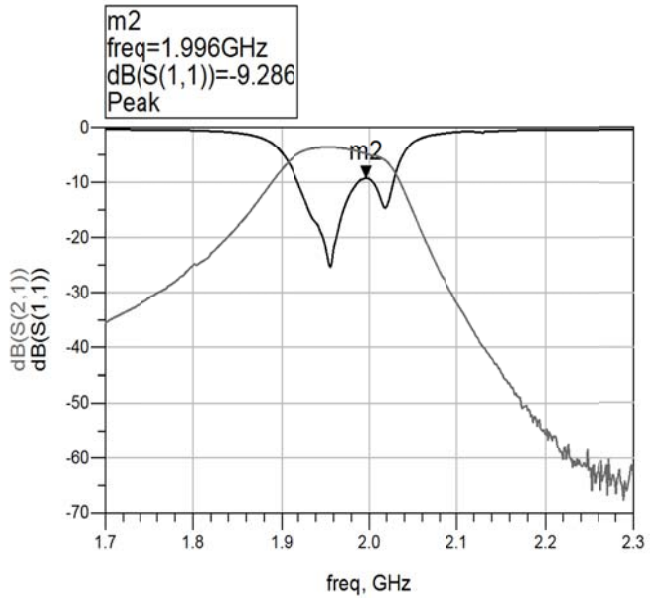

Figure 3-32: The measured S parameters of an intentionally detuned microstrip filter

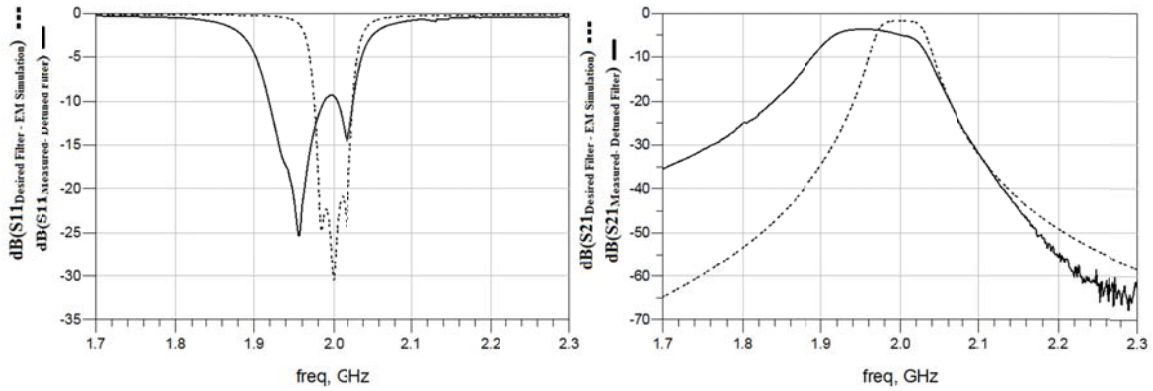

Figure 3-33: S parameters of the desired filter, from EM simulation, compared to measured S parameters of an intentionally detuned filter

Figure 3-34 shows a fabricated filter and an auxiliary circuit on the same board. The measured S parameters of the overall circuit are shown in Figure 3-35. The measured S parameters of the detuned filter are also shown in this figure. As can be seen, the measured return loss improves to more than 18 dB for the entire passband, while the 1-dB bandwidth is decreased to 3.36% (66 MHz), with a center frequency of 1.966 GHz. Figure 3-36 shows the net circuit S parameters in a wider frequency range to demonstrate the effect of the auxiliary circuit outside the passband. Note that the center frequencies of both filters are shifted to the left due to the fabrication inaccuracy in the filters' transmission line widths.

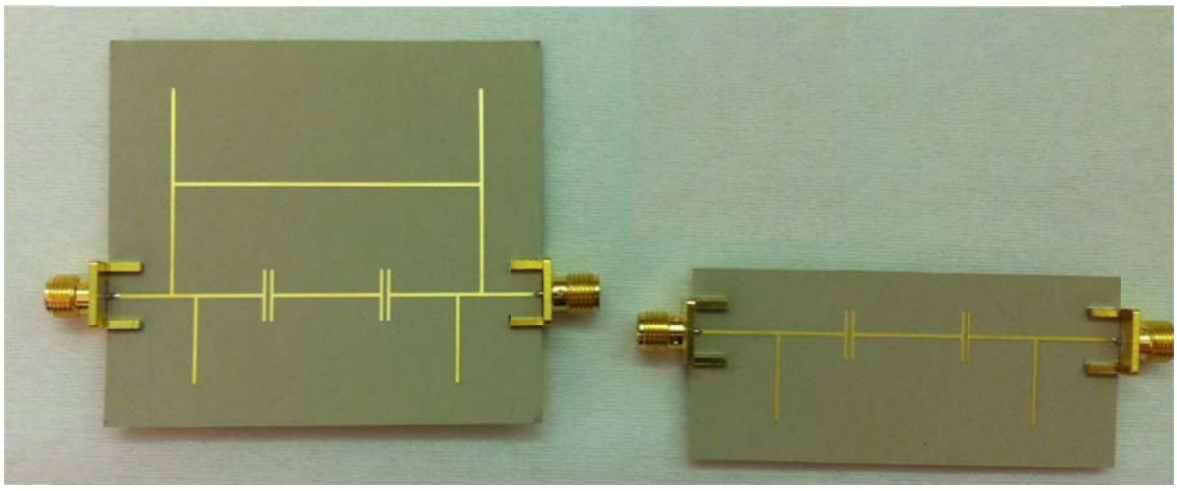

Figure 3-34: Fabricated filter and auxiliary circuit on the same board

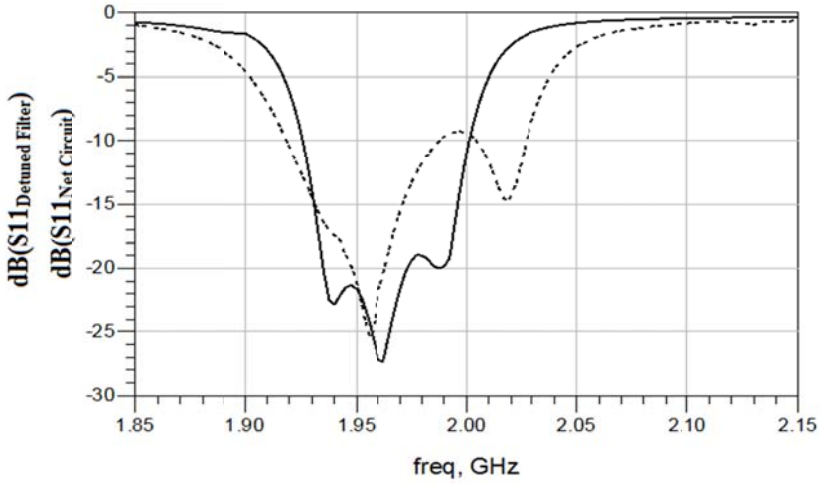

Figure 3-35: The measured S parameters of a net circuit and detuned filter

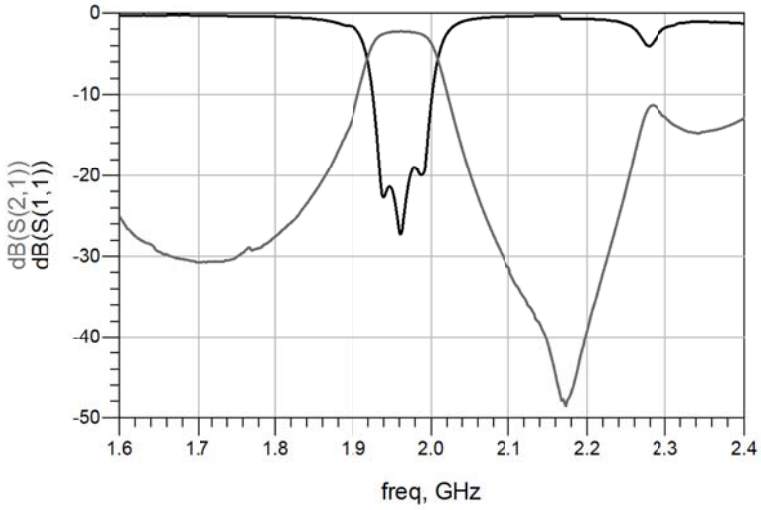

Figure 3-36: The measured S parameters of a net circuit in the frequency range of $f_0 \pm 6\Delta f$

3.5.2 The Cavity High-Frequency Filter

To prove the efficiency of the proposed method for filters with more than three poles, the auxiliary circuit is applied on a tunable cavity 6-pole filter. The filter is shown in Figure 3-37. The S parameter diagram of the cavity filter, prior to adding the auxiliary circuit, is shown in Figure 3-38. The return loss magnitude of the desired filter was intended to be more than 20 dB in the passband of the filter.

As illustrated in the figure, the filter is detuned from the desired behaviour and the magnitude of return loss is less than 18 dB in some frequencies in the passband. The measured return loss is less than the desired value, -20 dB, for 8.5% (40 MHz) of the passband. The measured return loss is 17.2 dB in some frequencies in the passband with a 2.11% (430 MHz) 1-dB bandwidth and a center frequency of 20.355 GHz.

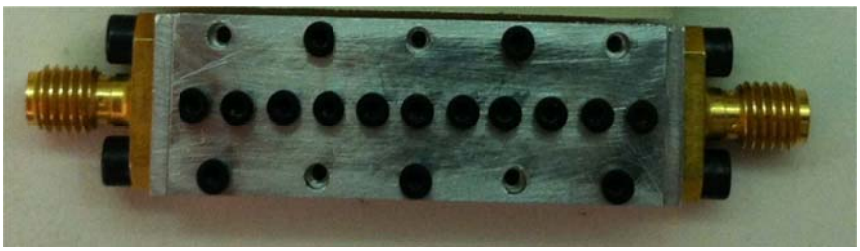

Figure 3-37: Tunable 6-pole cavity filter

The auxiliary circuit is implemented by the microstrip transmission lines on a separate board. The board is placed parallel to the detuned filter to improve its transmission response. Figure 3-39 shows a detuned filter connected to the fabricated microstrip circuit. An SMA T-junction and a 90-degree SMA bend are required for the connection. The effects of these two elements are considered in the simulation and design steps of the auxiliary circuit.

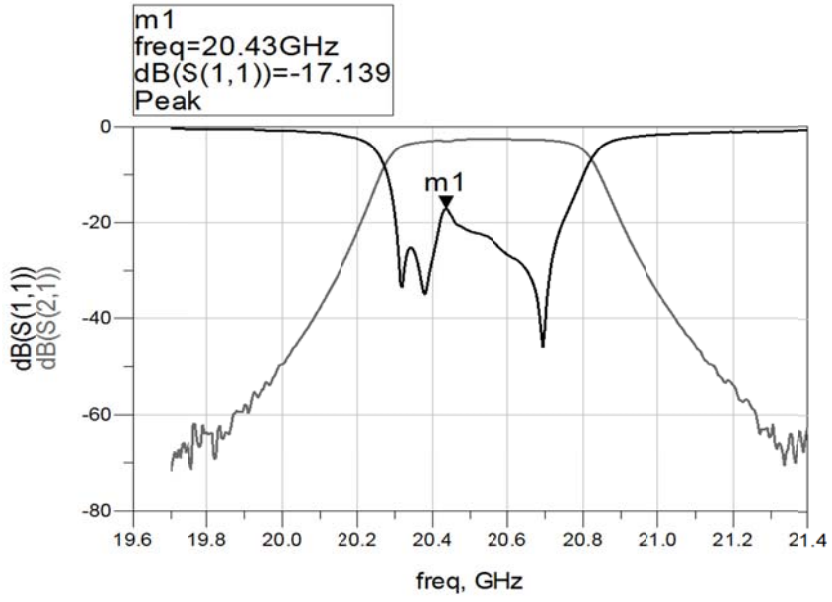

Figure 3-38: The measured S parameters of a 6-pole cavity filter

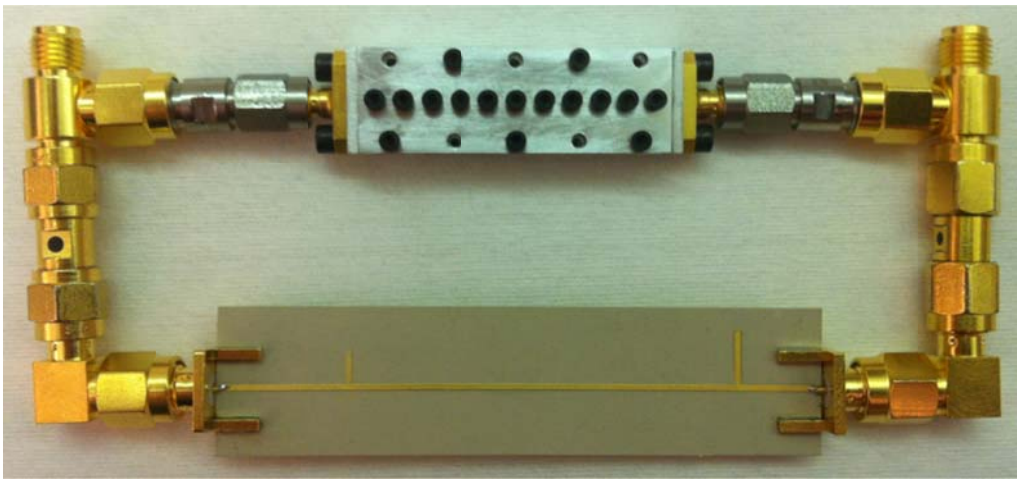

Figure 3-39: Detuned cavity filter parallel to a fabricated auxiliary circuit

The S parameters of a net circuit, including a detuned filter, T junction, bend, and fabricated microstrip auxiliary circuit, are shown in Figure 3-40. As demonstrated, the return loss magnitude of the net circuit is more than 20 dB for the entire passband. The measured return loss improves to 20 dB with a 2.07% (422 MHz) 1-dB bandwidth and a center frequency of 20.354 GHz.

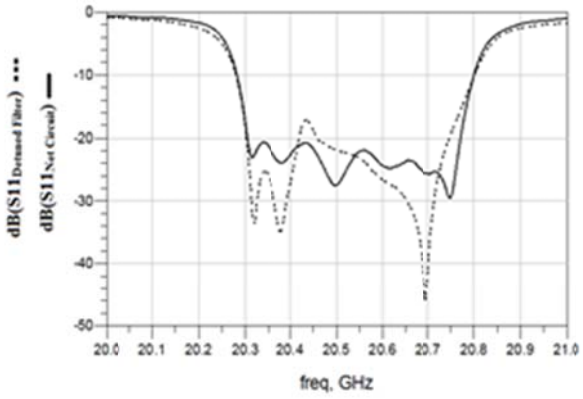

Figure 3-40: S parameters of a net circuit, including a detuned filter, T junction, bend, and fabricated microstrip auxiliary circuit compared to the S parameters of a detuned filter

Chapter 4
Center Frequency and Bandwidth Tuning of a Bandpass Microstrip Filter Using GaAs Varactors

4.1 Introduction

Microwave tunable filters have received increased attention over the past few decades due to their potential to replace switched-filter banks in multi-band communication systems. Planar technologies being utilized for tuning include RF-MEMS devices, semiconductor (silicon, GaAs) varactor diodes, and P-I-N diodes. The focus of recent work on tunable filters has shifted from maximizing tuning range to controlling filter behaviour as it is tuned.

In this chapter, we introduce a new type of center frequency and bandwidth tunable microstrip filter, which is realized using varactors. The innovation of this structure is in isolating the coupling elements from the resonators by proposing a novel structure for admittance inverters. The proposed filter exhibits low insertion loss in the passband, with full control over bandwidth and center frequency. Input couplings, resonance frequency of individual resonators, and inner couplings schemes are discussed in detail. Additionally, to validate the practicality of the proposed structure, measurements for the fabricated filter are presented.

The organization of this chapter is as follows. Motivations for the proposed structure and filter design are provided in section 4.2. The effects of varactors on both resonators and coupling structures are presented in section 4.3, along with the implementation of the tunable filter by adding the varactors. Finally, section 4.4 presents the EM simulation results.

4.2 Filter Design

Bandwidth tunability of microwave filters can be achieved by changing the coupling value of the inverters between the resonators. In microstrip filters, inverters are usually realized by a gap between resonators, as shown in Figure 4-1. To change the coupling value (J or K of the inverter) of microstrip gaps, either gap size or gap width needs to be changed. This method is difficult to implement on a microstrip filter that has already been fabricated. Attaching a varactor to gap walls is another solution for altering the coupling. However, as gap walls are directly connected to resonators, the resonance frequency of the adjacent resonator will also be impacted by the varactor. Moreover, to maintain the

symmetric structure of the equivalent circuit shown in Figure 1, two varactors must be attached to both sides of the gap.

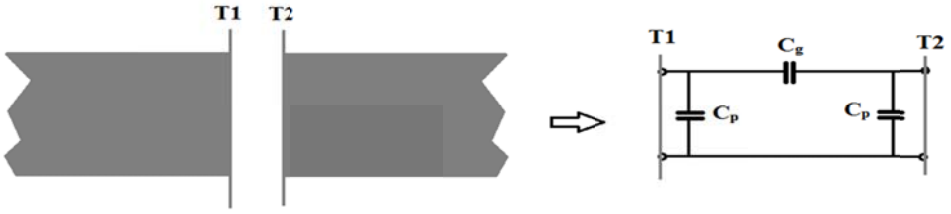

Figure 4-1: A microstrip gap and equivalent circuit model

4.2.1 A Novel Coupling Structure

The idea of designing tunable microstrip gaps by employing varactors suffers from the high phase loading effect of varactors on the adjacent resonators. To solve this problem, a novel structure is proposed for the microstrip couplers in this section. Figure 4-2 illustrates the proposed coupling structure for a tunable microstrip filter. The structure consists of two sets of coupled-lines and one transmission line that connects them. The top section of each coupled line is connected to the adjacent resonator.

The main advantage of this structure is isolating resonators and inverters. Since the bandwidth tenability can mainly be achieved by changing the coupling between resonators, using this structure makes the coupling value tunability (hence the bandwidth tunability) possible by changing the capacitance of the varactor attached to the center of the transmission line. The varactor should be connected to the middle of the transmission line, which is also the center of the structure, so that the inverter will keep its symmetry even after the capacitance of the varactor is changed.

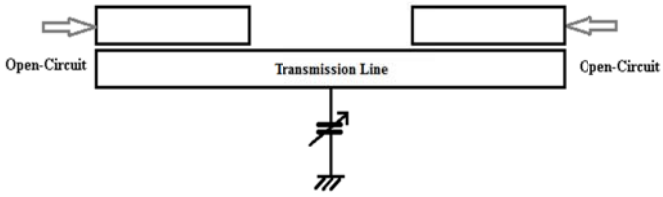

Figure 4-2: Proposed coupling structure for a tunable microstrip filter

Since the varactor is not directly attached to the resonators, the phase-loading effect caused by it is expected to be less than other microstrip inverters that have a direct connection to the resonator. Moreover, as the varactor can be connected to the center of this structure, one varactor is sufficient for tuning the coupling and maintaining symmetry at the same time. This statement can be tested by comparing the effect of adding a varactor on the phase-loading effect for a common microstrip coupling structure (similar to Figure 4-1) and the proposed coupling structure. Figure 4-3 shows a microstrip coupler with an attached varactor.

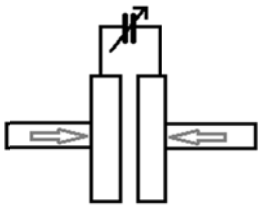

Figure 4-3: Microstrip coupler with an attached varactor

Figure 4-4 shows the phase-loading effect, as expressed in Equation (2-13), versus the varactor capacitance for both the proposed microstrip coupler and the micostrip coupler shown in Figure 4-3. The initial coupling values, J, and phase-loading effect value, ϕ, are the same for both couplers. As illustrated in this figure, the variation in the phase-loading effect of the proposed coupling structure after adding the varactor is negligible compared to the varactor impact on ϕ in the coupling structure shown in Figure 4-3.

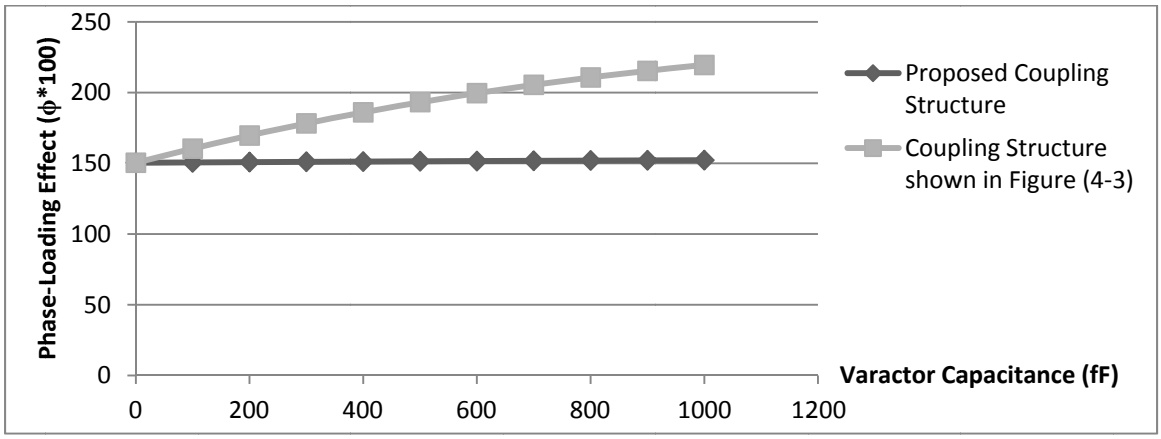

Figure 4-4: A microstrip coupler with an attached varactor

4.2.2 The Filter Structure

The design steps of the microstrip filter in this chapter are the same as in section 2.3.2. However, the microstrip gaps, employed as an admittance inverter in that section, are replaced with the proposed coupling structure in 4.2.1. Later in this chapter, GaAs Varactors will be attached to the proposed coupling structures to enable tuning of the coupling value. Varactors with different ranges of capacitances will also be employed to change the resonance frequency of resonators

The first step in designing a microstrip filter is calculating element values (g-values) for equal-ripple low-pass filter prototypes. Equations (2-1) to (2-8) show the expression for calculating element values. These values are a function of equal ripple level and number of poles and are independent from bandwidth and center frequency. Calculating the J values for admittance inverters is the second step. J values can be calculated by using element values and the ratio of bandwidth to center frequency. Equations (2-9), (2-10) and (2-11) are used to calculate J values.

In the microstrip filter design steps, the desired J values for admittance inverters are usually realized by microstrip gaps. As explained earlier, for tunability purposes, a new coupling structure is proposed in this chapter by using two similar gaps (Figure 4-2). In this section, this structure is employed to implement inter-resonator couplings. An important point in the design of the coupling structure is the resonance frequency of the transmission line that connects the two coupled lines. The length of this transmission line must be much shorter in comparison with the physical length of the resonators so that its resonance frequency will not interfere in the passband of the filter.

Equations (2-12) to (2-15) show the relationship between the S parameters of a coupling structure as a 2-port network and its J value as an admittance inverter. Note that the proposed coupling structure in Figure 4-2 can also be used for the input coupling. However, as the value of the input coupling is larger than the other couplings and its tuning range needs to be wide, we decided to use a single gap to realize the input coupling due to its greater sensitivity to varactors and hence wider coupling range.

In designing a proper inter-resonator admittance inverter, the dimensions of the proposed coupling structure are determined in such a way that their Jvalue is equal to the desired calculated J value. On the other hand, determining the input and output couplers requires more complex calculations. First, the R values can be calculated from the expressions (3-2) and (3-3), after which the maximum value

of the reflected group delay can be determined by using Equation (4-1). In this expression, τ is the group delay of S_{11}, Δf is the bandwidth of the filter, and R is the input resistor as well as an element of the coupling matrix, as defined in section 3.2. This maximum value should occur at the center frequency of the filter (f_0).

$$\tau(\omega_0) = \frac{4}{R.\Delta\omega} = \frac{4}{R.2\pi.\Delta f} \tag{4-1}$$

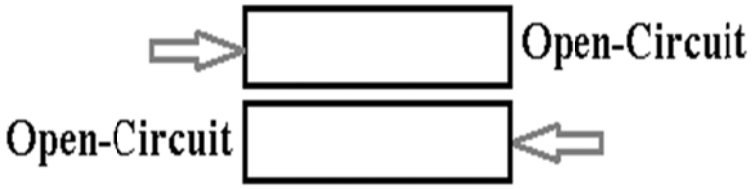

Figure 4-5: Input and output coupling structure

The final step is to design the resonators. The phase-loading effect, ϕ, of each coupler needs to be calculated before the length of the resonators. This parameter, which is defined in the expression (2-13), represents the loading effect of the coupler on the resonance frequency of the adjacent resonators. By knowing the loading phase (ϕ) of each coupler, the length of the resonators can easily be calculated by Equation (2-19). For miniaturization, a semi-square shape is used for the resonators. The layout of a complete 3-pole filter is shown in Figure 4-6, the dark parts being the filter's three resonators. After calculating the lengths of the microstrip resonators, a few degrees of iteration can be made to increase the accuracy of the final filter response, i.e., the coupling values of the inverters can be adjusted by considering the loading effects of the resonators on them.

Figure 4-6: Proposed structure for a 3-pole filter

4.3 Implementation of the Tunable Filter

A coupling matrix approach is used for the synthesis of the tunable filters. The fundamentals of the coupling matrix along with an introduction to M and R matrices were provided in section 3.2. The elements of the R matrix represent input and output couplings, while the M matrix secondary diagonal elements represent the inner couplings between the resonators. Each diagonal element of a coupling matrix represents one of the resonators. In this section, the tunability of center frequency, input/output couplings and inter-resonator couplings are analyzed individually. The effect of tuning one parameter on the others is analyzed at the end of this section.

4.3.1 Tuning the Center Frequency

For Chebyshev filters, the diagonal elements of a coupling matrix are zero. Each diagonal element represents a shift from the center frequency in the corresponding resonator. Tuning the center frequency is possible by tuning the resonant frequency of all resonators. Calculations of each resonator's resonance frequency will not be accurate if a single resonator is simulated without considering the loading effects of adjacent coupling structure and resonators. One reasonable method for finding the resonance frequency of a loaded resonator is by considering the next-closest coupling structures in the simulation.

Figure 4-7 shows a resonator with adjacent coupling structures. The phase-loading effect of the adjacent admittance inverters on the resonator is included in this 2-port network. As we can see, the center frequency tuning varactors is mounted on the center of this resonator. The duties of CR varactor include tuning the filter center frequency and compensating for loading effects when the filter bandwidth is tuned. The length of the resonator should be adjusted in such a way that the resonance frequency of the above structure will be set to the desired center frequency.

The main function of this varactor is tuning the center frequency of the filter. Hence, we should expect to see a shift in resonance frequency when the capacitance of the varactor increases. Figure 4-8 summarizes the effect of increasing CR capacitance on the resonance frequency of a resonator. The initial resonance frequency of this resonator is 2 GHz. The diagram shows that the resonance frequency decreases when the capacitance of CR increases. As depicted in this figure, the slope of the graph is almost constant and the trend of decreasing the resonance frequency is linear. The graph below shows that the center frequency of the filter can be tuned by changing the capacitance of

connected varactors to the resonators. Note that the resonance frequency can only be reduced by using this method. In other words, the filter needs to be designed in the highest frequency of tuning range. If this is done, then the center frequency can be reduced to lower frequencies by increasing the capacitance of the varactors connected to the resonators.

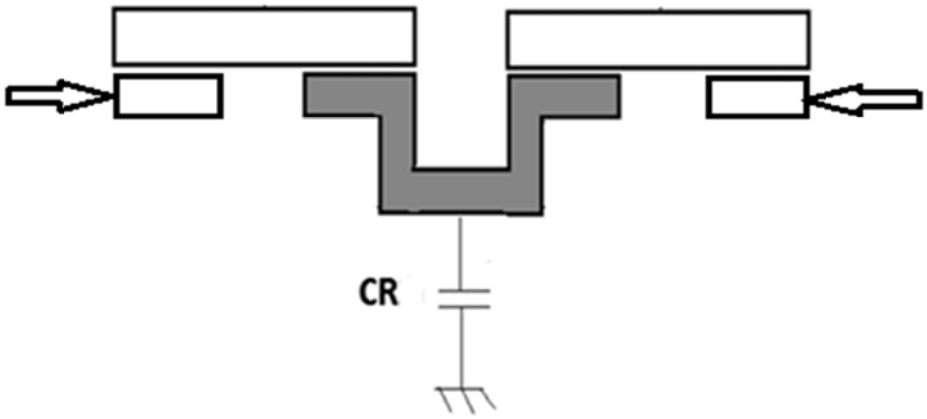

Figure 4-7: One resonator and adjacent coupling structures

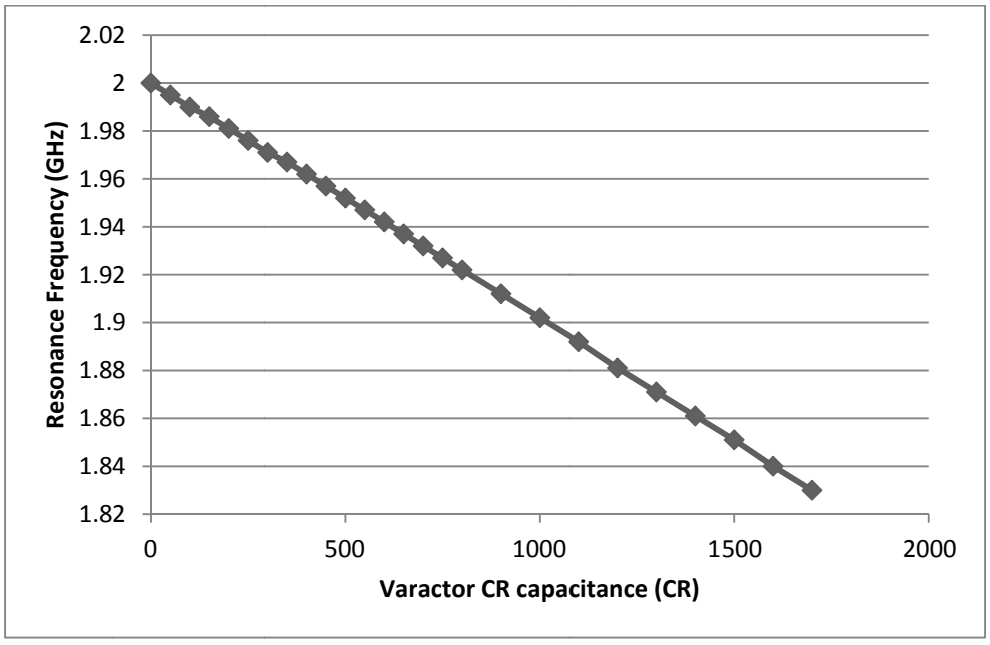

Figure 4-8: Resonance frequency versus the value of the varactor CR

4.3.2 Input Coupling Tuning

Based on Equation (2-9), the relationship between the input coupling value, J_{01}, and the filter bandwidth is provided in expression (4-2). This expression shows that, in tuning the bandwidth of a microwave filter, the input coupling of the filter has to be tuned as well. As shown in Figure 4-9, a varactor is mounted on the input coupling structure, directly in front of the coupled lines, to change the tune coupling value.

$$J_{input\ and\ output\ coupling} \propto \sqrt{bandwidth} \tag{4-2}$$

The reflected group delay method enables the extraction of input coupling. Expression (4-1) shows the relationship between the R parameters of the coupling matrix and the reflected group delay of a resonator measured at the resonant frequency. Figure 4-9 shows the input coupling structure with the first resonator and the next inter-resonator coupling structure. This structure includes the loading effect of the first resonator on the input coupling and can be used to calculate the effect of the varactor on the input coupling.

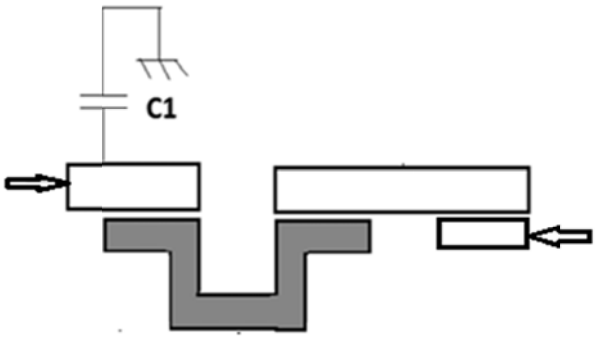

Figure 4-9: Input coupling structure with attached varactor, adjacent resonator and first inter-resonator coupling

The input coupling value is calculated by using reflected group delay. Increasing the value of the varactor C1 will change the maximum of the reflected group delay and hence the input coupling value. However, it will also change the frequency at which this maximum occurs. The shift in the frequency is the loading effect that needs to be adjusted later by other varactors. Figure 4-10 shows the different values of maximum reflected group delay of an input coupling structure versus different

values of varactor C1 attached to it. The initial reflected group delay value of this coupling structure, without any attached varactor, is 7.83×10^{-9}.

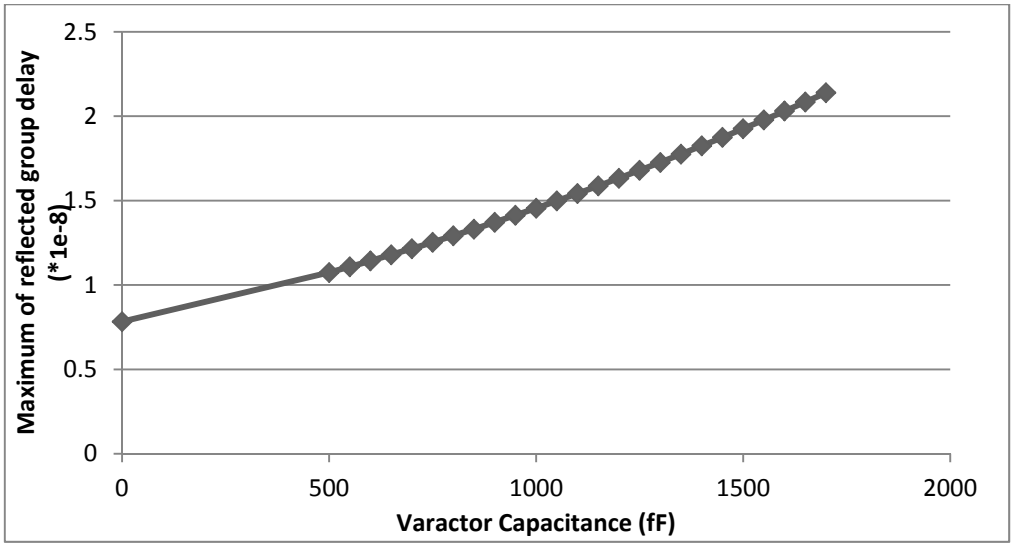

Figure 4-10: Maximum value of reflected group delay versus different values of varactor C1

The effect of this increase in the maximum reflected group delay on the behaviour of the filter can be analyzed by looking back at Equation (4-1). The left side of this equation, which is the maximum group delay of S_{11}, will increase by using higher values of varactors for C1.On the other hand, the value of R in the right side is only a function of g-values and hence it remains the same regardless of the change in the bandwidth. This means that the only variable in the right side will be the filter bandwidth. Since Δf is in the denominator on the right side, an increase in the maximum reflected group delay will result in a decrease in the bandwidth.

$$C1 \uparrow \Rightarrow \tau_{max} \uparrow \xRightarrow{equation\ (4-1)} Bandwidth \downarrow \tag{4-3}$$

Not all maximum reflected group delays used in Figure 4-10 occur in the filter center frequency, which is 2 GHz in this case. Figure 4-11 shows a frequency in which maximum group delay happens versus the value of varactor C1. The center frequency decreases when the capacitance of $C1$ increases. As will be explained later in this chapter, this effect will be adjusted by the other varactors, primarily the varactor attached to the adjacent resonator.

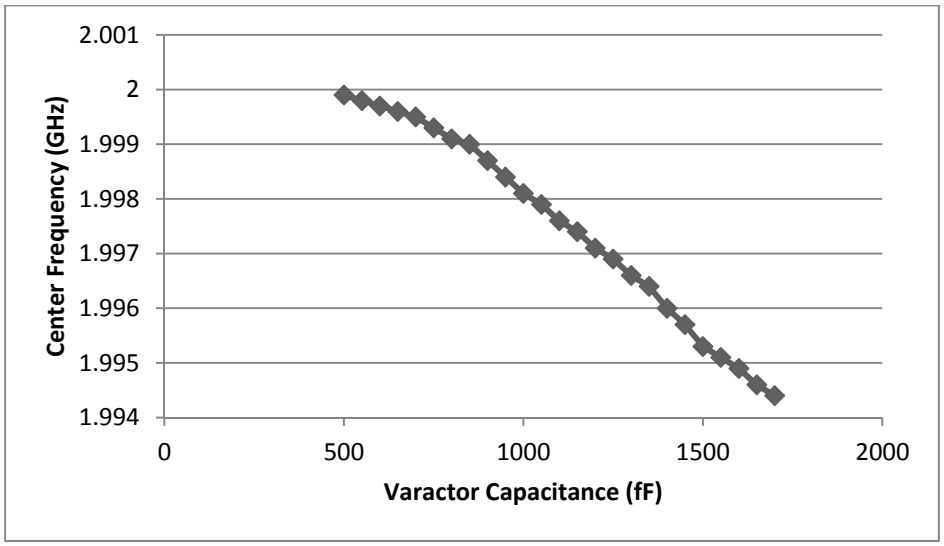

Figure 4-11: Frequency of maximum reflected group delay versus the value of varactor C1

4.3.3 Inter-Resonator Coupling

Extracting the inter-resonator coupling from a coupled circuit with two resonators is explained in detail in [46]. There are two resonant peaks in the S parameter diagrams of the coupled circuit with two resonators. If we name these two peaks f_1 and f_2, then the coupling coefficient can be calculated with the following expression. Thus, in tuning bandwidth microwave filters, the coupling coefficient between the adjacent resonators likewise needs to be tuned.

$$K = \frac{{f_2}^2 - {f_1}^2}{{f_2}^2 + {f_1}^2} \xrightarrow{for\ the\ narrowband\ circuits:\ f1.f2 \approx {f_0}^2} K \approx \frac{f_2 - f_1}{f_0} \tag{4-4}$$

As explained earlier, the proposed coupling structure in Figure 4-2 is employed for implementing the inter-resonator coupling. The J value of the proposed admittance inverter in Figure 4-2 can be calculated from the S parameters by using the expressions (2-12) to (2-15). The relationship between the inter-resonator coupling value and the bandwidth is stated in the following expressions, which shows that the inter-resonator coupling value is directly proportional to the filter bandwidth.

$$J_{inter-resonator} \propto bandwidth \tag{4-5}$$

The circuit model of the admittance inverter was shown in Figure 2-42. Adding the varactor C2 to the middle of this circuit will result in the equivalent circuit of Figure 4-12. If the $\Delta - Y$ transform is

applied to three elements of this circuit (namely, the two $B_s \times 2$ and the $C2$ capacitors), the circuit will be changed to what is shown in Figure 4-13.

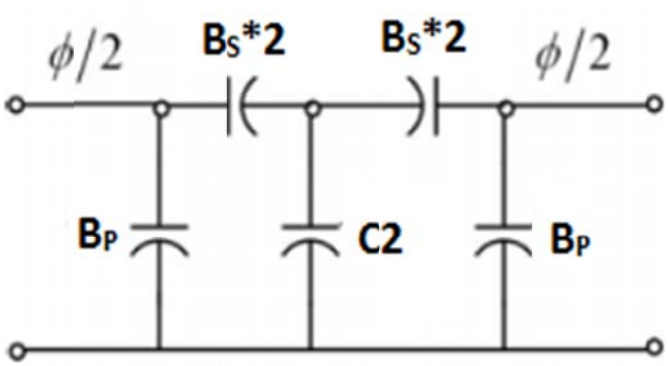

Figure 4-12: Equivalent circuit of admittance inverter after adding varactor C2.

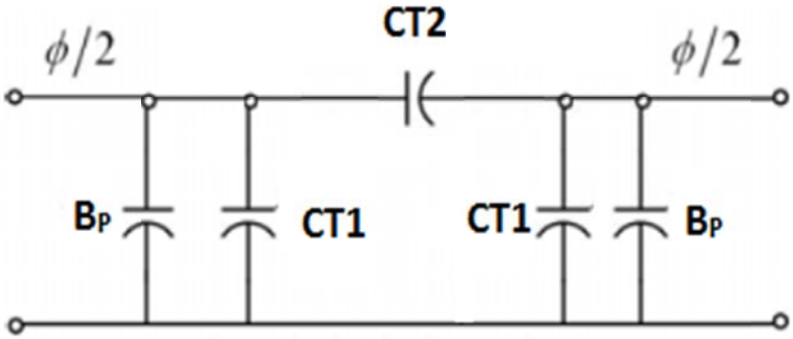

Figure 4-13: Equivalent circuit of proposed admittance inverter after applying $Y - \Delta$ transform

$$CT1 = \frac{C2 * (B_S/2)}{C2 + C2 + (B_S/2)} \tag{4-6}$$

$$CT2 = \frac{(B_S/2) * (B_S/2)}{C2 + C2 + (B_S/2)} \tag{4-7}$$

Since $CT1$ and B_P are parallel, we can replace them with one capacitor, and the final equivalent circuit will be similar to the initial circuit model for the impedance inverter. The only difference is the

value of the capacitors that result in a change in coupling values. This is exactly what we wanted in the first place: Changing the coupling value without disturbing the impedance inverter model. The graph in Figure 4-11 shows the new J values of an admittance inverter as the capacitance of C2 increases. The initial coupling value of this coupling structure, without any attached varactor, is 11.32×10^{-4}.

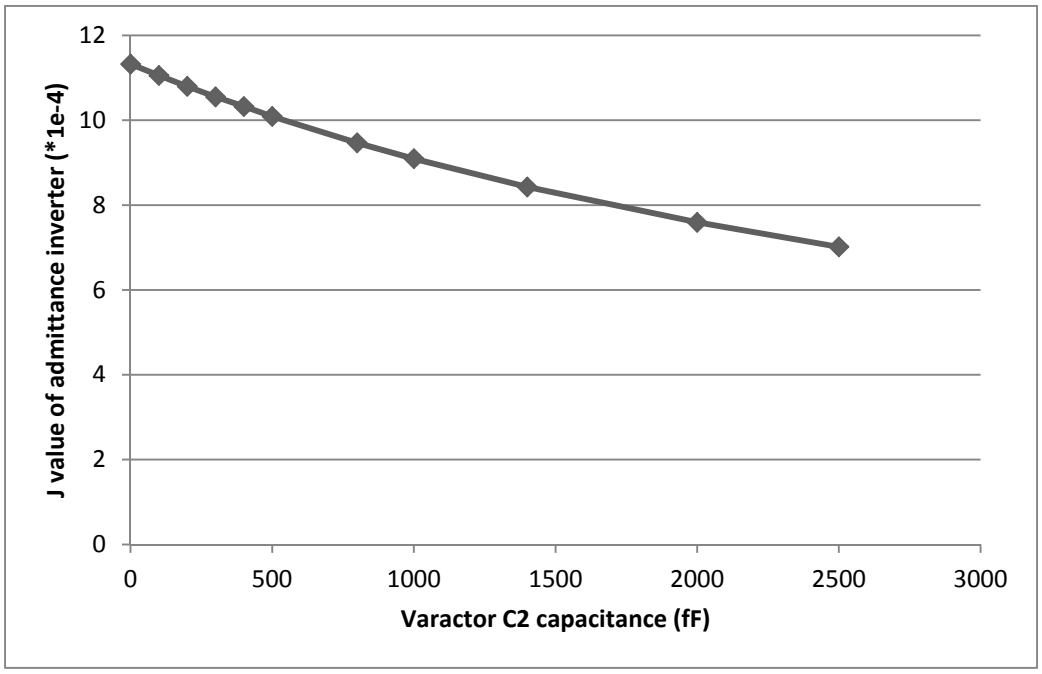

Figure 4-14: The J value of admittance inverter versus the value of varactor C2

As stated in expression (4-3), if the desired bandwidth of a Cheyshev filter increases, the inter-resonator coupling value will increase at the same pace. Figure 4-8 shows that the value of J decreases as the capacitance of C2 increases. Hence, this indicates that the bandwidth of the entire filter will decrease as a result of an increase in C2. Since increasing C1 has a reduction effect on the filter bandwidth as well, filters with minimum varactor values will have maximum bandwidth. Working from this perspective, decreasing bandwidth is possible by increasing varactor capacitances and decreasing inverter coupling values.

Unfortunately, the J value is not the only parameter that changes with the alteration in C2. The simulation result shows that increasing the capacitance of varactor C2 will slightly change the value

of the phase loading effect, ϕ. Figure 4-15 shows the calculated ϕ values of the same coupling structure after each alteration in varactor capacitance. The major effect of this change in ϕ appears in the resonance frequency of adjacent resonators. However, this problem can be solved by adjusting the resonance frequency of resonators with their connected varactors, CR1 and CR2 varactors.

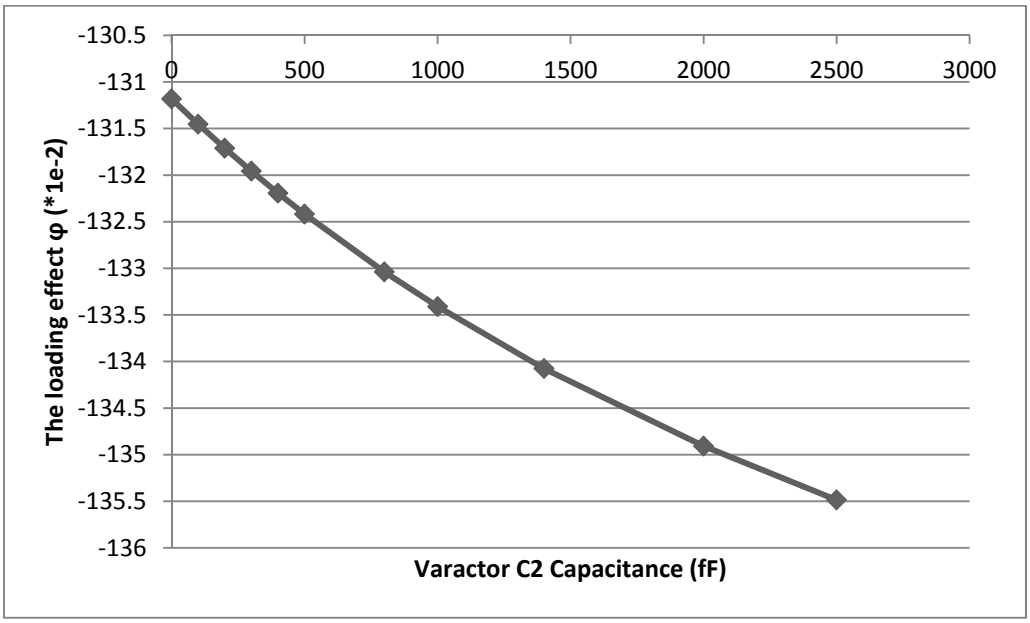

Figure 4-15: The ϕ values of admittance inverter versus the value of varactor C2

4.3.4 Tunable Filter Implementation

Figure 4-16 shows the final design of the filter after adding the varactors. Seven varactors have been used with four different capacitances: C1, C2, CR1 and CR2. The first varactor, C1, is used to tune the input and output coupling. C2 is attached to the middle of the inter-resonator coupling structure to tune the coupling value. In other words, the main duty of these two capacitors is to tune bandwidth. CR1 is applied to tune resonance frequency of the first and last resonators and to compensate for alterations in the phase loading effect caused by the other varactors. CR2 does the same to the second resonator and its adjacent couplers.

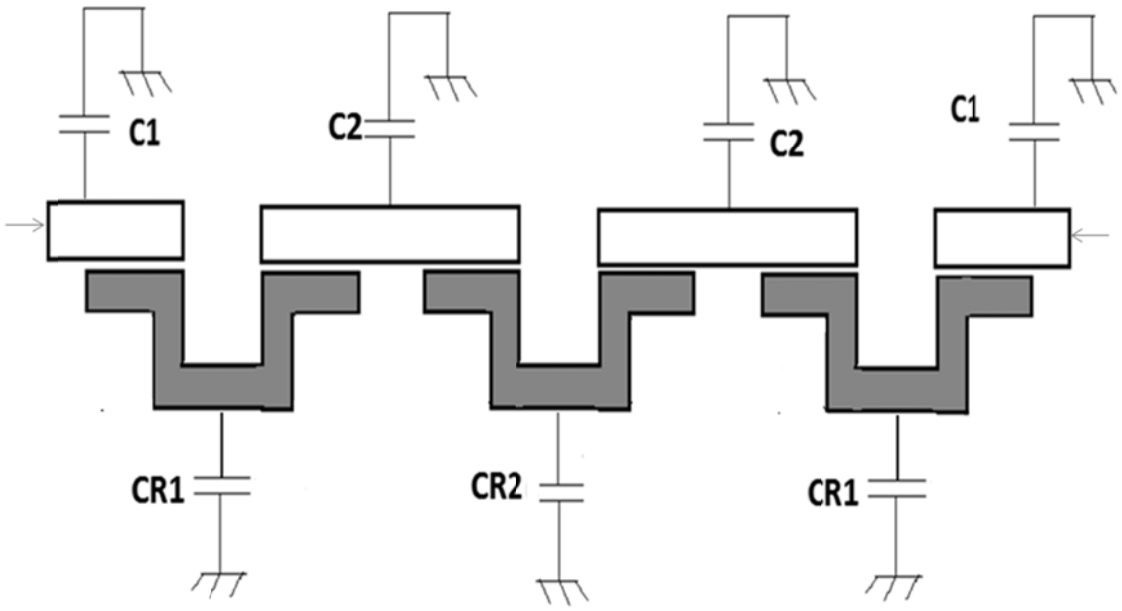

Figure 4-16: Final structure of the filter after adding capacitors

4.4 Simulation Results

Before presenting the simulation results for the complete filter, all of the important conclusions from the previous sections of this chapter will be summarized here. By considering the following points, a tunable microstrip filter with a center frequency range of 1.8 GHz to 2 GHz and a fractional bandwidth range of 3.5% to 0.5% has been designed and simulated. Figure 4-17 shows the layout of the tunable filter before attaching the varactors.

- The initial layout of the filter, without including the varactors, should be designed for the highest bandwidth in the tuning range. This is important mainly for the coupling structures.
- The initial layout of the filter, without including the varactors, should be designed for the highest canter frequency in the tuning range. This is important mainly for the resonators.
- The values of the two connected-to-the-resonator varactors should initially be set to a non-zero value.

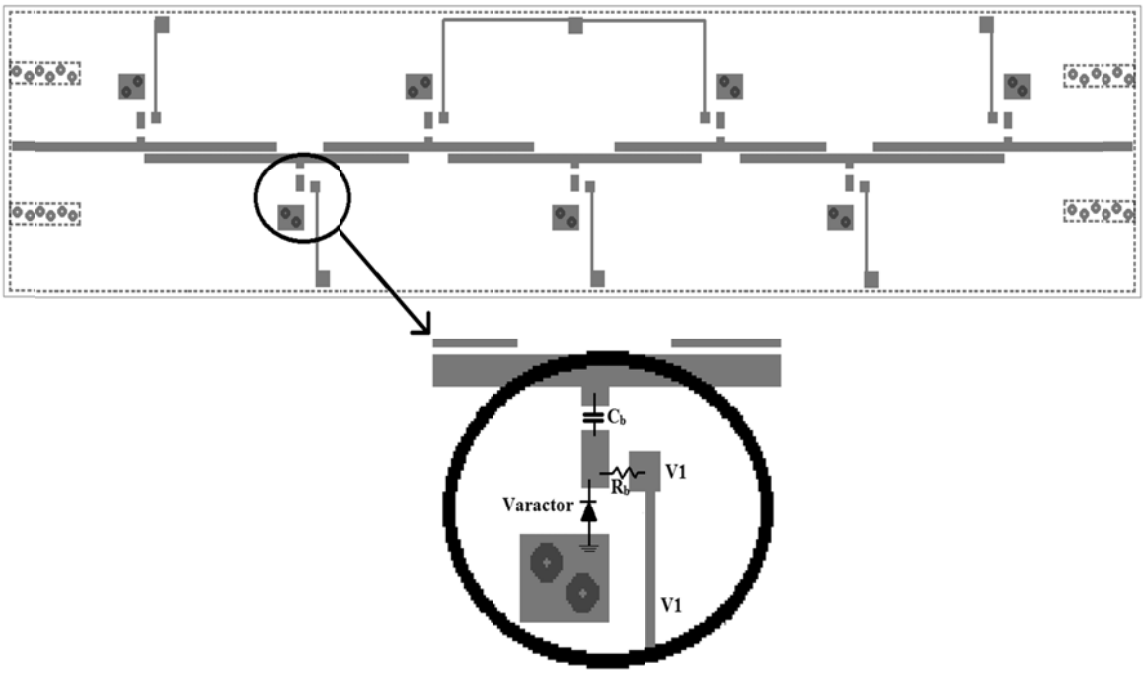

Figure 4-17: Layout of the bandwidth and center frequency tunable filter

As shown in Figure 4-17, the capacitor is realized by connecting a 0402 lumped bypass capacitor to a Schottky varactor diode (M/A COM MA45H201 for the resonators and M/A COM MA46H70 for the coupling structures). The chip capacitor is applied to realize a dc-biasing scheme. Due to the fixed value of the chip capacitor, the overall capacitance ratio of the capacitor-varactor set decreases. The bias circuit is realized using a resistor connected to the dc pad. A 0.635 mm Duroid substrate ($\varepsilon_r = 10.2$, Rogers RT/Duroid 6010.2) is used for the design.

The simulation results show a tunability range from 1.8 GHz to 2 GHz in the center frequency of the filter. The bandwidth tunability range is different in each center frequency. Figure 4-18 shows a bandwidth tunability of the filter while the center frequency is fixed on 1.95 GHz. As shown in this figure, the 1-dB bandwidth tunability range is from 60 MHz to 25 MHz. The insertion loss increases from 2.3 dB to 5 dB while the bandwidth is reduced from the maximum to the minimum value. The capacitor values for each state are provided in Table 4-1 at the end of this chapter.

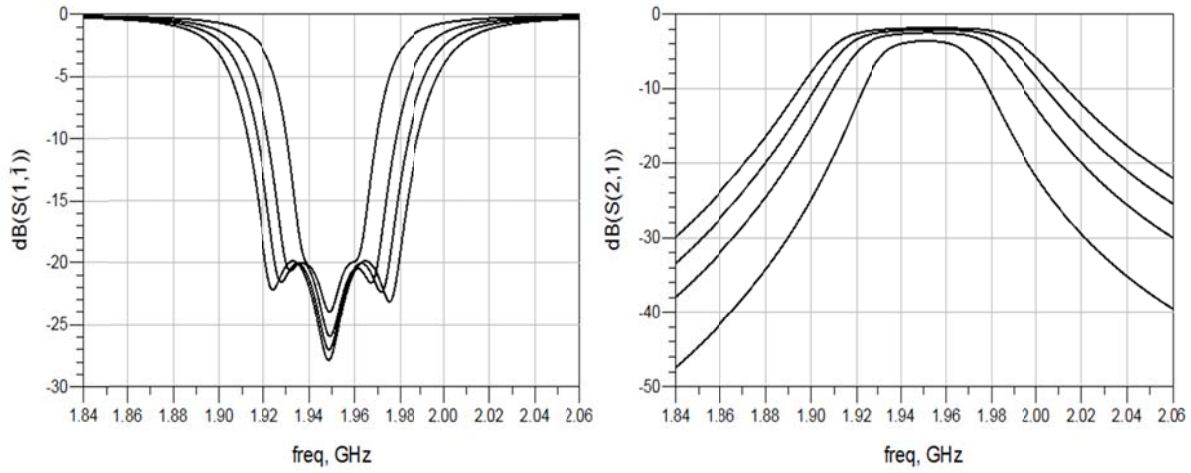

Figure 4-18: Tuning the bandwidth from 60 MHz to 25 MHz, with a fixed center frequency of 1.95 GHz

Tuning the center frequency with a fixed bandwidth is another interesting feature of this filter. Figure 4-19 shows the center frequency tunability of this filter from 1.9 GHz to 2 GHz while the bandwidth is constant and equal 40 MHz across the entire range. The insertion loss is almost constant during the center frequency tuning range and is approximately equal to 3 dB. Finally, the capacitor values for different filter center frequencies and bandwidths are provided in Table 4-1.

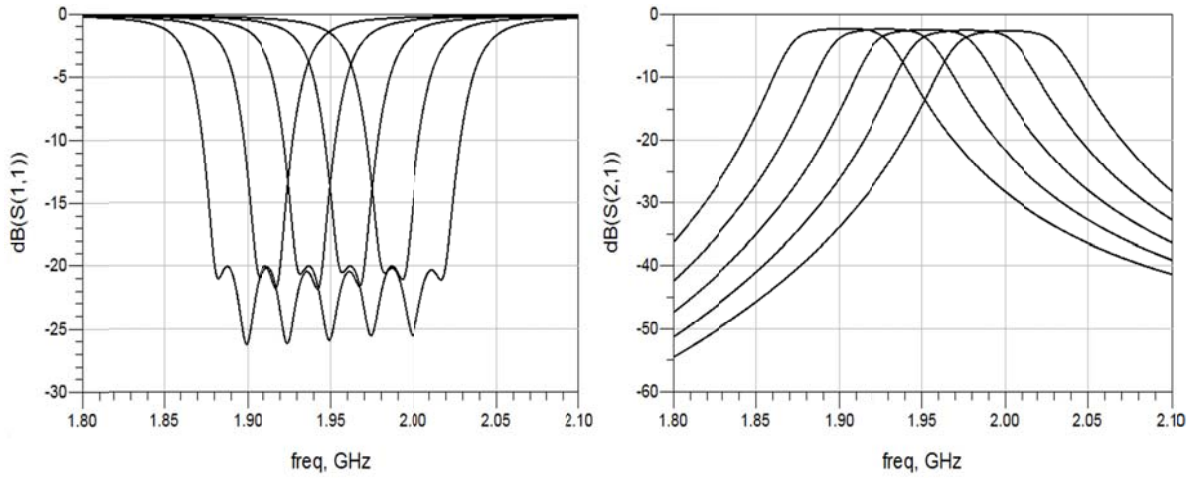

Figure 4-19: Tuning the center frequency from 1.9 GHz to 2 GHz with a fixed bandwidth of 40 MHz

Table 4-1: The look-up table for the varactor values (all of the capacitances are in fF)

	3.5%	**3%**	**2%**	**1.5%**	**1%**
2 GHz	C1=0 C2=0 CR1=500 CR2=750	C1=235 C2=850 CR1=337 CR2=524	C1=838.4 C2=3585.9 CR1=0 CR2=84.4		
1.95 GHz		C1=118.1 C2=136 CR1=1519 CR2=1648	C1=788.9 C2=2771.1 CR1=1231 CR2=1260	C1=1317 C2=5361.6 CR1=1045 CR2=1051	C1=2124.7 C2=10281.9 CR1=822.8 CR2=835.8
1.9 GHz			C1=636.8 C2=1774.4 CR1=2316 CR2=2305	C1=1149.8 C2=4000 CR1=2168 CR2=2128	C1=1981.5 C2=8472.3 CR1=1983.5 CR2=1939.8
1.85 GHz			C1=437.8 C2=800 CR1=3298 CR2=3259	C1=973.1 C2=2805.4 CR1=3168 CR2=3090	C1=1764.9 C2=6574.5 CR1=3020.1 CR2=2928.8
1.8 GHz			C1=458.4 C2=548.4 CR1=4190 CR2=4126	C1=766.1 C2=1493.8 CR1=4130 CR2=4045	C1=1544 C2=4476.6 CR1=4001 CR2=3893

Chapter 5
Conclusions and Future Work

5.1 Contribution of This Work

This work and the research leading up to its execution contain a number of primary contributions to the area of tunable microwave filters, all of which can be divided into two main areas.

First of all, the thesis introduces a novel method for the post-fabrication tuning of microwave filters by designing and adding a passive distributed-element circuit parallel to the detuned filter. This novel idea, demonstrated by experimental results, has several advantages over tuning screws, which is currently the most common way of tuning filters. The quality factor of each resonator reduces significantly after adding the tuning screws, whereas the proposed method does not affect the Q of resonators. Since the designed circuit will be added parallel to the original filter, it will not affect the elements of the filter individually. Thus, the proposed circuit can be used for tuning, whether the filter is planar or cavity. The provided experimental results show the performance of this idea on both cavity and planar filters.

This thesis' second area of contribution is its novel center frequency and bandwidth tunable microstrip filter by using GaAs varactors. The new isolated coupling structure used in this filter makes bandwidth tuning possible by reducing the loading effect of the coupling elements on the resonators. The center frequency of this filter can be also tuned by utilizing a different set of varactors connected to the resonators.

5.2 Future Work

The presented method in Chapter 3 can be extended to a more complicated circuit by adding admittance inverters to the proposed circuit. In this thesis, we modeled the differences between the Y parameters of a detuned filter and ideal filter with a set of transmission lines. By adding an admittance inverter to these transmission lines, we can approximate the more complicated Y parameter differences.

The ultimate improvement to the added compensator circuit is making the transmission lines dimensions tunable. Implementing this tunability depends on the type of applied transmission line in

the added circuit. For example, if a microstrip filter is used, the length can be increased by wire-bonding the microstrip lines together.

Bibliography

[1] J. Dunsmore, "Tuning band pass filters in the time domain," *Proc. IEEE MTT-S Int. Microw. Symp. Digest*, vol. 3, pp. 1351-1354, June 1999.

[2] V. Miraftab and R. R. Mansour, "Fully automated RF/microwave tuning by extracting human experience using fuzzy controllers," *IEEE Trans. Circuits Syst. I: Reg. Papers,*, vol. 55, no. 5, pp. 1357-1367, 2008.

[3] J. Ness, "A unified approach to the design, measurement, and tuning of coupled-resonator filters," *IEEE Trans. Microw. Theory Tech.*, vol. 46, no. 4, pp. 343-351, April 1998.

[4] "Infineon. (2006) PMB 5701; SMARTi 3G - The First Single-Chip Multi-Band CMOS Radio Frequency (RF) UMTS Transceiver IC.," Infineon Technologies AG. 81726 Munich, Germany, [Online]. Available: http://www.infineon.com/cms/en/product/channel.html?channel=ff80808112ab681d0112ab6acf4c062f.

[5] J. Uher and J. R. Hofer, "Tunable microwave and milliemeter-wave bandpass," *IEEE Trans. Microwave Theory Tech.*, vol. 39, no. 1, p. 643–653, 1984.

[6] G. L. Matthaei, L. Young, and E. Jones, Microwave Filters Impedance-Matching Networks, and Coupling Structures, Norwood, MA: Artech House, 1980.

[7] W. J. Keane, "YIG filters aid wide open receivers," *Microwave J.*, vol. 17, no. 8, p. 1920–1980, Sep. 1980.

[8] I. C. Hunter and J.D. Rhodes, "Electronically tunable microwave bandpass filters," *IEEE Trans. Microwave Theory & Tech.*, vol. 30, no. 9, p. 1354–1360, Sep. 1982.

[9] A. Tombak, J.-P. Maria, F. T. Ayguavives, Z. Jin, G. T. Stauf, A. I. Kingon, and A. Mortazawi, "Voltage-controlled RF filters employing thin-film barium-strontium-titanate tunable capacitors," *IEEE Trans. Microwave Theory & Tech.*, vol. 51, no. 2, p. 462–467, Feb. 2003.

[10] A. R. Brown and G. M. Rebeiz, "A varactor-tuned RF filter," *IEEE Trans. Microw. Theory Tech.*, vol. 48, no. 7, pp. 1157-1160, July 2000.

[11] M. Sanchez-Renedo and J. I. Alonso, "Tunable planar combline filter with multiple source/load coupling," *Proc. IEEE MTT-S Int. Microw. Symp. Digest*, June 2005.

[12] S. Park and G. M. Rebeiz, "Low-loss two-pole tunable filters with three different predefined bandwidth characteristics," *IEEE Trans. Microwave Theory & Tech.*, vol. 56, no. 5, p. 1137–1148, May 2008.

[13] K. Entesari, K. Obeidat, A. R. Brown, and G. M. Rebeiz, "A 25-75 MHz RF MEMS tunable filter," *IEEE Trans. Microwave Theory & Tech.*, vol. 55, no. 11, p. 2399–2405, 2007.

[14] I.Reines, A. Brown, M. El-Tanani, A. Grichener, and G. M. Rebeiz, "1.6-2.4 GHz RF-MEMS tunable 3-pole suspended combline filter," *IEEE MTT-S Int. Microwave Symp. Dig.*, p. 133–136, June 2008.

[15] S. Park, M. A. El-Tanani, I. Reines, and G. M. Rebeiz, "Low-loss 4-6 GHz tunable filter with 3-bit high-Q orthogonal bias RF-MEMS capacitance network," *IEEE Trans. Microwave Theory & Tech.*, vol. 56, no. 10, pp. 2348-2388, Oct. 2008.

[16] M. A. El-Tanani, and G. M. Rebeiz, "High Performance 1.5-2.5 GHz RF-MEMS Tunable Filters for Wireless Applications," *IEEE Trans. on Microw. Theory Tech.*, vol. 58, no. 6, pp. 1629-1637, Jun. 2010.

[17] G. Sanderson, A. H. Cardona, T. C. Watson, D. Chase, M. Roy, J. M. Paricka, and R. A. York, "Tunable IF filter using thin-film BST varactors," *Proc. IEEE MTT-S Int. Microw. Symp. Digest*, pp. 679-682, June 2007.

[18] Y.-H. Chun, J.-S. Hong, P. Bao, T. J. Jackson, and M. J. Lancaster, "BST-varactor tunable dual-mode filter using variable Zc transmission line," *IEEE Microwave and Wireless Components Letters*, vol. 18, no. 3, pp. 167-169, March 2008.

[19] M.-T. Nguyen, W. D. Yan, and E. P. W. Horne, "Broadband tunable filters using high Q passive tunable ICs," *Proc. IEEE MTT-S Int. Microw. Symp. Digest*, pp. 951-954, June 2008.

[20] C. Rauscher, "Reconfigurable bandpass filter with a three-to-one switchable passband width," *IEEE Trans. Microw. Theory Tech.*, vol. 51, p. 573–577, Feb. 2003.

[21] Cesar Lugo Jr., Dane Thompson, John Papapolymerou, "Reconfigurable bandpass filter with variable bandwidth at 5.8 GHz using a capacitive gap variation technique," *Proc. 33rd Eur. Microwave Conf.*, vol. 3, pp. 923-926, Munich, Germany, Oct. 2003.

[22] J. I. A. M. Sanchez-Renedo, R. Gomez-Garcia and C. Briso-Rodriguez, "Tunable combline filter with continuous control of center frequency and bandwidth," *IEEE Trans. Microwave Theory & Tech.*, vol. 53, no. 1, pp. 191-199, Jan. 2005.

[23] K. Kawai, H. Okazaki, and S. Narahashi, "Center frequency and bandwidth tunable filter employing tunable comb-shaped transmission line resonator and J-inverters," in *36th European Microwave Conference*, Sept. 2006.

[24] H. Joshi, H. H. Sigmarsson, S. Moon, D. Peroulis and W. J. Chappell, "High Q narrow-band tunable filters with controllable bandwidth," *IEEE MTT-S International Microwave Symposium Digest*, pp. 629-632, May 2009.

[25] C. Lugo, G. Wang, J. Papapolymerous, Z. Zhao, X. Wang, and A. T. Hunt, "Frequency and bandwidth agile millimeter-wave filter using ferroelectric capacitors and MEMS cantilevers," *IEEE Trans. Microwave Theory Tech.*, vol. 55, pp. 376-382, 2007.

[26] X. Liu, L. P. Katehi, W. J. Chappell, and D. Peroulis, "A 3.4 - 6.2 GHz continuously tunable electrostatic MEMS resonator with quality factor of 460-530," *IEEE MTT-S International Microwave Symposium Digest*, pp. 1149-1152, June 2009.

[27] E. Fourn, C. Quendo, E. Rius, A. Pothier, P. Blondy, C. Champeaux, J. C. Orlianges, A. Catherinot, G. Tanne, C. person, and F. Huret, "Bandwidth and central frequency control on tunable bandpass filter by using MEMS cantilevers," *IEEE MTT-S International Microwave Symposium Digest*, pp. 523-526, June 2003.

[28] C. Palego, A. Pothier, A. Crunteanu, M. Chatras, P. Blondy, C. Champeaux, P. Tristant, and A. Catherinot, "Two-pole lumped-element programmable filter with MEMS pseudodigital capacitor banks," *IEEE Trans. Microwave Theory & Tech.*, vol. 56, no. 3, p. 729–735, Mar. 2008.

[29] H. Joshi, H. H. Sigmarsson, S. Moon, D. Peroulis, and W. J. Chappell, "High-q fully reconfigurable tunable bandpass filters," *IEEE Trans. Microw. Theory Tech.*, vol. 57, no. 12, pp. 3525-3533, 2009.

[30] Hao-Han Hsu, A.D. Margomenos, D. Peroulis, "A monolithic RF-MEMS filter with continuously-tunable center-frequency and bandwidth," *Silicon Monolithic Integrated Circuits in RF Systems (SiRF)*, pp. 169-172, Jan. 2011.

[31] Yi-Chyun Chiou, and G. M. Rebeiz, "Yi-Chyun Chiou, and Gabriel M. Rebeiz," *IEEE Trans. Microwave Theory & Tech*, vol. 59, no. 11, pp. 2872-2878 , Nov. 2011.

[32] R. S. Elliott, An Introduction to Guided Waves and Microwave Circuits, Englewood Cliffs, NJ: Prentice–Hall, 1993.

[33] R. J. Cameron, C. M. Kudsia, and R. R. Mansour, Microwave Filters for Communications Systems: Fundamentals, Design, and Applications, John Wiley & Sons Inc., 2007.

[34] Advance Design System 2005A, Agilent Technologies, Inc., Palo Alto, CA, USA, 2005.

[35] SONNET Software Inc., "Sonnet 12.56," *North Syracuse, NY*, 2009.

[36] J. Zhou, G. Zhang and M.J. Lancaster, "Passive microwave filter tuning using bond wires," *Microwaves, Antennas & Propagation, IET*, vol. 1, no. 3, pp. 567-571, Jun. 2007.

[37] J. Zhou, M.J. Lancaster, and F. Huang, "Coplanar quarter-wavelength quasi-elliptic filters without bond-wire bridges," *IEEE Trans. Microw. Theory Tech.*, vol. 52, no. 4, p. 1150–1156, 2005.

[38] P. Harscher, R. Vahldieck, and S. Amari, "Automated filter tuning using generalized low-pass

prototype networks and gradient-based parameter extraction," *IEEE Trans. Microw. Theory Tech.*, vol. 49, no. 12, p. 2532–2538, 2001.

[39] H.-T. Hsu, H.-W. Yao, K. Zaki, and A. Atia, "Computer-aided diagnosis and tuning of cascaded coupled resonators," *IEEE Trans. Microw. Theory Tech.*, vol. 50, no. 4, pp. 1137-1145, Apr. 2002.

[40] G. Pepe, F.-J. Gortz, and H. Chaloupka, "Sequential tuning of microwave filters using adaptive models and parameter extraction," *IEEE Trans. Microw. Theory Tech.*, vol. 53, no. 1, pp. 22-31, 2005.

[41] S. Pal, C. Stevens, and D. Edwards, "Tunable HTS microstrip filters for microwave electronics," *Electron. Lett.*, vol. 41, no. 5, pp. 286-288, 2005.

[42] N.J. Parker, S.W. Goodyear, D.J.P. Ellis, and R.G. Humphreys, "Tuning superconducting microwave filters by laser trimming," *IEEE MTT-S Int. Microwave Symposium Digest*, vol. 3, pp. 1971-1974, Jun. 2002.

[43] T. Zuo, L. Fang, S. Yan, X. Zhao, T. Zhou,S. You,W. Ma, H. Yue and Q. Xie, "A computer-aided method for postproduction tuning of HTS filters," *Supercond. Sci. Tech.*, vol. 20, pp. 1184-1188, 2007.

[44] M. Meng and K.-L. Wu, "An analytical approach to computer-aided diagnosis and tuning of lossy microwave coupled resonator filters," *IEEE Trans. Microw. Theory Tech.*, vol. 57, no. 12, pp. 3188-3195, Dec. 2009.

[45] G. Pepe, F.-J. Gortz, and H. Chaloupka, "Computer-aided tuning and diagnosis of microwave filters using sequential parameter extraction," *Proc. IEEE MTT-S Int. Microw. Symp. Digest*, vol. 3, pp. 1373-1376, April 2004.

[46] J.-S. Hong and M. J. Lancaster, Microstrip Filters for RF/Microwave Applications, K. Chang, Ed. John Wiley & Sons Inc., 2001.

[47] A. E. Atia and A. E. Williams, "Narrow-bandpass waveguide filters," *IEEE Trans. Microw. Theory Tech.*, vol. 20, no. 4, pp. 258-265, 1972.

[48] C. G. Montgomery, R. H. Dicke, and E. M. Purcell, Principles of Microwave Circuits, Stevenage, U.K: Peregrinus, 1987.

[49] W. Meng and K-L. Wu, "Analytical Diagnosis and Tuning of Narrowband Multicoupled Resonator Filters," *IEEE Trans. Microw. Theory Tech.*, vol. 54, no. 10, pp. 3765-3771, 2006.

[50] MATLAB 7.1, The Mathworks, Inc., Natick, MA USA, 2005.